



**MATHEUS CORDAZZO DIAS**

**THE FIBER RECALCITRANCE OF COMMERCIAL  
EUCALYPTUS PULPS AFFECTING THE EFFECTIVENESS  
OF PRETREATMENTS AND THE PRODUCTION OF  
CELLULOSE NANOFIBRILS**

**LAVRAS – MG  
2022**

**MATHEUS CORDAZZO DIAS**

**THE FIBER RECALCITRANCE OF COMMERCIAL EUCALYPTUS PULPS  
AFFECTING THE EFFECTIVENESS OF PRETREATMENTS AND THE  
PRODUCTION OF CELLULOSE NANOFIBRILS**

Doctoral Thesis presented to the Federal University of Lavras, as part of the requirements of the Graduate Program in Wood Science and Technology, concentration area in Wood Science and Technology, research line Processing and Utilization of Lignocellulosic Materials and Derivatives to obtain the degree of Doctor of Science in Wood Science and Technology.

Prof. Dr. Saulo Rocha Ferreira  
Advisor

Prof. Dr. Gustavo Henrique Denzin Tonoli  
Co-Advisor

Prof. Dr. Mohamed Naceur Belgacem  
Co-Advisor

**LAVRAS – MG  
2022**

Ficha catalográfica elaborada pelo Sistema de Geração de Ficha Catalográfica da Biblioteca  
Universitária da UFLA, com dados informados pelo(a) próprio(a) autor(a).

Dias, Matheus Cordazzo.

The fiber recalcitrance of commercial Eucalyptus pulps  
affecting the effectiveness of pretreatments and the production of  
cellulose nanofibrils / Matheus Cordazzo Dias. - 2022.

138 p. : il.

Orientador(a): Saulo Rocha Ferreira.

Coorientador(a): Gustavo Henrique Denzin Tonoli, Mohamed  
Naceur Belgacem.

Tese (doutorado) - Universidade Federal de Lavras, 2022.

Bibliografia.

1. Cell wall. 2. Nanofibrillated cellulose. 3. Recalcitrance. I.  
Ferreira, Saulo Rocha. II. Tonoli, Gustavo Henrique Denzin. III.  
Belgacem, Mohamed Naceur. IV. Título.

**MATHEUS CORDAZZO DIAS**

**THE FIBER RECALCITRANCE OF COMMERCIAL EUCALYPTUS PULPS  
AFFECTING THE EFFECTIVENESS OF PRETREATMENTS AND THE  
PRODUCTION OF CELLULOSE NANOFIBRILS**

**A RECALCITRÂNCIA DAS FIBRAS DE POLPAS COMERCIAIS DE EUCALIPTO  
QUE AFETAM A EFICÁCIA DE PRÉ-TRATAMENTOS E A PRODUÇÃO DE  
NANOFIBRILAS DE CELULOSE**

Doctoral Thesis presented to the Federal University of Lavras, as part of the requirements of the Graduate Program in Wood Science and Technology, concentration area in Wood Science and Technology, research line Processing and Utilization of Lignocellulosic Materials and Derivatives to obtain the degree of Doctor of Science in Wood Science and Technology.

**APPROVED** on February 21, 2022.

Dr. Saulo Rocha Ferreira	UFLA
Dr. Gustavo Henrique Denzin Tonoli	UFLA
Dr. Marcelo Coelho dos Santos M. Soares	KLABIN S.A
Dr. Holmer Savastano Junior	FZEA/USP
Dr. Mario Guimarães Junior	CEFET-MG
Dr. Mohamed Naceur Belgacem	GRENOBLE INP/UGA

Prof. Dr. Saulo Rocha Ferreira  
Advisor

**LAVRAS – MG  
2022**

## DEDICATÓRIA

Dedico esta tese à minha família, por seu amor incondicional, dedicação e por todo o apoio que me deram ao longo desta jornada.

## AGRADECIMENTOS

Agradeço em primeiro lugar, Deus, pois sem ELE eu não teria chegado até aqui. Aos meus pais, João Guilherme e Maria Lúcia, porque confiaram em mim e me deram esta oportunidade de realizar mais um passo desta jornada sem medir esforços para tornar este sonho realidade. Sem seu apoio e compreensão, nada disso teria sido possível, pois eles foram fundamentais para a realização de meu trabalho. A vocês, eu lhes expresso minha maior gratidão. Aos meus irmãos, Guilherme e Andressa, que sempre estiveram ao meu lado me apoiando durante os momentos de tristeza, felicidade, angústia e ansiedade desta longa jornada. Um reconhecimento especial à minha irmã Andressa e ao meu cunhado Samuel por me terem dado de presente o meu sobrinho Renato, que desde seu nascimento encheu meu coração de amor e felicidade.

Aos meus queridos amigos que a UFLA me deu, com os quais desfrutei de momentos de prazer, aprendizado, motivação e amizade. Obrigado por torcerem por mim e me encorajarem não só na academia, mas na vida.

A *École Internationale du Papier, de la Communication Imprimée et des Biomatériaux* e o LGP2, pertencente ao *Institut Polytechnique de Grenoble* - França e todo seu pessoal, estudantes e funcionários, por me receberem tão bem durante meu doutorado sanduíche, onde tive a oportunidade de ganhar experiência como pesquisador.

Ao meu orientador Saulo Rocha Ferreira e aos meus coorientadores Gustavo Henrique Denzin Tonoli e Mohamed Naceur Belgacem, por todo o aprendizado, apoio e paciência ao longo desta jornada, fazendo-me crescer pessoal e profissionalmente.

Gostaria de agradecer ao Programa de Pós-graduação em Ciência e Tecnologia da Madeira da UFLA e à CAPES, por me conceder a bolsa de doutorado, e pela oportunidade de desenvolver parte do meu doutorado na França, concedendo uma bolsa através do Programa de Doutorado Sanduíche no Exterior, garantindo que o curso de pós-graduação fosse totalmente desenvolvido.

*“Nossas virtudes e nossos fracassos  
são inseparáveis,  
como força e matéria.  
Quando eles se separam,  
O homem deixa de existir.”*

**Nikola Tesla**

## RESUMO

Este estudo teve como objetivo principal avaliar a influência das propriedades de diferentes polpas comerciais de *Eucalyptus* sp. na eficiência de pré-tratamentos e seu impacto no processo de obtenção de NFC. Para tal, foram utilizados dois tipos diferentes de polpas celulósicas, sendo elas: polpa kraft branqueada, além de polpa kraft liner não branqueada com alto teor de lignina. Na primeira etapa caracterizou-se as propriedades químicas e morfológicas detalhadas dos materiais. Na segunda etapa, pré-tratamentos alcalinos com hidróxido de sódio (NaOH) foram realizados nas polpas branqueadas em diferentes concentrações e tempo de reação para obtenção de fibras com diferentes conteúdos de hemiceluloses. Na terceira etapa, para as polpas não branqueadas, foram utilizados dois pré-tratamentos enzimáticos seguidos: O primeiro com uma enzima laccase com o objetivo de degradar a lignina sem removê-la e o segundo com uma enzima endoglucanase para hidrolisar a celulose. As NFC foram obtidas nanofibrilação mecânica utilizando um moinho nanofibrilador e o consumo energético foi monitorado. Posteriormente as NFC obtidas foram caracterizadas para analisar o impacto dos pré-tratamentos na sua qualidade. O primeiro artigo (Artigo 1) buscou avaliar as propriedades das NFC com diferentes teores de hemiceluloses e polimorfos de celulose II. Foi encontrada uma ligação entre estes polissacarídeos e as propriedades das NFC. Foi observada uma diminuição da cristalinidade (de 69 para 63%) e mudanças na estrutura cristalina da celulose submetida a um ambiente alcalino, promovendo a conversão parcial da celulose I em celulose II (de 2 para 42%) e impedindo a produção de NFC em concentrações de NaOH superiores a 5%. A maioria dos tratamentos mostrou comportamento de fluido pseudoplástico, exceto pelo tratamento de NaOH 10% durante 2 horas, que mostrou comportamento de fluido newtoniano. O índice de qualidade do tratamento NaOH 5% foi o mais alto ( $68 \pm 3$  e 22% de economia de energia em comparação com a amostra não tratada), seguido pela amostra não tratada ( $63 \pm 3$ ); e os NaOH 10% tratados por 1 e 2 horas tiveram índices de qualidade de  $51 \pm 3$  e  $32 \pm 1$ , respectivamente. O segundo artigo (Artigo 2) buscou avaliar o impacto de um pré-tratamento enzimático combinado de laccase e endoglucanase para a produção de nanofibrilas de celulose contendo lignina (LCNF). Este pré-tratamento melhorou a qualidade das LCNF ( $61 \pm 3$  a  $71 \pm 2$ ) e proporcionou a redução do consumo energético em 42%. As LCNF obtidas após os pré-tratamentos enzimáticos melhoraram a resistência mecânica em 24% e exibiu boa permeabilidade ao vapor d'água ( $2,42 \text{ g.mm/m}^2 \cdot \text{kPa.dia}$ ) e propriedades de barreira à graxa (kit nº 12). A reologia das LCNF exibiu comportamento não newtoniano. Este estudo mostrou que os tratamentos alcalinos causaram diferentes níveis de hemiceluloses e conversão parcial em celulose II. Foi demonstrado o impacto positivo da mudança no teor de hemicelulose e na estrutura da celulose tratadas com NaOH 5% para produção de NFCs. A Laccase mostrou-se eficaz no ataque à lignina ajudando a diminuir a recalcitrância da parede celular e tornando as cadeias de celulose mais expostas ao contato físico para a ação da Endoglucanase.

**Palavras-chave:** Celulose microfibrilada (CMF). Celulose nanofibrilada (CNF). Consumo energético. Nanotecnologia. Parede celular. Recalcitrância.



## ABSTRACT

The principal objective of this study was to evaluate the influence of different *Eucalyptus* sp. commercial pulp properties on the pretreatment efficiency and its impact on the CNFs production process. To achieve this, two distinct types of pulps were used: bleached kraft pulp, and an unbleached kraft liner pulp with high lignin content. In the first step, the detailed chemical and morphological properties of the materials were characterized. In the second stage, alkaline pretreatments with sodium hydroxide (NaOH) were performed on the bleached pulps at different concentrations and reaction times to obtain fibers with different hemicellulose contents. In the third stage, for the unbleached pulps, two enzymatic pretreatments were used in a sequence: The first with a laccase enzyme aiming to degrade lignin without removing it and the second with an endoglucanase enzyme to hydrolyze cellulose. The CNFs were obtained by mechanical nanofibrillation using a nanofibrillator grinder and the energy consumption was monitored. Subsequently, the obtained CNFs were characterized to understand the influence of the pretreatments on their quality. The present research is divided in two chapters (articles): The first article (Article 1) attempted to evaluate the properties of CNFs with different hemicellulose and cellulose polymorph II contents. A connection was found between these polysaccharides and CNFs properties. A decrease in crystallinity (from 69 to 63%) and changes in the crystalline structure of cellulose subjected to an alkaline environment were observed, promoting partial conversion of cellulose I to cellulose II (from 2 to 42%) and preventing CNFs production at NaOH concentrations higher than 5%. Most treatments showed pseudoplastic fluid behavior, except for the 10% NaOH treatment for 2 hours, which showed Newtonian fluid behavior. The quality index of the 5% NaOH treatment was the highest ( $68 \pm 3$  and 22% energy savings compared to the untreated sample), followed by the untreated sample ( $63 \pm 3$ ); and the 10% NaOH treated for 1 and 2 hours had quality indices of  $51 \pm 3$  and  $32 \pm 1$ , respectively; The second article (Article 2) aimed to evaluate the impact of a combined enzymatic pretreatment of laccase and endoglucanase to produce lignin-containing cellulose nanofibrils (LCNF). This pretreatment improved the quality of LCNF ( $61 \pm 3$  to  $71 \pm 2$ ) and provided a reduction in energy consumption by 42%. LCNF obtained after the enzymatic pretreatments improved the mechanical strength by 24% and exhibited good water vapor permeability ( $2.42 \text{ g}\cdot\text{mm}/\text{m}^2\cdot\text{kPa}\cdot\text{day}$ ) and grease barrier properties (kit no. 12). The rheology of LCNF exhibited non-Newtonian behavior. This study showed that the alkali treatments can promote positive influence on the change in hemicellulose content and cellulose structure treated with 5% NaOH to produce CNFs. Laccase was shown to be effective in attacking lignin, contributing to decreasing the recalcitrance of the cell wall and increasing the exposure of cellulose chains to physical contact for the action of endoglucanase.

**Keywords:** Cell wall. Energy consumption. Microfibrillated cellulose (MFC). Nanofibrillated cellulose (NFC). Nanotechnology. Recalcitrance.

## LIST OF ILLUSTRATIONS

### PART I

<b>FIGURE 1.</b> THE STRUCTURE OF WOOD, FROM MACROSCOPIC TO MOLECULAR SCALE. ....	23
<b>FIGURE 2.</b> CHEMICAL STRUCTURE OF LIGNIN. ....	25
<b>FIGURE 3.</b> MONOMERS OF THE SUGARS THAT MAKE UP THE HEMICELLULOSE OF WOOD. ....	27
<b>FIGURE 4.</b> PART OF THE CHEMICAL STRUCTURE OF A) GALACTOGLUCOMANNAN AND B) ARABINOGLUCOXYLAN. ....	28
<b>FIGURE 5.</b> CELLULOSE MOLECULAR STRUCTURE. ....	30
<b>FIGURE 6.</b> UNIT CELL MODELS OF A) CELLULOSE IB E B) CELLULOSE II. ....	31
<b>FIGURE 7.</b> A THREE-DIMENSIONAL PERSPECTIVE OF THE LIGNIN-CARBOHYDRATE COMPLEX (LCC) IN THE WOOD CELL WALL. ....	32
<b>FIGURE 8.</b> A REPRESENTATION OF THE KNOWN LINKAGES BETWEEN LIGNIN AND CARBOHYDRATES IN THE WOOD CELL WALL. ....	33
<b>FIGURE 9.</b> ILLUSTRATION OF NaOH ACTING ON THE CELLULOSIC FIBER AND REMOVING SUGARS (HEMICELLULOSE). ....	37
<b>FIGURE 10.</b> MECHANISMS OF ACTION OF ENZYMES THAT ACT ON CELLULOSE. ....	38
<b>FIGURE 11.</b> MECHANISM OF ACTION OF THE ENZYME LACCASE IN PLANT BIOMASS. ....	39

### ARTICLE I

<b>FIGURE 1.</b> A) DISPERSION STATES OF THE 0.1 WT.% CNF SUSPENSIONS AT 0, 10, 30 MIN, 1, 2, 3, 4, 5, 6, 7, 8, AND 24 H. INFLUENCE OF TIME ON CNF SUSPENSION STABILITY IN WATER. ....	69
<b>FIGURE 2.</b> TYPICAL TRANSMISSION ELECTRON MICROSCOPY (TEM) AND DIAMETER DISTRIBUTION OF CNFs AND IMAGES FROM (A AND F) UNTREATED_N; (B AND G) TOCNF; (C AND H) NA5_2_N; (D AND H) NA10_1_N; AND (E AND J) NA10_2_N. THE GREEN ARROWS INDICATE MORE INDIVIDUALIZED CNFs, WHILE PURPLE ARROWS INDICATE MORE ELECTRODENSE REGIONS AND CONSEQUENTLY LESS INDIVIDUALIZED CNFs. ....	70
<b>FIGURE 3.</b> TYPICAL X-RAY PATTERNS OF EUCALYPTUS CNF SAMPLES OBTAINED FROM FIBER PULPS BEFORE AND AFTER TEMPO AND ALKALINE TREATMENTS. CHARACTERISTIC PEAKS AND THE ASSOCIATED LATTICE PLANES ARE INDICATED FOR CELLULOSE IB (BLACK DASHED LINES) AND CELLULOSE II (RED DASHED LINES), RESPECTIVELY. AN AMORPHOUS HALO OF CELLULOSE II WITH AN FWHM OF 9 IS USED AS A REFERENCE FOR CRYSTALLINE FRACTION CALCULATION. ....	72
<b>FIGURE 4.</b> APPARENT VISCOSITY VS. SHEAR RATE FOR THE CNF SUSPENSIONS UNDER DIFFERENT CONDITIONS. ....	74
<b>FIGURE 5.</b> THE RELATIONSHIP BETWEEN APPARENT VISCOSITY AND HEMICELLULOSE CONTENTS IN THE DIFFERENT CNFs AFTER NANOFIBRILLATION. * EUC TEMPO WAS NOT CONSIDERED IN THE CORRELATION BECAUSE, UNLIKE THE OTHER FIBERS, IT WAS A CHEMICALLY MODIFIED FIBER. SCHEMATIC REPRESENTATION SHOWING HOW HEMICELLULOSE INFLUENCES THE SEPARATION OF CELLULOSE MICROFIBRILS. A) REPRESENTATION OF CELLULOSE NANOFIBRILS COMPOSED OF CRYSTALLINE AND AMORPHOUS DOMAINS, BOTH FORMED BY ORDERED AND DISORDERED REGIONS OF CELLULOSE CHAINS; B) FIBERS WITH HIGHER HEMICELLULOSE CONTENT BEING CUT DURING NANOFIBRILLATION AND BEING EASILY INDIVIDUALIZED; AND C) NANOFIBRILS FROM FIBERS WITH A LOW HEMICELLULOSE CONTENT	

## ARTICLE II

<b>FIGURE 1:</b> DISPERSION STATES OF THE 0.1 WT.% ULCNF AND EST_LCNF SUSPENSIONS AT 0, 10, 30 MIN, 1, 2, 3, 4, 5, 6, 7, 8, AND 24 H. INFLUENCE OF TIME ON LCNF SUSPENSIONS STABILITY IN WATER. ....	101
<b>FIGURE 2:</b> TYPICAL TRANSMISSION ELECTRON MICROSCOPE (TEM) IMAGES AND DIAMETER DISTRIBUTION OF CNF FROM: A) UNTREATED LIGNIN-CELLULOSE NANOFIBRILS (ULCNF), AND B) ENZYMES TREATED LIGNIN-CELLULOSE NANOFIBRILS (EST_LCNF). ....	103
<b>FIGURE 3:</b> TYPICAL X-RAY DIFFRACTION (XRD) PATTERNS OF EUCALYPTUS LCNF SAMPLES OBTAINED FROM FIBER PULPS A) BEFORE AND B) AFTER ENZYMATIC PRETREATMENTS....	104
<b>FIGURE 4:</b> RHEOLOGICAL BEHAVIOR OF LCNF SUSPENSIONS. A) APPARENT VISCOSITY VS. SHEAR RATE FOR THE LCNF SUSPENSIONS, AND B) STORAGE ( $G'$ ) AND LOSS ( $G''$ ) MODULI OF SUSPENSIONS WITH 1.0% (W/W) LCNF AS A FUNCTION OF FREQUENCY FOR: LIGNIN-CELLULOSE NANOFIBRILS OBTAINED FROM CONTROL) AND LACCASE AND CELLULOSE ENZYMES TREATED AND STRUCTURAL RECOVERY IN 3ITT EXPERIMENTS PLOTTED AS C) TRANSIENT VISCOSITY RECOVERY IN ROTATIONAL TEST, AND D) TRANSIENT VISCOSITY RECOVERY IN ROTATIONAL TEST WITH NORMALIZED TRANSIENT VISCOSITY ( $H^+/H^0$ ). ....	105
<b>FIGURE 5:</b> AVERAGE CONTACT ANGLE AND WETTABILITY VALUES (A) AND WVTR AND WPA VALUES (B) FOR UNTREATED AND ENZYMES TREATED LIGNIN-CELLULOSE NANOFIBERS. ....	109
<b>FIGURE 6.</b> DYNAMIC NANOPAPER CONTACT ANGLES FOR THE UPPER AND LOWER SIDES OF UNTREATED LIGNIN-CELLULOSE NANOFIBRILS (ULCNF) AND ENZYME-TREATED LIGNIN-CELLULOSE NANOFIBRILS (EST_LCNF). POLAR SOLVENTS (DEIONIZED WATER, GLYCEROL AND ETHYLENE GLYCOL) AND APOLAR SOLVENTS (DIODOMETHANE AND 1-BROMONAPHTALENE) WERE USED. ....	112
<b>FIGURE 7: A)</b> EVOLUTION OF ENERGY CONSUMPTION FOR EACH PASS AND <b>B)</b> TIME SPENT VS. NANOFIBRILLATION PASS FOR ULCNF AND EST_LCNF. THE BLACK ARROWS INDICATE THE POINT AT WHICH IT WAS OBSERVED THAT THE SUSPENSIONS ACQUIRED A CONSISTENT GEL APPEARANCE. ....	114

## LIST OF TABLES

### ARTICLE I

- TABLE 1:** AVERAGE AND STANDARD DEVIATION OF THE CELLULOSE AND HEMICELLULOSE CONTENTS OF EUCALYPTUS FIBERS (F) BEFORE AND AFTER TEMPO AND ALKALINE TREATMENTS. \* DIFFERENT LETTERS IN THE SAME COLUMN INDICATE SIGNIFICANT ( $p \leq 0.05$ ) DIFFERENCES BETWEEN THE SAMPLES FOR TUKEY'S TEST. ND = NOT DETECTED..... 67
- TABLE 2:** AVERAGE AND STANDARD DEVIATION VALUES OF THE CRYSTALLINE FRACTION (CF) AND CRYSTALLITE SIZE (CS) FOR EUCALYPTUS CNFs PRODUCED UNDER DIFFERENT CONDITIONS. DIFFERENT LETTERS IN THE SAME COLUMN INDICATE SIGNIFICANT ( $p \leq 0.05$ ) DIFFERENCES BETWEEN THE SAMPLES FOR TUKEY'S TEST. .... 73
- TABLE 3:** PARAMETERS OF THE NEWTON MODEL FOR EUC10% 2H AND POWER LAW AND HERSCHEL-BULKLEY MODELS FOR UNTREATED\_N, TOCNF\_N, NA5\_2\_N, AND N10\_1\_N. .... 75
- TABLE 4:** AVERAGE AND STANDARD DEVIATION VALUES OF TENSILE STRENGTH, YOUNG'S MODULUS, AND ELONGATION AT BREAK OF THE NANOSTRUCTURED FILMS FROM CNFs UNDER DIFFERENT CONDITIONS. \*IT WAS IMPOSSIBLE TO PERFORM THE TEST ON EUC10% 2H BECAUSE IT WAS NOT POSSIBLE TO FORM FILMS FOR THIS TREATMENT. DIFFERENT LETTERS IN THE SAME COLUMN INDICATE SIGNIFICANT ( $p \leq 0.05$ ) DIFFERENCES BETWEEN THE SAMPLES FOR TUKEY'S TEST. .... 79
- TABLE 5:** SIMPLIFIED QUALITY INDICES OF CNFs PRODUCED BY DIFFERENT TREATMENTS. DIFFERENT LETTERS IN THE SAME COLUMN INDICATE SIGNIFICANT ( $p \leq 0.05$ ) DIFFERENCES BETWEEN THE SAMPLES FOR TUKEY'S TEST. .... 81

### ARTICLE II

- TABLE 1:** EXPERIMENTAL DESIGN AND CODING OF SAMPLES. .... 91
- TABLE 2:** EFFECT OF LACCASE AND CELLULASE MEDITATED ENZYMATIC HYDROLYSIS TREATMENTS OF UNBLEACHED EUCALYPTUS KRAFT PULP ON FIBERS' MORPHOLOGICAL PROPERTIES. \*DIFFERENT LETTERS IN THE SAME COLUMN INDICATE SIGNIFICANT ( $p \leq 0.05$ ) DIFFERENCES BETWEEN THE SAMPLES FOR THE TUKEY'S TEST..... 98
- TABLE 3:** AVERAGE AND STANDARD DEVIATION OF THE CHEMICAL COMPONENTS CONTENT OF EUCALYPTUS FIBERS BEFORE AND AFTER ENZYMATIC TREATMENTS. \*DIFFERENT LETTERS IN THE SAME COLUMN INDICATE SIGNIFICANT ( $p \leq 0.05$ ) DIFFERENCES BETWEEN THE SAMPLES FOR THE TUKEY'S TEST. ND = NOT DETECTED..... 100

<b>TABLE 4:</b> PARAMETERS OF THE HERSCHEL-BULKLEY MODEL AND INITIAL APPARENT VISCOSITY AND AT $100 \text{ s}^{-1}$ (H100) FOR ULCNF AND EsT_LCNF.....	106
<b>TABLE 5:</b> VALUES OF STORAGE MODULUS ( $G'$ ), GEL STIFFNESS ( $G'/G''$ ) AND LOSS TANGENT VALUE ( $\text{TAN } \Delta(G''/G')$ ) OBTAINED FROM THE MECHANICAL SPECTRA AT $25^\circ\text{C}$ AND $0.1 \text{ RAD S}^{-1}$ FOR LCNF SUSPENSIONS AT CONCENTRATIONS OF 1 WT%. .....	107
<b>TABLE 6:</b> GREASE RESISTANCE (OIL KIT NUMBER) AND SURFACE FREE ENERGY (SFE) FOR THE NANOPAPERS OF ULCNF AND EsT_LCNF. *DIFFERENT LETTERS IN THE SAME ROW INDICATE SIGNIFICANT ( $p \leq 0.05$ ) DIFFERENCES BETWEEN THE SAMPLES FOR THE TUKEY'S TEST. ....	111
<b>TABLE 7:</b> QUALITY INDEXES OF LIGNIN-CELLULOSE NANOFIBRILS PRODUCED BY DIFFERENT CONDITIONS. DIFFERENT LETTERS IN THE SAME COLUMN INDICATE SIGNIFICANT ( $p \leq 0.05$ ) DIFFERENCES BETWEEN THE SAMPLES FOR THE TUKEY'S TEST.....	115

## SUMMARY

<b>THESIS PRESENTATION</b> .....	16
<b>CHAPTER I: INTRODUCTION, BACKGROUND, MOTIVATION, OBJECTIVES, THEORETICAL REFERENCE, AND CONCLUDING REMARKS</b> .....	17
<b>1. INTRODUCTION</b> .....	17
<b>2. BACKGROUND</b> .....	19
<b>3. MOTIVATION</b> .....	20
<b>4. OBJECTIVES</b> .....	21
<b>4.1 General objective</b> .....	21
<b>4.2 Specific objectives</b> .....	21
<b>5. THEORETICAL REFERENCE</b> .....	22
<b>5.1 Plant cell wall ultrastructure</b> .....	22
<b>5.2 The recalcitrance of lignocellulosics</b> .....	23
<b>5.2.1 Lignin</b> .....	24
<b>5.2.2 Hemicellulose</b> .....	26
<b>5.2.3 Cellulose</b> .....	29
<b>5.3 Lignin-carbohydrate complex</b> .....	31
<b>5.4 Cellulose nanofibrils</b> .....	34
<b>5.5 Pre-treatment of lignocellulosic biomass</b> .....	35
<b>5.5.1 Alkaline pre-treatments</b> .....	36
<b>5.5.2 Enzymatic pre-treatments</b> .....	37
<b>6. CHAPTER I: CONCLUDING REMARKS</b> .....	40
<b>7. BIBLIOGRAPHIC REFERENCES</b> .....	41
<b>CHAPTER II: ARTICLE 1</b> .....	60
<b>1. Introduction</b> .....	60
<b>2. Experimental</b> .....	61
<b>2.1 Materials</b> .....	61
<b>2.2 Alkaline treatment of cellulose kraft pulp</b> .....	62
<b>2.3 TEMPO-mediated oxidation treatment of cellulose kraft pulp</b> .....	62
<b>2.4 Monosaccharide's quantification</b> .....	62
<b>2.5 Cellulose nanofibers (CNF) production</b> .....	63
<b>2.6 Micro size area (<math>\mu\text{m}^2</math>)</b> .....	63
<b>2.7 Transmission Electron Microscopy (TEM)</b> .....	63
<b>2.8 X-ray diffraction (XRD)</b> .....	64
<b>2.9 Rheological behavior</b> .....	65

2.10	CNF films casting .....	65
2.11	Transparency at 550 nm (%) .....	66
2.12	Mechanical properties of CNF films.....	66
2.13	Simplified quality index (*Q.I.).....	66
2.14	Statistical analysis .....	67
3.	Results and discussion.....	67
3.1	Hemicellulose quantification .....	67
3.2	Turbidity, visual inspection, and stability of the CNF suspensions.....	68
3.3	CNF morphology .....	69
3.5	X-ray diffraction (XRD) .....	71
3.6	Rheological behavior.....	74
3.7	Mechanical performance of the CNF films.....	79
3.8	Effect of modifications on quality of cellulose nanofibers .....	80
4	Conclusions .....	81
	Supporting information .....	82
	Acknowledgments .....	82
	Conflict of interest.....	82
5	References .....	82
	CHAPTER III: ARTICLE 2 .....	87
1.	Introduction .....	88
2.	Experimental section.....	90
2.1	Materials .....	90
2.2	Characterization of the pulp fibers.....	90
2.3	Enzymatic pretreatments .....	91
	2.3.1 Laccase mediated enzymatic hydrolysis.....	91
	2.3.2 Endoglucanase mediated enzymatic hydrolysis.....	91
2.4	LCNF production by mechanical nanofibrillation.....	92
2.5	Turbidity, visual inspection, stability, and Zeta potential of LCNF suspensions.....	92
2.6	Light Microscopy (LM) .....	92
2.7	Transmission Electron Microscopy (TEM) .....	93
2.8	Nano-structured papers preparation .....	93
2.9	Porosity (%).....	93
2.10	X-Ray diffraction (XRD) .....	94
2.11	Rheological parameters .....	94
	2.11.1 Viscoelastic properties .....	95
	2.11.2 3 Interval thixotropy test recovery measurements (3ITT).....	95

2.12 Mechanical properties.....	95
2.13 Contact angle, surface wettability and surface free energy of nanopapers .....	96
2.14 Barrier properties .....	96
2.15 Simplified quality index (Q.I*).....	96
2.16 Statical analysis .....	97
<b>3. Results and discussion.....</b>	<b>97</b>
3.1 Effect of enzymatic treatments on fiber properties.....	97
3.2 Turbidity, visual inspection, stability, and Zeta potential of LCNF suspensions.....	101
3.3 Morphological properties of LCNF .....	103
3.4 Crystallographic characterization .....	104
3.5 Rheological behavior.....	105
3.6 Contact angle, wettability, free surface energy and barrier properties .....	109
3.7 Energy consumption .....	113
3.8 Quality of lignin-cellulose nanofibrils .....	115
<b>4. Conclusions .....</b>	<b>116</b>
<b>Acknowledgments .....</b>	<b>117</b>
<b>Conflict of interest.....</b>	<b>117</b>
<b>References .....</b>	<b>118</b>
<b>CHAPTER IV: CONCLUSIONS OF THE THESIS.....</b>	<b>123</b>
<b>CHAPTER V: SUGGESTIONS FOR FUTURE WORKS .....</b>	<b>125</b>
<b>CHAPTER VI: APPENDICES.....</b>	<b>126</b>
<b>APPENDIX 1: TEMPO - mediated oxidation of cellulosic fibers.....</b>	<b>126</b>
<b>APPENDIX 2: Preparation of phosphate buffer solution with pH = 4.5 .....</b>	<b>129</b>
<b>APPENDIX 3: Preparation of phosphate buffer solution with pH pH 5 .....</b>	<b>132</b>
<b>APPENDIX 4: Enzymatic hydrolysis mediated by the Laccase enzyme (60 LAMU/g).....</b>	<b>135</b>
<b>APPENDIX 5: Enzymatic hydrolysis mediated by the Cellulase enzyme (300 ECU/g) .....</b>	<b>137</b>



## THESIS PRESENTATION

This thesis is presented in the form of chapters. The first part includes a chapter I, which covers five sections: (1) Introduction; (2) Motivation; (3) Objectives; (4) Theoretical framework and (5) Considerations. This first chapter aims to introduce the reader to the object of study of this thesis, providing tools that help understand the topics covered. Chapter II of this thesis addresses the first paper (Article 1) developed in this work entitled “Influence of hemicellulose content and cellulose crystal change on cellulose nanofibers properties”. Chapter III brings the second article (Article 2) entitled " Eco-friendly laccase and cellulase enzymes pretreatment for optimized production of high content lignin-cellulose nanofibrils" developed during the post-graduate doctoral sandwich period at Institut Polytechnique de Grenoble - France. Finally, the thesis has the chapter IV, "Conclusions of the Thesis," followed by chapter V with suggestions for future work and chapter VI of Appendices.

## **CHAPTER I: INTRODUCTION, BACKGROUND, MOTIVATION, OBJECTIVES, THEORETICAL REFERENCE, AND CONCLUDING REMARKS**

### **1. INTRODUCTION**

With the concern that the impacts of climate change may cause, and that has already started to be felt around the world, mainly due to human activities that use fossil fuels as raw material for the most diverse purposes, the understanding that it is even more necessary to find alternatives for the consumption of this raw material is growing.

The obtaining of different conventional synthetic polymers causes impacts from their production to their inadequate disposal in the environment, where they take hundreds of years to decompose and have created serious problems, especially for marine life, since most of these materials end up in the oceans.

One possibility that has been pointed out to reduce the impact of these materials on the environment is the substitution of petroleum-based polymers by natural polymers, also known as biopolymers.

Lignocellulosic biomass may be a promising alternative as a source of these biopolymers to replace fossil fuels. In this sense, cellulose stands out before other polymers, whether natural or synthetic. Besides being the most abundant biopolymer on Earth, it is renewable, biodegradable, and comes mainly from managed forests, and can also be obtained from agroindustrial waste, possessing properties that have been of great importance to humankind, having served the population as the primary source of raw material for paper, clothing, and construction materials among many others.

Still referring to cellulose, obtaining and using this biopolymer in nanoscale, in which at least one of its dimensions is equal to or smaller than 100 nm, has aroused the interest of the entire scientific and technological community due to the improved properties inherent to this material in nanoscale. However, the large energy requirement for its production is the major bottleneck that persists as a barrier in the production of nanocellulose on large scales.

Several studies have been conducted to offer alternatives through pretreatments of plant fibers to reduce the energy consumption required for these processes. These pretreatments can be performed mechanically, however chemical, enzymatic pre-treatments or their combination can also lead to significant improvements in terms of energy consumption. However, although there is a range of studies on the effect of different fiber pre-treatments as facilitators to obtain cellulose nanofibrils, information on how the intrinsic characteristics of different plant fibers

will influence the effectiveness of these pre-treatments, how these can affect the delamination of the cell wall is still limited.

This work aimed to evaluate the influence of the chemical and morphological properties of different plant fibers in the recalcitrance and efficiency of chemical and enzymatic pretreatments and their impact on the process of obtaining cellulose nanofibrils. It is expected to generate fundamental knowledge of how these pretreatments (Alkaline pretreatment using Sodium Hydroxide and enzymatic pretreatments using Laccase and Endoglucanase enzymes) influence the intrinsic properties of distinct types of fibers, and the impact on fiber recalcitrance, in addition to developing more efficient pretreatments for produce cellulose and lignocellulose nanofibrils according to the characteristic of the material.

## 2. BACKGROUND

Studies related to the production, characterization, and application of cellulose fibers and nanofibrils have been gaining prominence in different segments. The development of nanocomposites with the incorporation of cellulose nanofibrils assumes a prominent role in the demand for materials from renewable sources and biodegradable nature. Since the beginning of the century, there has been a greater effort to develop commercially viable and adequate processes to deconstruct vegetable cellulose fibers into their individualized structural components, called cellulose nanofibrils. Among the types of nanocellulose, the cellulose nanofibrils (CNF) or microfibrillated cellulose (MFC), obtained by mechanical processes, present themselves as a type of nanocellulose with exciting potential for industrial application, whose main advantages are the ease of operation of the equipment, the possibility of using fewer chemical reagents, and the relatively low cost for obtaining.

Cellulose nanofibrils are more attractive raw materials compared to fibers (on a macro scale) due to their large surface area and high mechanical ability to function as reinforcement in polymeric or cementitious composites or their barrier property that can be widely used in the development of biodegradable food packaging. Their nanoscale dimensions and their ability to form a tightly interwoven nanoporous network have encouraged the emergence of new high-value applications. Knowledge of the cellulosic feedstock is essential for industrial applications, as well as for the processing and quality of the final product and its subsequent application on an industrial scale. The geometric properties (shape, length, and diameter) of cellulosic nanofibrils are highly dependent on the extraction process and the initial condition of the cellulosic feedstock.

### **3. MOTIVATION**

Biomaterials of plant origin have been identified as future substitutes for those materials of natural origin or not, in which their exploitation activity and manufacturing process cause considerable damage to the environment in the short, medium, or long term. Within these biomaterials, natural and biodegradable polymers, especially cellulose, have been gaining more and more interest in research and development activities in academia and industry. In this context, cellulose nanofibrils, which is derived from plant fibers, has been highlighted as a promising and multifunctional material. Therefore, there is a huge diversity of research in the literature that studies the application of this material in different situations, such as in the food, pharmaceutical, and biomedical areas, civil construction, composite materials, etc. However, it is not simple to extract these nanostructures from lignocellulosic biomass fibers due to their natural deconstruction resistance, known as recalcitrance. This hinders and increases the cost of large-scale production, making its application still limited. Therefore, understanding how this recalcitrance is related to biomass constituents becomes essential for the maximum use of these resources with the greatest operational efficiency, developing new pre-treatments or optimizing them.

## **4. OBJECTIVES**

### **4.1 General objective**

The primary purpose of this research is to investigate the influence of recalcitrance of different Eucalyptus commercial pulps on the effectiveness of pretreatments and its impact on the process of obtaining cellulose nanofibrils.

### **4.2 Specific objectives**

As specific objectives, the present research aimed to:

1. To investigate the influence of pre-treatments on different commercial pulps (associating the effects generated with their morphology and chemical composition);
2. To investigate the influence of the modifications obtained after pre-treatments on the efficiency in the process of obtaining nanofibrils (mechanical nanofibrillation);
3. To suggest a quality index for the cellulose nanofibrils produced under the different conditions;
4. Evaluate the energy efficiency of pretreatments in the mechanical nanofibrillation process.

## 5. THEORETICAL REFERENCE

### 5.1 Plant cell wall ultrastructure

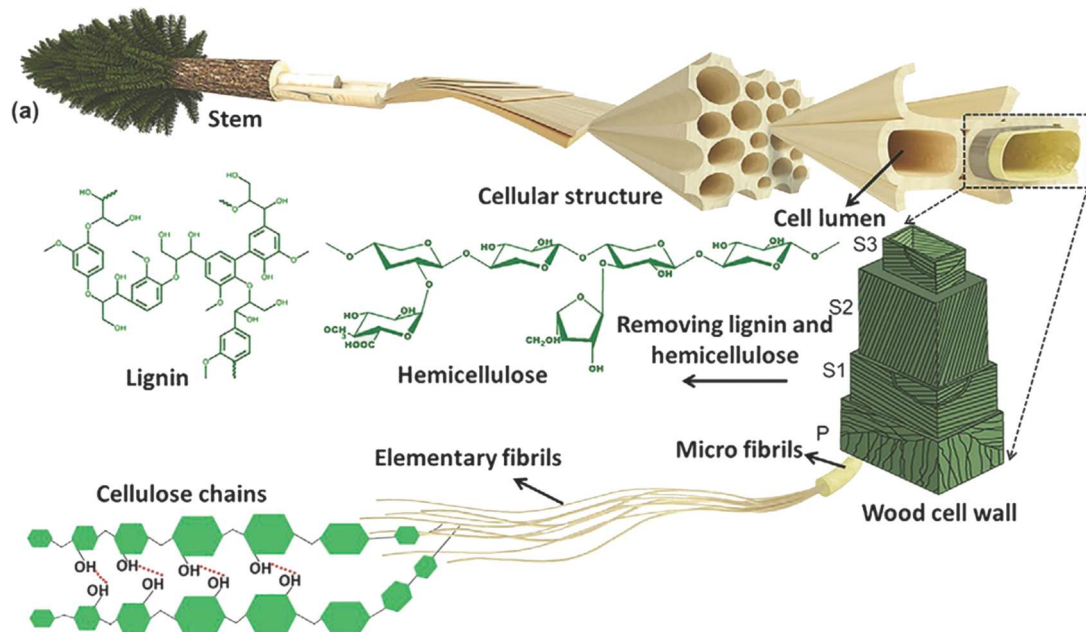
Wood cells are produced in the vascular cambium from meristematic cells, divided into fusiform and radial initials. Since the cells derived from fusiform initials standing on the stem occupy an important part of the xylem, woods show remarkable anisotropy. The main functions of the xylem tissue are the conduction of water from the roots to the aerial parts, provide mechanical support, and physiological function, such as starch storage. Although these functions are common in both softwoods and hardwoods, the xylem of the hardwoods are more evolved in comparison to softwoods, being adapted for each function (HON; SHIRAISHI, 2001).

Conifers have more primitive anatomy than hardwoods, presenting as cells the axial tracheids (that occupy up to 95% of the wood volume and carry out conduction and support functions for the wood, presenting an average length of 2 to 5 mm), radial and axial parenchyma and radial tracheids. Hardwoods, on the other hand, present specialized cells for conduction and sustentation. The vessel elements are the main elements of differentiation between the coniferous and hardwoods. In the latter, they are responsible for conducting liquids and gases in the wood. The fibers play the sole role of mechanical support in hardwoods, being smaller than the tracheids, with an average length of 0.5 to 2.5 mm (PHILIPP; D'ALMEIDA, 1988; BURGER; RICHTER, 1991).

According to Fengel e Wegener (1989), the concentric arrangement of the cell wall layers is caused by differences in chemical composition and by different orientations of the structural elements. Therefore, in this order of magnitude, the components must be subdivided into structural components, i.e., cellulose, and substructural components, i.e., hemicellulose and lignin. When the hemicellulose and lignin are removed, the texture of the cellulosic elements, called fibrils, is visible.

The wood fiber wall consists of several layers that show differences in their structure and chemical composition (Figure 1). These layers are the middle lamella, primary wall, and secondary wall (JOFFRE et al. 2016).

**Figure 1.** The structure of wood, from macroscopic to molecular scale.



Source: Liu et al. (2021).

The middle lamella is the intercellular region, with the function of holding adjacent cells together, not being part of the cell wall. Initially, it is composed mainly of peptidic substances, and subsequently, the middle lamella become highly lignified. The primary wall is elastic and plastic during the early stages of cell growth and extension. It is composed of an unstructured network of cellulose microfibrils randomly deposited, except near the corners of the cell, where they are arranged axially along the length of the cell. The microfibrils are embedded in a matrix of hemicellulose and pectic compounds. The primary wall becomes lignified only after deposition of the secondary wall. The thickness of the primary wall is thin, ranging between 0.1 and 0.2  $\mu\text{m}$ , making it difficult to distinguish or isolate it from the middle lamella (WALKER et al. 1993).

The secondary wall of wood cells is composed of three layers named S1, S2, and S3. These layers are connected by the composite middle lamella (CML), composed of the primary wall and the middle lamella. The S2 layer is the central and thickest layer and is the essential structural component of the cell wall, providing mechanical support for the tissue (RAFSANJANI et al. 2014).

## 5.2 The recalcitrance of lignocellulosics

Lignocellulosic biomass is composed of cellulose, hemicellulose, and lignin, plus other minor components that create a complex matrix structure that presents natural recalcitrance.



This is directly linked to its structure, resulting from these main constituent molecules and their interactions. Cellulose, hemicellulose, and lignin are the polymers that form the plant cell wall, a very compact, stable, and resistant structure (LORENCI WOICIECHOWSKI et al., 2020).

The properties of its monomers and the interaction between these polymers make this structure present biological, chemical and mechanical resistance that hinders the separation and recovery of its three main components, which characterizes the recalcitrance of plant biomass (LORENCI WOICIECHOWSKI et al., 2020).

Due to this characteristic, for more effective utilization of this biomass of vegetal origin, it is essential to perform pre-treatments on this material in order to make the cellulose more accessible by modifying its physical and/or chemical structure, facilitating the conversion of plant fibers into various by-products (KUMAR; SHARMA, 2017).

Recalcitrance can be divided into structural factors such as the degree of polymerization of cellulose, degree of crystallinity, pore size and volume, the specific surface area of cellulose, and chemical factors, which include the characteristics of each polymer chemically composes the biomass. (PELLEGRINI; SEPULCHRO; POLIKARPOV, 2020; ZOGHLAMI; PAËS, 2019).

The extensive knowledge of the three main chemical constituents that form the plant cell wall is essential and helps elucidate the phenomena that occur and its behavior in response to external phenomena to which the plant fibers may be subjected. The following subtopics approach these constituents to understand the work better and better comprehend the recalcitrance phenomenon. Recalcitrance can be defined as the ability of the fiber to resist the attack of different agents, which can be physical, mechanical, chemical, and biological. Keeping its initial characteristics intact.

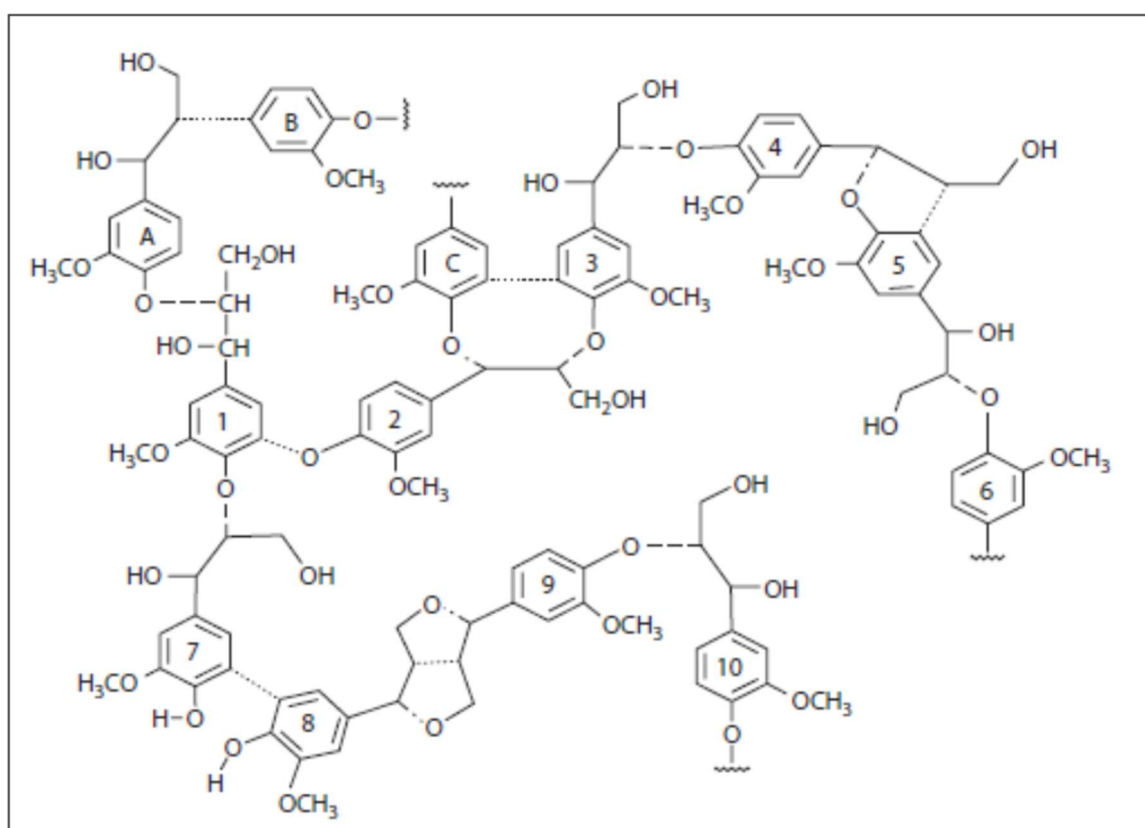
### **5.2.1 Lignin**

Lignin is the third major component that forms the plant cell wall and is the most significant non-carbohydrate component (YOO et al., 2020). In mature wood, its amount varies between 18 and 38% of the tissue composition (BROWNING, 1963). It is a three-dimensional aromatic and amorphous polymer of a rigid and complex structure formed from the polymerization of coumaryl alcohol, coniferyl alcohol, and sinapyl alcohol units (FENGEL; WEGENER, 1989).

It is the substance that gives rigidity to the plant cell wall and acts as a cementing agent holding the cells together (PHILIPP; D'ALMEIDA, 1988). It can still be considered as a three-dimensional amorphous polyphenol type polymer of siringyl (S), guaiacyl (G), and p-hydroxyphenyl (H) units and some non-canonical subunits in monomers that are not repeated

(Figure 2) and are still associated with hemicellulose not only by physical bonding but also by covalent bonds. It is widely accepted that lignin structure differs considerably due to different conditions of extraction, isolation, and different types of plants (GUO et al. 2017; ROWELL, 2012). According to the units of percussive alcohols in which they are formed, lignin can be divided into three major classes. First, the lignin of coniferous wood consists of coniferyl alcohol units. Second, hardwoods (dicotyledonous angiosperms) are composed of lignin formed by coniferyl and sinapyl alcohol units. Finally, the lignin of grasses and annual monocot angiosperms comprises coniferyl, sinapyl, and p-coumaryl units. (SUHAS; CARROTT; RIBEIRO CARROTT, 2007).

**Figure 2.** Example of structure of lignin.



Source: Heitner et al. (2010).

Lignin also presents abrasiveness and low density. Youssefian and Rahbar (2015) found, studying bamboo fibrils, that the density of lignin of this material being equal to 1.33 g/cm<sup>3</sup>. These characteristics make lignin interesting for use as a filler to replace inorganic fillers. With specific polymers, in suitable formulations, lignin can form partially or even completely biodegradable composites (STEWART, 2008). Many studies have been developed in which lignin is used as a substitute for phenol to formulate new adhesives for wood (FERDOSIAN et

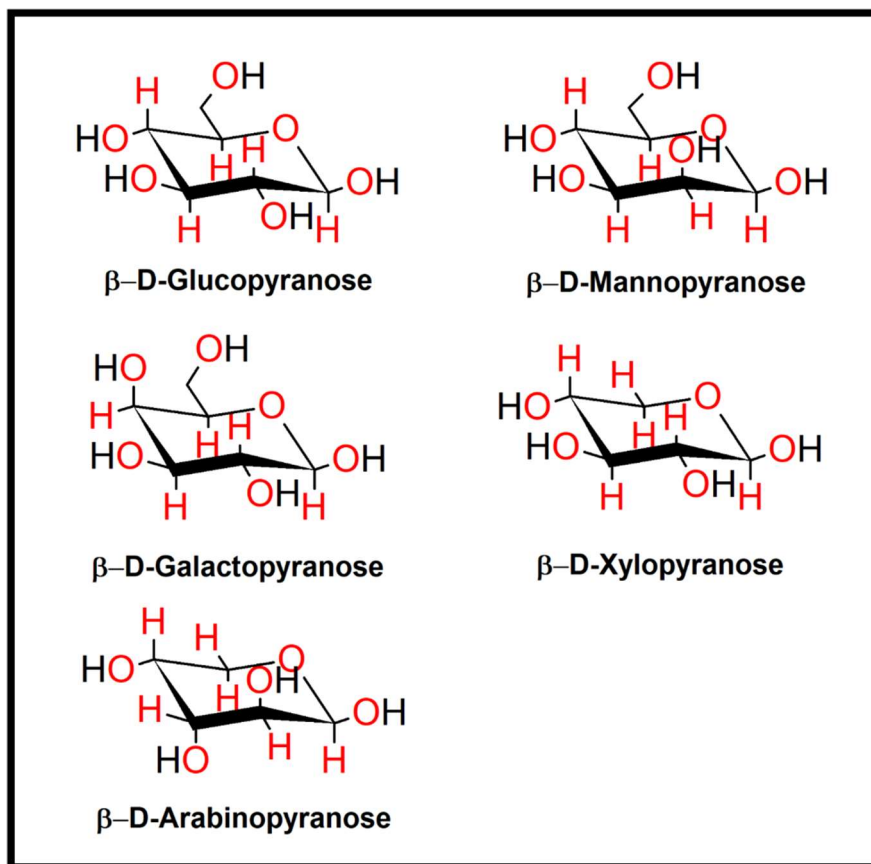
al. 2017; WANG; YU; DI, 2018), in biomedicine (FIGUEIREDO et al. 2018), composites, and nanocomposites (MA et al. 2017; YE et al. 2017), among other purposes

Literature has described that lignin is one of the most significant factors in the recalcitrance of lignocellulosic biomass. (LI; PU; RAGAUSKAS, 2016) Due to its structure, lignin can inhibit the action of enzymes on cellulose through physical barriers, such as hydrophobicity, surface charges, electrostatic interactions, and hydrogen bonding interactions that limit the accessibility of enzymes by decreasing enzyme yield (HUANG et al., 2016; LI et al., 2020).

### **5.2.2 Hemicellulose**

Hemicellulose are polysaccharides in plant cell walls that have  $\beta$ -(1  $\rightarrow$  4) linkages and vertical structures with an equatorial configuration. Hemicellulose are formed by different monomers of sugars (Figure 3) and includes xyloses, glucose, mannoses, arabinoses, galactoses, with smaller amounts of other sugars. These types of hemicellulose are present in the cell walls of all land plants except the  $\beta$ - (1  $\rightarrow$  3,1  $\rightarrow$  4)-glucans, which are restricted to Poales and a few other groups. The detailed structure of hemicellulose and their abundance varies widely among different species and cell types (ROWELL, 2012; SCHELLER; ULVSKOV, 2010).

**Figure 3.** Monomers of the sugars that make up the hemicellulose of wood.

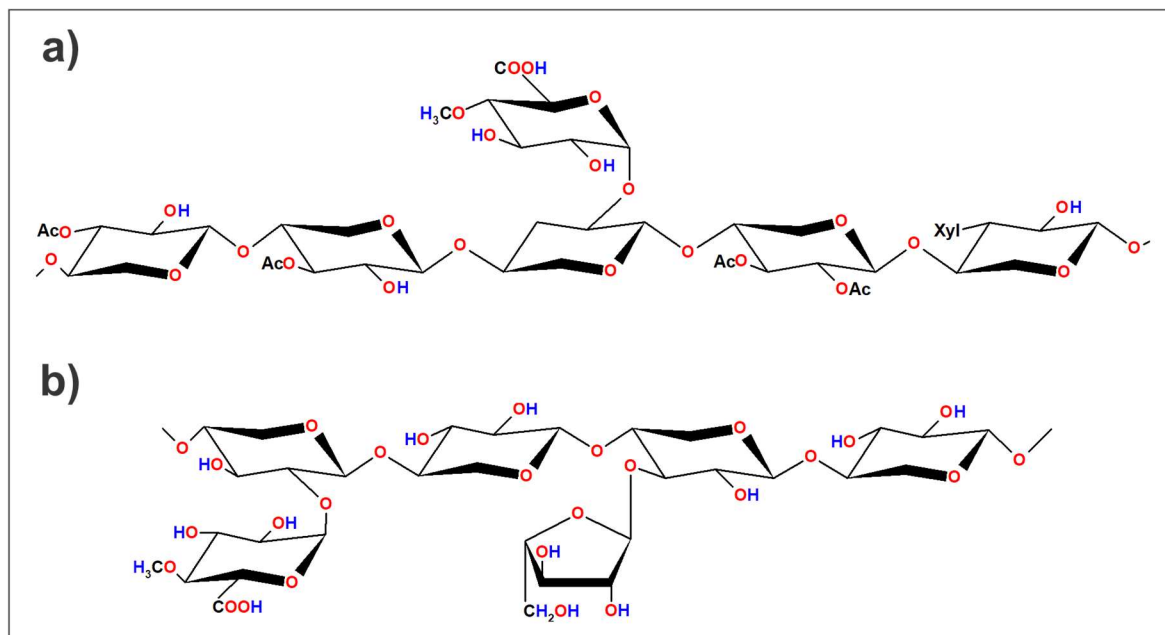


Source: From the author (2021).

They are still closely associated with cellulose and lignin in all higher plants, where they represent 20 - 30% of the plant dry mass and have shown to be a promising resource in the production of films, barriers, and hydrogels (FENGEL; WEGENER, 1989; KISHANI et al., 2018). Furthermore, although less abundant than cellulose, these polysaccharides cooperate significantly for the mechanical strength of delignified wood fibers and papers made from these fibers (DAHLMAN; JACOBS; SJÖBERG, 2003). Hemicellulose are the second most abundant class of hydrophilic polysaccharides in nature (PENG et al., 2008).

Hemicellulose has much lower molar masses when compared to cellulose, ranging from 100-200 units (RODRIGUES MOTA et al., 2018) and contains a considerable degree of branching between its chains (Figure 4), possessing a highly amorphous nature, unlike cellulose, and is more susceptible to chemical hydrolysis under milder conditions (ROWELL, 2012). The types of hemicellulose present in each material also vary according to the origin of the material. Taking as example *Pinus* (coniferous) and *Eucalyptus* (hardwood) pulps, we may observe that conifers present glucomannans and xylans, while hardwoods present only xylans in their chemical composition (LAHTINEN et al. 2014).

**Figure 4.** Part of the chemical structure of a) O-Acetyl-4-O-methylglycuronoxylan from hardwoods and b) Arabin-4-O-methylglycuronoxylan from softwoods.



Source: From the author (2021).

A large proportion of hydroxyl groups are bound in intra- and intermolecular hydrogen bonds, and some of these bonds naturally bind water to cellulose molecules. This hydrophilic character hinders the development of hemicellulose-based materials. Therefore, chemical modifications have been suggested to produce water-resistant materials (PENG, 2008).

Several studies state that hemicellulose, like lignin, acts as a physical barrier limiting access to enzymes. It has been reported that removing hemicellulose by dilute acid or steam explosion pretreatment could improve the accessibility of enzymes to cellulose by increasing the conversion of cellulose to sugars (KRUYENISKI et al., 2019; SANTOS et al., 2018). However, as a pretreatment to obtain cellulose nanofibrils, hemicelluloses may not be considered a considerable barrier since it is not the goal to convert cellulose to minor sugars.

Regarding the role of hemicelluloses in the process of obtaining cellulose nanofibrils, there are studies in the literature that point to the presence of these polysaccharides as facilitators in the process of nanofibrillation, where the hemicelluloses act by inhibiting fiber coalescence, making the delamination of the cell wall easier (DIAS; MENDONÇA; DAMÁSIO, 2019; PARK et al., 2017).

#### 5.2.2.1 Xylans

Xylans are a diverse group of polysaccharides with the typical structure of  $\beta$ -linked xylose residues (1  $\rightarrow$  4), the most abundant hemicellulose found in nature (SCHELLER; ULVSKOV, 2010).

In hardwood, the xylan chains are bound, at irregular intervals, with 4-O-methyl glucuronic acid groups with an  $\alpha$ - (1  $\rightarrow$  2)-glycosidic bonds on the xylose units. As a result, many of the OH groups on C2 and C3 of the xylose units are replaced by O-acetyl groups. At the same time, coniferous wood xylans differ from hardwood xylans by the lack of acetyl groups and the presence of arabinofuranose units linked by  $\alpha$ - (1  $\rightarrow$  3)-glycosidic bonds to the xylan skeleton. Thus, coniferous wood xylans are arabinan-4-O methylglucuronoxylans (FENGEL; WEGENER, 1989).

#### 5.2.2.2 Mannans

Mannans are polysaccharides containing a main linear structure that may consist entirely of mannose, as in mannans and galactomannans, or with mannose and glucose in non-repetitive pattern glucomannans and galactoglucomannans that link to each other via  $\beta$  - (1  $\rightarrow$  4) linkages (SCHELLER; ULVSKOV, 2010; PHILIPP; D'ALMEIDA, 1988).

For hardwood species, glucomannans form lightly ramified chains, and the ratio between mannose and glucose monomers is between 1.5 - 2.0: 1 while for coniferous species, acetyl, and galactose groups link to the glucomannan structure, and the ratio between mannose and glucose monomers is 3:1 (PHILIPP; D'ALMEIDA, 1988).

#### 5.2.2.3 Galactans

They are highly ramified, water-soluble polysaccharides, having a linear structure containing galactose units linked together by  $\beta$  - (1  $\rightarrow$  3) linkages and side chains of galactose monomers, galactose and arabinose monomers, arabinose monomers, and only glucuronic acid units joined by  $\beta$  - (1  $\rightarrow$  6) linkages. In hardwoods, galactans still have raminose units (PHILIPP; D'ALMEIDA, 1988).

### 5.2.3 Cellulose

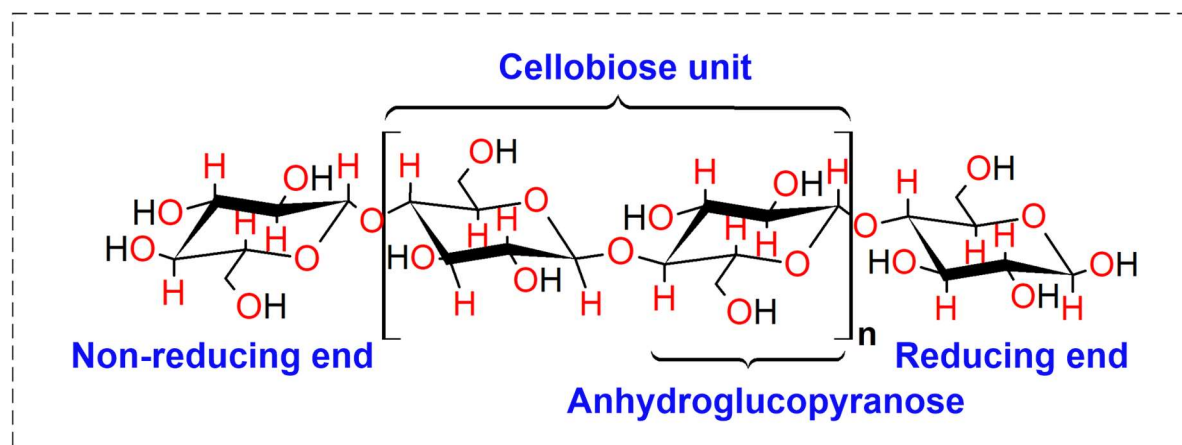
Cellulose is the most abundant organic compound found in nature that can be obtained from various sources with an annual global production estimated in tens of billions of tons, being present in the cell wall of plant cells and its main constituent, representing about 50% of its chemical composition (HABIBI et al., 2010).

According to Gellersted e Henriksson (2009), its function is different in various kinds of organisms. In plants, oomycetes, and probably in some bacteria, cellulose is found in the cell wall. In tunicates, cellulose forms a tunic that envelops the entire animal, and in *Acetobacter* bacteria, cellulose is produced in extracellular fibrils forming sheets on which the bacteria float.

Cellulose is formed from anhydroglucopyranose, which is a natural monomer consisting of repeating  $\beta$ - (1 $\rightarrow$ 4)- D-glucopyranose units (Figure 5), where this repeating unit is called

cellobiose, forming a long linear chain polymer with a high molecular weight ((MORÁN et al., 2008). The size of the cellulose chains, measured by the degree of polymerization, varies according to their source. For example, on the wood, they are reported to vary in size from 300 - 1700 units; in native wood pulp, the chain size is approximately 10,000 units (BLANCO et al., 2018).

**Figure 5.** Cellulose molecular structure.



Source: From the author (2021).

The linear cellulose molecules are deposited in multiple overlapping layers, with the axial position of the hydroxyl groups stabilizing the structure through intra- and inter-molecular hydrogen bonds, creating microfibrils with a hydrophobic interior and hydrophilic exterior, which together form macrofibrils (LORENCI WOICIECHOWSKI et al., 2020).

Cellulose occurs naturally in wood, cotton, bamboo, and other plant materials and can also be found in algae, tunicates, and some bacteria (HENRIKSSON et al., 2007; IWAMOTO; NAKAGAITO; YANO, 2007; KLEMM et al., 2006)

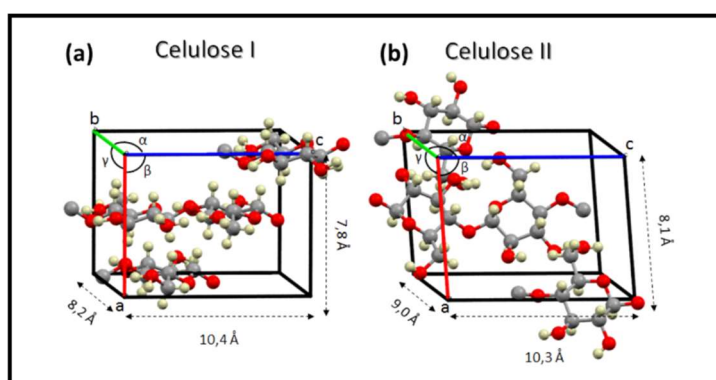
In nature, cellulose chains are arranged in an ordered manner to form compact cellulose nanocrystals, also known as cellulose nanowhiskers, which are stabilized through inter- and intramolecular hydrogen bonds located between the hydroxyls of hydroxyls carbons 3 and 6 (ALEMDAR; SAIN, 2008). These bonds make the nanocrystals completely insoluble in water, and most organic solvents, leading to a material with mechanical strength limited only by the forces of the adjacent atoms and has amorphous regions where the chains are arranged irregularly (KAMEL, 2007; MARCHESSAULT; SUNDARARAJAN, 1983).

According to Burger e Richter (1991), during cell division in plant tissue, the middle lamella is the first separation membrane to appear between the new pair of cells formed, and its function is to promote the union of these cells. Next, there is the deposition of cellulose microfibrils inside the cell irregularly, forming the primary wall. The primary wall accompanies

the cell until its differentiation, and then there is the deposition of microfibrils in the primary membrane that follow a specific orientation in three distinct layers, forming the secondary wall. These layers are known as S1, S2, and S3.

There are several types of crystalline cellulose structures (I, II, III, and IV), being the native cellulose or cellulose I (Figure 6), the crystalline form most found in nature and presenting the best mechanical properties. The most important and studied are I and II (JIN et al., 2016; MORÁN et al., 2008; OSULLIVAN, 1997).

**Figure 6.** Unit cell models of a) cellulose I e b) cellulose II.



Source: From the author (2021).

Cellulose II has different unit cells than cellulose I. Cellulose I has dimensions of 7.8 Å in a, 8.2 Å in b, and 10.4 Å in c with angle  $\gamma$  equal to 96.5°, while cellulose II has dimensions of 8.1 Å in a, 9.0 Å in b, 10.3 Å in c, and angle  $\gamma$  equal to 117.1° (MACRAE et al., 2008).

Cellulose II can be obtained through a process known as mercerization that uses the alkaline solution, usually sodium hydroxide (NaOH), in concentrations that can vary from 12.0%, 17.5%, and 20.0% (JIN et al., 2016; SHARMA et al., 2015; WANG et al., 2014). Or through the dissolution of cellulose and its subsequent regeneration (PHILIPP; D'ALMEIDA, 1988). It also has more sites for hydrogen bond formation due to its antiparallel packing, resulting in a more stable structure (KROON-BATENBURG; KROON, 1997). Furthermore, the use of biopolymers, mainly cellulose on a nanometric scale, such as cellulose nanofibrils, has been pointed out as a renewable and biodegradable raw material in several applications, showing itself as a proposed solution for the recent industrial challenge to successfully face the environmental problems caused by traditional petroleum-based polymers (MOHANTY; MISRA; HINRICHSSEN, 2000).

### 5.3 Lignin-carbohydrate complex

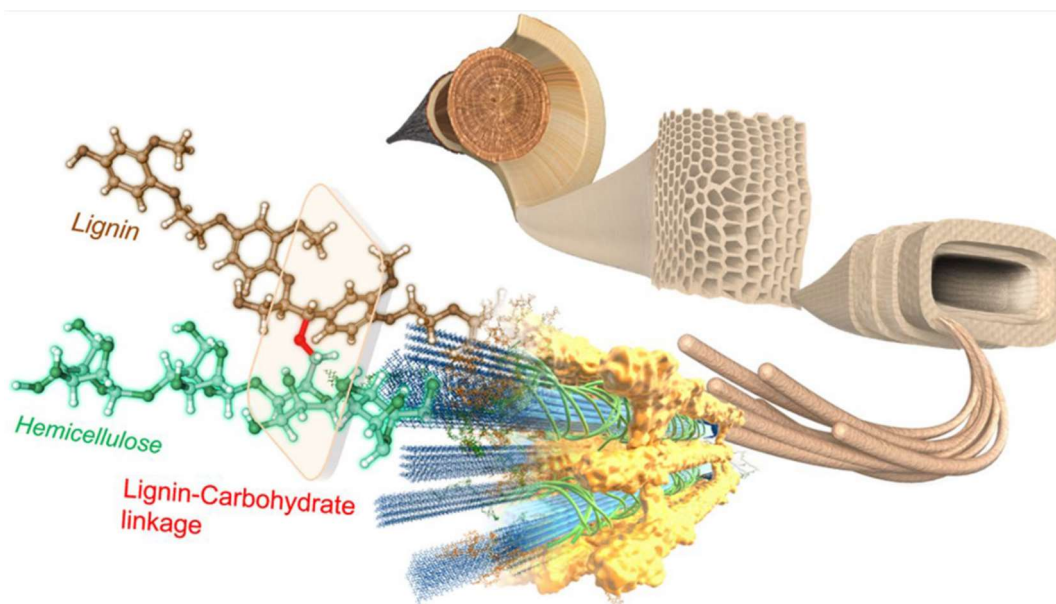
As explained in the previous sections, the plant cell wall is mainly formed by three distinct main polymers: Cellulose, hemicellulose, and lignin. These components do not exist



individually in the wall structure and are linked together in what is called the lignin-carbohydrate complex (LCC) through stable chemical linkages. (YOO et al., 2020; ZHAO et al., 2020)

The occurrence of these bonds between lignin and carbohydrates ultimately hinders the selective separation and isolation of lignin and carbohydrate preparations from lignocellulosic. In addition, the bonds between lignin and carbohydrates also hinder the efficient selective separation of wood components in biorefinery processes (BALAKSHIN; CAPANEMA; BERLIN, 2014). Lignin is mainly bound with hemicelluloses by covalent bonds, mainly at the benzene ring's carbon- $\alpha$  and C-4 positions. Presumably, lignin-carbohydrate intermolecular chemical bonds to a small extent exist natively between lignin, hemicelluloses, and cellulose (DU; GELLERSTEDT; LI, 2013; ZHAO et al., 2020).

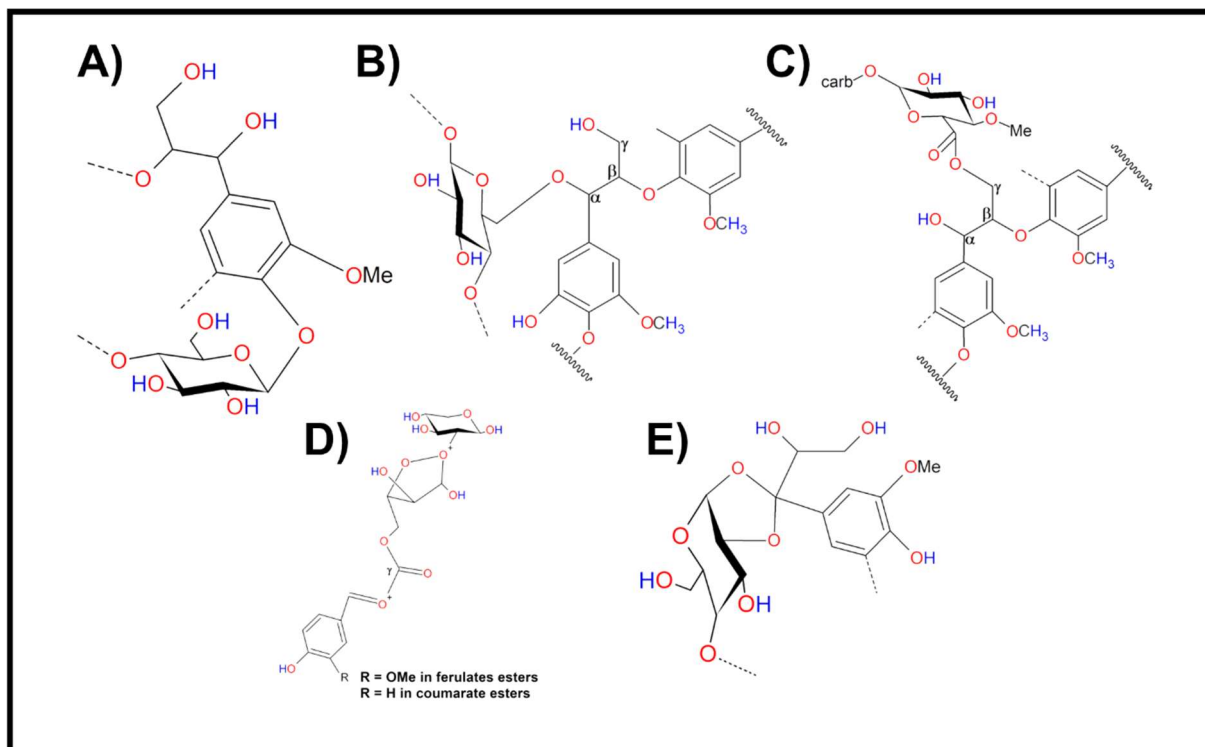
**Figure 7.** A three-dimensional perspective of the lignin-carbohydrate complex (LCC) in the wood cell wall.



Source: Nishimura et al. (2018).

In the scientific literature, five types of linkages between lignin and carbohydrates (cellulose and hemicellulose) are suggested to exist: Phenylglycosides, benzyl ethers,  $\gamma$ -esters, ferrule/cumarate esters, and hemiacetal/acetal linkages (GIUMMARELLA et al., 2019).

**Figure 8.** A representation of the known linkages between lignin and carbohydrates in the wood cell wall.



A) Phenyl-glycosides, B) Benzyl ethers, C)  $\gamma$ -esters, D) Ferrule/coumarate esters and E) Hemiacetal/acetal linkages. Source: From the author (2021)

The phenyl glycoside and hemiacetal/acetal bonds are not well elucidated compared to the other types of linkages. (GIUMMARELLA; LAWOKO, 2016). The benzyl ether bond is present in two different forms: 1) the bond form between the  $\alpha$ -position of lignin and the primary OH groups of glucose, galactose, mannose, and arabinose monomers; 2) that between the  $\alpha$ -position of lignin and the secondary OH groups of sugar monomers, mainly with xylose (YOO et al., 2020; YOU et al., 2015). The benzyl ester bond is another important LCC bond that connects the lignin and the carbohydrates via the carbohydrates' uronic acid and the lignin's hydroxyl group (TARASOV; LEITCH; FATEHI, 2018). Many angiosperms, such as *Graminea* and *Caryophyllales*, contain esterified ferulic acid, and to some extent, p-coumaric structures covalently linked to carbohydrates. In grasses, the presence of feruloyl arabinoxylan provides a convenient and reliable tool for cross-linking polysaccharides (GIUMMARELLA et al., 2019).

Thus, further studies of LCC structure can help determine appropriate processes to break lignin-carbohydrate bonds and thereby individualize the lignocellulosic components of biomass in an effective and more cost-efficient manner (BALAKSHIN; CAPANEMA; BERLIN, 2014).

#### 5.4 Cellulose nanofibrils

Cellulose nanofibrils, also referred to in the literature as Microfibrillated Cellulose (MFC), Microfibrillar Cellulose (MFC), Nanofibrillated Cellulose (NFC), or even Cellulose Filaments (CF) (NECHYPORCHUK; BELGACEM; BRAS, 2016; RAJINIPRIYA et al., 2018) are the fibrillar units resulting from the linear combination of cellulose macromolecules, containing both amorphous and crystalline regions of cellulose, with the ability to form interwoven networks (GUIMARÃES JR et al. 2015). They were successfully isolated in the laboratory for the first time by (TURBAK; SNYDER; SANDBERG, 1983).

Cellulose nanofibrils have a considerable length to diameter ratio (Aspect Ratio) and higher mechanical properties, with tensile strength and modulus of elasticity estimated to be around 100-140 MPa and 12-21 GPa, respectively (GUIMARÃES et al., 2015a; ROL et al., 2017).

For having a large aspect ratio, large specific surface area with reactive hydroxyl groups, and the possibility of obtaining them from natural sources and agro-industrial residues, cellulose nanofibrils have been attracting attention of researchers and industrial sectors all over the world (JONOBI et al. 2015; SOUZA, 2010), is seen as exciting material for several applications (HENRIKSSON et al. 2007; SIRÓ; PLACKETT, 2010; SYVERUD et al. 2011). More recently, studies on the production and application of CNFs have gained significant prominence. For example, they can be applied as a reinforcing agent to improve mechanical and barrier properties (GUIMARÃES JUNIOR; TEIXEIRA; TONOLI, 2018; KLEMM et al., 2011), in the paper industry (MIRMEHDI et al., 2018), biomedical and pharmaceutical products (JORFI; FOSTER, 2015), cementitious composites (FONSECA et al., 2016) and electronic devices (ARANTES et al., 2017). In addition, it provides a wide variety of possible surface functionalizations (MISSOUM; BELGACEM; BRAS, 2013).

As previously mentioned, NFCs can be obtained from different natural sources, which is a great advantage compared to other materials. Furthermore, the characteristics of the nanofibrils vary according to the fiber source, being able to adapt the species and the production method according to the desired use. Several papers in the literature report the production of CNFs from wood (BUFALINO et al., 2014, 2015a; GUIMARÃES et al., 2015a, 2015b; SCATOLINO et al., 2017a, 2017b) and non-timber resources such as bagasse and rice straw (HASSAN et al., 2014), hemp stem (KLEMM et al., 2011; PANTHAPULAKKAL; SAIN, 2013), banana racks (ZULUAGA et al., 2009), bamboo (GUIMARÃES et al., 2015a), *Aloe vera* (CHENG et al., 2014), sisal and abaca leaves (ALILA et al., 2013), curauá (CAMPOS et al., 2013), cocoa industry waste (SOUZA et al., 2019), açai industry waste (BRAGA et al.,

2021), and oat straw (LAGO, R. C., DE OLIVEIRA A. L., DIAS, M. C., DE CARVALHO, E. E. N., TONOLI, G. H. D., BARROS VILAS BOAS, 2020).

Chemical or mechanical processes can be applied to obtain cellulose nanofibrils, where in the first, there is partial hydrolysis, initially of the amorphous region of the cellulose to obtain the nanocrystals (or whiskers). In the second, there is the deconstruction of the cell wall structure that generates smaller structures that contain crystalline and amorphous regions.

Mechanical methods for obtaining nanofibrils cited in the literature are: (1) by shearing, usually performed using a stone mill (SYVERUD et al. 2011); (2) high-pressure homogenizer (DAVOUDPOUR et al. 2015), (3) microfluidizer (SIQUEIRA et al. 2011), (4) mechanical stirring (CHERIAN et al. 2008); (5) cryo crushing (low-temperature maceration) (CHAKRABORTY et al. 2005) and more recently by a (6) twin-screw extruder (BANVILLET et al., 2021a; ESPINOSA et al., 2020; ROL et al., 2017).

The mechanical methods are the most used to produce nanofibrils, but they demand a high energy cost (ABDUL KHALIL et al. 2014; JOSSET et al. 2014; SAITO et al. 2006).

According to Siró e Plackett (2010), it was not uncommon that energy consumption values of mechanical nanofibrillation reached figures around 20,000-30,000 kW.h/ton, which impeded for a long time the production of CNFs on an industrial scale. Several pretreatments have been proposed for lignocellulosic biomass to reduce energy consumption and enable the industrial production of CNFs. Chemical or enzymatic pre-treatments can reduce energy consumption to values around 1,000 kWh/ton of cellulosic fiber (SIRÓ; PLACKETT, 2010).

Many studies have proposed pre-treatments to reduce energy consumption during the production of nanofibrils, among which we can highlight the enzymatic pre-treatments (ARANTES et al., 2020; BANVILLET et al., 2021a), which are less aggressive to the structure of the nanofibrils and are also environmentally friendly, as they do not produce toxic residues.

### **5.5 Pre-treatment of lignocellulosic biomass**

There are different pre-treatment possibilities, such as physical, chemical, biological, and/or their combinations. However, the primary objective of any pretreatment is to promote the breakdown of cellulose, hemicellulose, and lignin so that these polymers are converted into smaller fragments with greater specific surface area, thus facilitating and increasing the yield to obtain different by-products from cellulose.

Chemical and enzymatic pretreatments have been used to weaken the structure of cellulose fibers and facilitate nanofibrillation, reducing energy consumption and creating CNFs with functional groups. Many pretreatment methods have been reported in the literature, which

can be divided into three categories: (1) chemical modifications, which alter the fibers, (2) enzymatic method that cuts the fibers, and (3) other types of pretreatment (ROL et al., 2019).

Below, two types of lignocellulosic biomass pretreatments that were explored in this work will be described:

### 5.5.1 Alkaline pre-treatments

Alkaline pretreatments are generally carried out at ambient temperature and pressure. The most used alkalis are the hydroxyl derivatives of sodium, potassium, calcium, and ammonium salts. Among these hydroxyl derivatives, sodium hydroxide (NaOH) is considered the most effective (KUMAR; SHARMA, 2017; KUMAR; WYMAN, 2009).

The first work that investigated the influence of a pre-treatment using NaOH to cause swelling of the fibers in order to facilitate nanofibrillation of cellulosic fibers was by Abe, (2016). In this paper, the author analyzed the use of NaOH solutions to facilitate nanofibrillation of ball mill dried pulps. Ball milling in 8% NaOH loosened the hydrogen bonds between microfibrils of and produced cellulose nanofibrils with a uniform diameter of approximately 12-20 nm.

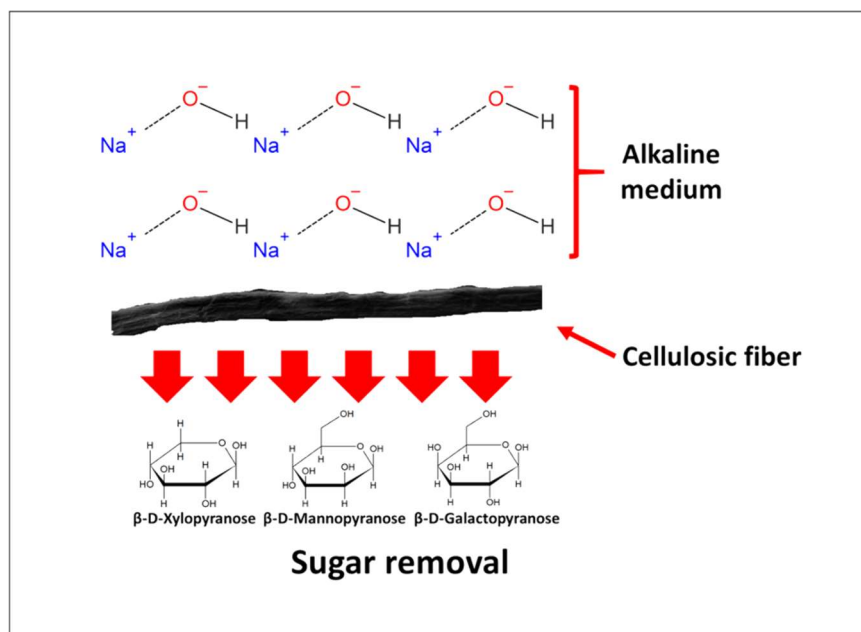
16% NaOH solution was also evaluated and although it also increased nanofibrillation, the shape of the original microfibrils disappeared after neutralization, and an integrated, continuous network formed by the interdigitation of cellulose nanofibers was observed.

Alkaline reagents degrade ester side chains and glycosides, leading to structural modification of lignin, swelling of cellulose, decrystallization of cellulose, and solvation of hemicellulose (ABE, 2016; CHENG et al., 2010; IBRAHIM et al., 2011; SILLS; GOSSETT, 2011).

Lee et al., (2018) demonstrated that cellulose nanofibrils produced after pretreatment with low concentration NaOH (2%) showed enhanced thermal stability with a dispersing agent (carboxymethylcellulose) at low temperature. They showed average onset and maximum thermal decomposition temperatures of 305°C and 343°C, respectively, higher than those of control NFCs (283°C and 310°C).

Dias and collaborators (2019) showed that pretreatment with 5% NaOH solution for two hours at 80°C leads to partial removal of hemicellulose (Figure 9), where up to a range between 9-12% facilitates obtaining Eucalyptus cellulose nanofibrils representing a 38% energy saving.

**Figure 9.** Illustration of NaOH acting on the cellulosic fiber and removing sugars (hemicellulose).



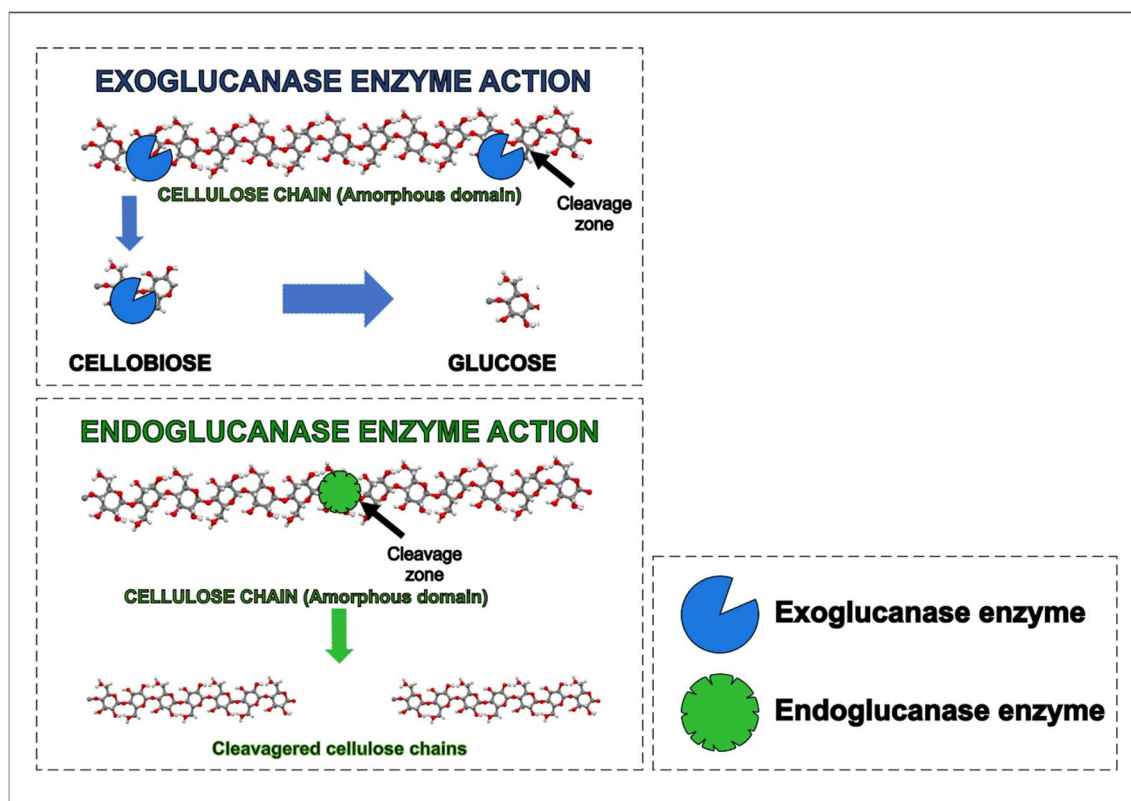
Source: From the author (2021).

### 5.5.2 Enzymatic pre-treatments

The use of enzymes in cellulose treatment has been reported as a way to optimize bioethanol production (SHOKRKAR; EBRAHIMI; ZAMANI, 2018; SINGHANIA et al., 2013; VASIĆ; KNEZ; LEITGEB, 2021) in addition to facilitating the mechanical refining of cellulose pulps (CUI; MEDDEB-MOUELHI, 2015; GIL et al., 2009; TORRES et al., 2012). The first studies on enzymatic pre-treatments to facilitate the obtainment of cellulose nanofibrils were developed in 2007 by (HENRIKSSON et al., 2007; PÄÄKKO et al., 2007) and since then, this pretreatment method has become more and more established in the industry due to its ease and efficiency (ARANTES et al., 2020).

In the enzymatic breakdown of cellulose molecules, there are two main classes of enzymes concerning their mechanism of action on the fiber structure: (1) Exoglucanases or cellobiohydrolases, which act by cleaving the ends of the cellulose chain, and (2) Endoglucanases, which cleave the inner part of the chain. These enzymes first reduce the cellulose into cellobioses and subsequently hydrolyze them into glycosides (ARANTES et al., 2020), as illustrated in Figure 7.

Figure 10. Mechanisms of action of enzymes that act on cellulose.



Source: From the author (2021).

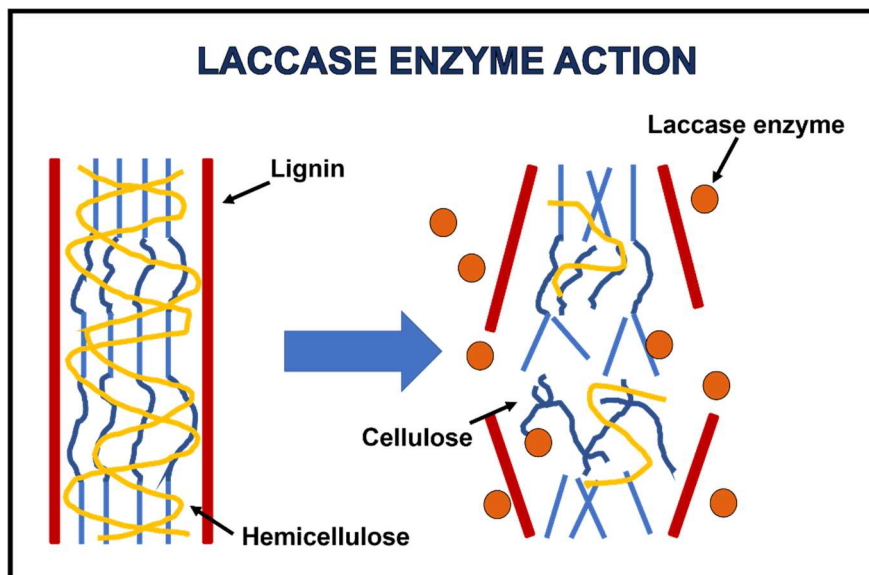
The enzymatic hydrolysis of cellulose is a process that requires physical contact between the glycosidic hydrolases and their substrates, which can be obstructed by lignin in several ways (SIPPONEN et al., 2017). In unbleached pulps, insoluble lignin may block the access of enzymes to carbohydrate surfaces or may irreversibly bind enzymes and prevent the access of enzymes to their substrate. The fate of the catalytic activity of the adsorbed cellulases is under debate since there are reports of lignin-bound cellulases retaining most of the activity (RODRIGUES et al., 2012). Thus, making it a challenge to develop new pretreatments that attack the other compounds to make cellulose isolation more effective.

More recently, several new enzymes have been tested, such as hemicellulases, lytic polysaccharide monooxygenases (LPMO), and laccases. These enzymes do not directly hydrolyze cellulose fibers but instead improve the accessibility of cellulose to cellulase and, in doing so, improve fibrillation (ROL et al., 2019).

Laccase enzymes have emerged as important biotechnological catalysts because of their environmentally friendly nature and mild working conditions. They are multi-copper enzymes capable of catalyzing the direct oxidation of a wide range of aromatic compounds, such as lignin monomers, generating reactive radicals, using molecular oxygen as the oxidant (GARCIA-

UBASART et al., 2012; NLANDU et al., 2020). Figure 11 illustrates the mechanism of action of the enzyme laccase in plant biomass, acting mainly on lignin.

**Figure 11.** Mechanism of action of the enzyme laccase in plant biomass.



Source: From the author (2021).

In bioethanol production, pretreatment with a laccase mediator system has been applied to remove inhibitory compounds in saccharification. In paper production, the use of laccases between steam explosion and kraft pulping increases the delignification rate, even when applied to substrates with high lignin content (MARTIN-SAMPEDRO et al., 2011). The catalytic degradation of lignin has always been a challenge. However, Steinmetz et al., (2020) have demonstrated in their study the potential of laccase as a depolymerizing agent for lignin in a semi-continuous depolymerization process under mild conditions (aqueous medium near room temperature), helping to improve knowledge of biological catalyst work for the production of high-value aromatic compounds.

Given the above, using the enzyme laccase as a pre-stage before pretreatment of cellulose with cellulase enzymes may be a viable alternative to increase the yield and quality of cellulose nanofibrils that contain high lignin contents in their composition.



## 6. CHAPTER I: CONCLUDING REMARKS

In this chapter, the motivation for the development of this work was presented, and a literature review was also provided with important information for the reader's immersion and a better understanding of the topics covered, as well as to ensure the scientific basis of this study.

It has been seen that lignocellulosic biomass is formed by a complex and well-defined structure, known as cell wall, where carbohydrates are closely linked with lignin by a complex of chemical bonds in the fiber structure. Which ultimately affects the accessibility of cellulose to the attack of chemical and/or biological agents, enzymes, or mechanical agents, making it difficult to isolate and deconstruct the fibers into smaller structures.

The study of the topics covered in the review served as a basis for defining the experiments adopted in this research. Overcoming the natural recalcitrance of biomass is still a challenge to cheapen the production of cellulose nanofibrils, and that pretreatments of biomass have been developed and applied for different purposes. It became clear the need to verify the association of fiber components in its recalcitrance and its response to pre-treatments and their effects on energy consumption for mechanical nanofibrillation.

This work is expected to contribute by understanding how the morphological structure and chemical composition of different plant fibers influence their deconstruction in different pre-treatments. Thus, seeking to indicate more efficient pre-treatments according to the raw materials characteristics and to achieve energy efficiency for the large-scale production of cellulose nanofibrils for the most diverse applications.

## 7. BIBLIOGRAPHIC REFERENCES

- ABDUL KHALIL, H. P. S. et al. Production and modification of nanofibrillated cellulose using various mechanical processes: A review. **Carbohydrate Polymers**, v. 99, p. 649–665, 2014.
- ABE, K. Nanofibrillation of dried pulp in NaOH solutions using bead milling. **Cellulose**, v. 23, n. 2, p. 1257–1261, 2016.
- AGODA-TANDJAWA, G. et al. Rheological characterization of microfibrillated cellulose suspensions after freezing. **Carbohydrate Polymers**, v. 80, n. 3, p. 677–686, 2010.
- ALEMDAR, A.; SAIN, M. Isolation and characterization of nanofibers from agricultural residues - Wheat straw and soy hulls. **Bioresource Technology**, v. 99, n. 6, p. 1664–1671, 2008.
- ALEXANDER, W. J.; GOLDSCHMID, O.; MITCHELL, R. L. Relation of Intrinsic Viscosity to Cellulose Chain Length. Degree of Polymerization Range below 400. **Industrial & Engineering Chemistry**, v. 49, n. 8, p. 1303–1306, 1957.
- ALILA, S. et al. Non-woody plants as raw materials for production of microfibrillated cellulose (MFC): A comparative study. **Industrial Crops and Products**, v. 41, n. 1, p. 250–259, 2013.
- ARANTES, A. C. C. et al. Renewable hybrid nanocatalyst from magnetite and cellulose for treatment of textile effluents. **Carbohydrate Polymers**, v. 163, p. 101–107, 2017.
- ARANTES, V. et al. **The current status of the enzyme-mediated isolation and functionalization of nanocelluloses: production, properties, techno-economics, and opportunities.** [s.l.: s.n.]. v. 27
- ARANTES, V.; SADDLER, J. N. Access to cellulose limits the efficiency of enzymatic hydrolysis: The role of amorphogenesis. **Biotechnology for Biofuels**, v. 3, p. 1–11, 2010.
- AROLA, S. et al. The role of hemicellulose in nanofibrillated cellulose networks. **Soft Matter**, v. 9, n. 4, p. 1319–1326, 2013.
- AZEVEDO, C. A. et al. Relationship between Surface Properties and Fiber Network Parameters of Eucalyptus Kraft Pulps and Their Absorption Capacity. **Surfaces**, v. 3, n. 3, p. 265–281, 2020.
- BALAKSHIN, M.; CAPANEMA, E.; BERLIN, A. **Isolation and Analysis of Lignin–Carbohydrate Complexes Preparations with Traditional and Advanced Methods.** 1. ed. [s.l.] Elsevier B.V., 2014. v. 42
- BALEA, A. et al. Nanocelluloses: Natural-based materials for fiber- reinforced cement

- composites. A critical review. **Polymers**, v. 11, n. 3, 2019.
- BALLESTEROS, J. E. M. et al. Potential of the hornification treatment on eucalyptus and pine fibers for fiber-cement applications. **Cellulose**, v. 24, n. 5, p. 2275–2286, 2017.
- BANVILLET, G. et al. Cellulose fibers deconstruction by twin-screw extrusion with in situ enzymatic hydrolysis via bioextrusion. **Bioresource Technology**, v. 327, n. December 2020, p. 124819, 2021a.
- BANVILLET, G. et al. Alkaline treatment combined with enzymatic hydrolysis for efficient cellulose nanofibrils production. **Carbohydrate Polymers**, v. 255, n. November 2020, 2021b.
- BAYU, A. et al. How to Read and Interpret FTIR Spectroscopy of Organic Material. **Indonesian Journal of Science & Technology**, v. 4, n. 1, p. 97–118, 2019.
- BERGLUND, L. et al. Production potential of cellulose nanofibers from industrial residues: Efficiency and nanofiber characteristics. **Industrial Crops and Products**, v. 92, p. 84–92, 2016.
- BEYENE, D. et al. Characterization of cellulase-treated fibers and resulting cellulose nanocrystals generated through acid hydrolysis. **Materials**, v. 11, n. 8, 2018.
- BLANCO, A. et al. **Nanocellulose for industrial use: Cellulose nanofibers (CNF), cellulose nanocrystals (CNC), and bacterial cellulose (BC)**. [s.l.] Elsevier Inc., 2018.
- BORUAH, P. et al. Exploring the lignolytic potential of a new laccase producing strain *Kocuria* sp. PBS-1 and its application in bamboo pulp bleaching. **International Biodeterioration and Biodegradation**, v. 143, n. June, p. 104726, 2019.
- BRAGA, D. G. et al. Cellulose nanostructured films from pretreated açai mesocarp fibers: Physical, barrier, and tensile performance. **Cerne**, v. 27, n. 1, p. 1–14, 2021.
- BUFALINO, L. et al. New products made with lignocellulosic nanofibers from Brazilian amazon forest. **IOP Conference Series: Materials Science and Engineering**, v. 64, n. 1, 2014.
- BUFALINO, L. et al. Nanocellulose Films from Amazon Forest Wood Wastes: Structural and Thermal Properties. **Key Engineering Materials**, v. 668, p. 110–117, 2015a.
- BUFALINO, L. et al. How the chemical nature of Brazilian hardwoods affects nanofibrillation of cellulose fibers and film optical quality. **Cellulose**, v. 22, n. 6, p. 3657–3672, 2015b.
- CAMPOS, A. et al. Obtaining nanofibers from curauá and sugarcane bagasse fibers using enzymatic hydrolysis followed by sonication. **Cellulose**, v. 20, n. 3, p. 1491–1500, 2013.
- CARVALHO, D. M. DE et al. Impact of the chemical composition of cellulosic materials on the nanofibrillation process and nanopaper properties. **Industrial Crops and Products**, v.

- 127, n. November 2018, p. 203–211, 2019.
- CECCON, F. et al. Enhanced microfibrillated cellulose-based film by controlling the hemicellulose content and MFC rheology. v. 218, n. March, p. 307–314, 2019.
- CHAKRABORTY, A.; SAIN, M.; KORTSCHOT, M. Cellulose microfibrils: A novel method of preparation using high shear refining and cryocrushing. **Holzforschung**, v. 59, n. 1, p. 102–107, 2005.
- CHAUSSY, D.; MARTIN, C.; ROUX, J. C. Rheological behavior of cellulose fiber suspensions: Application to paper-making processing. **Industrial and Engineering Chemistry Research**, v. 50, n. 6, p. 3524–3533, 2011.
- CHEN, G. et al. Fiber characterization of old corrugated container bleached pulp with laccase and glycine pretreatment. **Biomass Conversion and Biorefinery**, 2021.
- CHEN, H. et al. Lignin containing cellulose nanofibril application in pMDI wood adhesives for drastically improved gap-filling properties with robust bondline interfaces. **Chemical Engineering Journal**, v. 360, n. November 2018, p. 393–401, 2019.
- CHEN, Q. et al. Effects of laccase on lignin depolymerization and enzymatic hydrolysis of ensiled corn stover. **Bioresource Technology**, v. 117, p. 186–192, 2012.
- CHEN, Y. et al. Correction to: Comparative characteristics of TEMPO-oxidized cellulose nanofibers and resulting nanopapers from bamboo, softwood, and hardwood pulps. **Cellulose**, v. 25, n. 1, p. 895, 2018.
- CHENG, S. et al. Aloe vera rind cellulose nanofibers-reinforced films. **Journal of Applied Polymer Science**, v. 131, n. 15, p. 1–9, 2014.
- CHENG, Y. et al. Evaluation of High Solids Alkaline Pretreatment of Rice Straw. **Applied Biochemistry and Biotechnology**, v. 162, p. 1768–1784, 2010.
- CHERIAN, B. M. et al. A novel method for the synthesis of cellulose nanofibril whiskers from banana fibers and characterization. **Journal of Agricultural and Food Chemistry**, v. 56, n. 14, p. 5617–5627, 2008.
- CHU, S.; SUBRAHMANYAM, A. V.; HUBER, G. W. The pyrolysis chemistry of a  $\beta$ -O-4 type oligomeric lignin model compound. **Green Chemistry**, v. 15, n. 1, p. 125–136, 2013.
- CLARO, P. et al. Curaua and eucalyptus nanofiber films by continuous casting: mixture of cellulose nanocrystals and nanofibrils. **Cellulose**, v. 26, n. 4, p. 2453–2470, 2019.
- CUI, L.; MEDDEB-MOUELHI, F. Effect of commercial cellulases and refining on kraft pulp properties : Correlations between treatment impacts and enzymatic activity components. v. 115, p. 193–199, 2015.
- CZAIKOSKI, A.; DA CUNHA, R. L.; MENEGALLI, F. C. Rheological behavior of cellulose

nanofibers from cassava peel obtained by combination of chemical and physical processes.

**Carbohydrate Polymers**, v. 248, n. May, p. 116744, 2020.

DAHLMAN, O.; JACOBS, A.; SJÖBERG, J. Molecular properties of hemicelluloses located in the surface and inner layers of hardwood and softwood pulps. **Cellulose**, v. 10, n. 4, p. 325–334, 2003.

DANG, Z.; ZHANG, J.; RAGAUSKAS, A. J. Characterizing TEMPO-mediated oxidation of ECF bleached softwood kraft pulps. **Carbohydrate Polymers**, v. 70, n. 3, p. 310–317, 2007.

DAVOUDPOUR, Y. et al. Optimization of high pressure homogenization parameters for the isolation of cellulosic nanofibers using response surface methodology. **Industrial Crops and Products**, v. 74, p. 381–387, 2015.

DEKA, A.; DEY, N. Rheological studies of two component high build epoxy and polyurethane based high performance coatings. **Journal of Coatings Technology and Research**, v. 10, n. 3, p. 305–315, 2013.

DELGADO-AGUILAR, M. et al. The key role of lignin in the production of low-cost lignocellulosic nanofibres for papermaking applications. **Industrial Crops and Products**, v. 86, p. 295–300, 2016.

DESMAISONS, J. et al. A new quality index for benchmarking of different cellulose nanofibrils. **Carbohydrate Polymers**, v. 174, p. 318–329, 2017.

DIAS, M. C.; MENDONÇA, M. C.; DAMÁSIO, R. A. P. Influence of hemicellulose content of Eucalyptus and Pinus fibers on the grinding process for obtaining cellulose micro / nanofibrils. **Holzforschung**, v. 73, n. 11, p. 1035–1046, 2019.

DIMIC-MISIC, K. et al. Rheological properties comparison of aqueous dispersed nanocellulose derived from a novel pathway-produced microcrystalline cellulose or by conventional methods. **Applied Rheology**, v. 28, n. 6, p. 1–15, 2018.

DIMIC-MISIC, K.; GANE, P. A. C.; PALTAKARI, J. Micro and nanofibrillated cellulose as a rheology modifier additive in CMC-containing pigment-coating formulations. **Industrial and Engineering Chemistry Research**, v. 52, n. 45, p. 16066–16083, 2013.

DU, X.; GELLERSTEDT, G.; LI, J. Universal fractionation of lignin – carbohydrate complexes ( LCCs ) from lignocellulosic biomass : an example using spruce. **The plant journal**, v. 74, p. 328–338, 2013.

ESPINOSA, E. et al. Use of multi-factorial analysis to determine the quality of cellulose nanofibers: effect of nanofibrillation treatment and residual lignin content. **Cellulose**, v. 3, 2020.

FARLEY, A. et al. Influence of chemical pretreatments on plant fiber cell wall and their

- implications on the appearance of fiber dislocations. 2020.
- FERDOSIAN, F. et al. Bio-based adhesives and evaluation for wood composites application. **Polymers**, v. 9, n. 2, 2017.
- FERREIRA, S. R. et al. Effect of hornification on the structure, tensile behavior and fiber matrix bond of sisal, jute and curauá fiber cement based composite systems. **Construction and Building Materials**, v. 139, p. 551–561, 2017.
- FERRER, A. et al. Effect of residual lignin and heteropolysaccharides in nanofibrillar cellulose and nanopaper from wood fibers. **Cellulose**, v. 19, n. 6, p. 2179–2193, 2012.
- FIGUEIREDO, P. et al. Properties and chemical modifications of lignin: Towards lignin-based nanomaterials for biomedical applications. **Progress in Materials Science**, v. 93, p. 233–269, 2018.
- FONSECA, C. S. et al. Micro/nanofibrilas celulósicas de eucalyptus em fibrocimentos extrudados [Eucalyptus cellulosic micro/nanofibrils in extruded fibercement]. **Cerne**, v. 22, n. 1, p. 59–68, 2016.
- FOSTER, E. J. et al. **Current characterization methods for cellulose nanomaterials** *Chemical Society Reviews* Royal Society of Chemistry, , 2018. Disponível em: <<http://dx.doi.org/10.1039/c6cs00895j>>
- FRENCH, A. D. Idealized powder diffraction patterns for cellulose polymorphs. **Cellulose**, v. 21, n. 2, p. 885–896, 2014.
- FRENCH, A. D. Increment in evolution of cellulose crystallinity analysis. **Cellulose**, v. 27, n. 10, p. 5445–5448, 2020.
- FUKUZUMI, H. et al. Transparent and high gas barrier films of cellulose nanofibers prepared by TEMPO-mediated oxidation. **Biomacromolecules**, v. 10, n. 1, p. 162–165, 2009.
- FUKUZUMI, H. et al. Dispersion stability and aggregation behavior of TEMPO-oxidized cellulose nanofibrils in water as a function of salt addition. **Cellulose**, v. 21, n. 3, p. 1553–1559, 2014.
- GARCÍA-ABUÍN, A. et al. Viscosimetric behaviour of carboxymethyl cellulose - Arabic gum mixtures: A new step to modelling. **Carbohydrate Polymers**, v. 80, n. 1, p. 26–30, 2010.
- GARCIA-UBASART, J. et al. A new procedure for the hydrophobization of cellulose fibre using laccase and a hydrophobic phenolic compound. **Bioresource Technology**, v. 112, p. 341–344, 2012.
- GELLERSTEDT, G.; EK, M.; HENRIKSSON, G. **Wood chemistry and biotechnology**. [s.l.: s.n.]. v. 1
- GENG, L. et al. Rheological Properties of Jute-Based Cellulose Nanofibers under Different

- Ionic Conditions. **In: Umesh A, Rajai A, Akira I (eds) Nanocelluloses: their preparation, properties, and applications. ACS Symposium Series.**, p. 113–132, 2018.
- GHANNAM, M. ; ESMAIL, M. . Rheological properties of carboxymethyl cellulose (CMC) solutions. **Journal of Applied Polymer Science**, v. 64, n. 2, p. 289–301, 1998.
- GIL, N. et al. Use of enzymes to improve the refining of a bleached Eucalyptus globulus kraft pulp. v. 46, p. 89–95, 2009.
- GIUMMARELLA, N. et al. A critical review on the analysis of lignin carbohydrate bonds. **Green Chemistry**, v. 21, n. 7, p. 1573–1595, 2019.
- GIUMMARELLA, N.; LAWOKO, M. Structural Basis for the Formation and Regulation of Lignin-Xylan Bonds in Birch. **ACS Sustainable Chemistry and Engineering**, v. 4, n. 10, p. 5319–5326, 2016.
- GRÜNEBERGER, F. et al. Rheology of nanofibrillated cellulose/acrylate systems for coating applications. **Cellulose**, v. 21, n. 3, p. 1313–1326, 2014.
- GU, F. et al. Water retention value for characterizing fibrillation degree of cellulosic fibers at micro and nanometer scales. **Cellulose**, v. 25, n. 5, p. 2861–2871, 2018.
- GUIMARÃES JUNIOR, M.; TEIXEIRA, F. G.; TONOLI, G. H. D. Effect of the nanofibrillation of bamboo pulp on the thermal, structural, mechanical and physical properties of nanocomposites based on starch/poly(vinyl alcohol) blend. **Cellulose**, v. 25, n. 3, p. 1823–1849, 2018.
- GUIMARÃES, M. et al. Preparation of Cellulose Nanofibrils from Bamboo Pulp by Mechanical Defibrillation for Their Applications in Biodegradable Composites. **Journal of Nanoscience and Nanotechnology**, v. 15, n. 9, p. 6751–6768, 2015a.
- GUIMARÃES, M. et al. Starch/PVA-based nanocomposites reinforced with bamboo nanofibrils. **Industrial Crops and Products**, v. 70, p. 72–83, 2015b.
- GUO, H. et al. Valorization of Lignin to Simple Phenolic Compounds over Tungsten Carbide: Impact of Lignin Structure. **ChemSusChem**, v. 10, n. 3, p. 523–532, 2017.
- GUPTA, A. et al. Rheological and thermo-mechanical properties of poly(lactic acid)/lignin-coated cellulose nanocrystal composites. **ACS Sustainable Chemistry and Engineering**, v. 5, n. 2, p. 1711–1720, 2017.
- HAKEEM, K. R.; JAWAID, M.; ALOTHMAN, O. Y. **Rheological Properties and Processing of Polymer Blends with Micro- and Nanofibrillated Cellulose.** [s.l: s.n.].
- HASSAN, M. et al. Effect of xylanase pretreatment of rice straw unbleached soda and neutral sulfite pulps on isolation of nanofibers and their properties. **Cellulose**, v. 25, n. 5, p. 2939–2953, 2018.

- HASSAN, M. L. et al. Enzyme-assisted isolation of microfibrillated cellulose from date palm fruit stalks. **Industrial Crops and Products**, v. 55, p. 102–108, 2014.
- HE, M. et al. Production and Characterization of Cellulose Nanofibrils from Different Chemical and Mechanical Pulps. **Journal of Wood Chemistry and Technology**, v. 38, n. 2, p. 149–158, 2018.
- HEITNER, C.; DIMMEL, D. R.; SCHMIDT, J. A. **Lignins and Lignans: Advances in Chemistry**. Boca Raton: CRC PRESS, 2010.
- HENRIKSSON, M. et al. An environmentally friendly method for enzyme-assisted preparation of microfibrillated cellulose (MFC) nanofibers. **European Polymer Journal**, v. 43, n. 8, p. 3434–3441, 2007.
- HOEGGER, I. C. et al. Mechanical deconstruction of lignocellulose cell walls and their enzymatic saccharification. **Cellulose**, v. 20, n. 2, p. 807–818, 2013.
- HORIKAWA, Y. et al. Prediction of Lignin Contents from Infrared Spectroscopy: Chemical Digestion and Lignin/Biomass Ratios of *Cryptomeria japonica*. **Applied Biochemistry and Biotechnology**, v. 188, n. 4, p. 1066–1076, 2019.
- HORSEMAN, T. et al. Preparation and property assessment of neat lignocellulose nanofibrils (LCNF) and their composite films. **Cellulose**, v. 24, n. 6, p. 2455–2468, 2017.
- HUANG, C. et al. Understanding the Nonproductive Enzyme Adsorption and Physicochemical Properties of Residual Lignins in Moso Bamboo Pretreated with Sulfuric Acid and Kraft Pulping. **Applied Biochemistry and Biotechnology**, v. 180, n. 8, p. 1508–1523, 2016.
- HUBBE, M. A. et al. Rheology of nanocellulose-rich aqueous suspensions: A review. **BioResources**, v. 12, n. 4, p. 9556–9661, 2017.
- IBÁ. Report 2020. **Indústria Brasileira de Árvores**, p. 66, 2020.
- IBRAHIM, M. M. et al. Comparison of alkaline pulping with steam explosion for glucose production from rice straw. **Carbohydrate Polymers**, v. 83, n. 2, p. 720–726, 2011.
- IGLESIAS, M. C. et al. The effect of residual lignin on the rheological properties of cellulose nanofibril suspensions. **Journal of Wood Chemistry and Technology**, v. 0, n. 0, p. 1–12, 2020.
- IKEDA, S.; NISHINARI, K. “Weak gel”-type rheological properties of aqueous dispersions of nonaggregated  $\kappa$ -carrageenan helices. **Journal of Agricultural and Food Chemistry**, v. 49, n. 9, p. 4436–4441, 2001.
- IMANI, M. et al. Coupled Effects of Fibril Width, Residual and Mechanically Liberated Lignin on the Flow, Viscoelasticity, and Dewatering of Cellulosic Nanomaterials.



- Biomacromolecules**, v. 21, n. 10, p. 4123–4134, 2020.
- IOELOVICH, M. Cellulose as a nanostructured polymer: A short review. **BioResources**, v. 3, n. 4, p. 1403–1418, 2008a.
- IOELOVICH, M. Cellulose As a Nanostructured Polyme.Pdf. v. 3, n. Ioelovich 1999, p. 1403–1418, 2008b.
- IOTTI, M. et al. Rheological Studies of Microfibrillar Cellulose Water Dispersions. **Journal of Polymers and the Environment**, v. 19, n. 1, p. 137–145, 2011.
- ISOGAI, A.; SAITO, T.; FUKUZUMI, H. TEMPO-oxidized cellulose nanofibers. **Nanoscale**, v. 3, n. 1, p. 71–85, 2011.
- IWAMOTO, S.; ABE, K.; YANO, H. The effect of hemicelluloses on wood pulp nanofibrillation and nanofiber network characteristics. **Biomacromolecules**, v. 9, n. 3, p. 1022–1026, 2008.
- IWAMOTO, S.; NAKAGAITO, A. N.; YANO, H. Nano-fibrillation of pulp fibers for the processing of transparent nanocomposites. **Applied Physics A: Materials Science and Processing**, v. 89, n. 2, p. 461–466, 2007.
- JIN, E. et al. On the polymorphic and morphological changes of cellulose nanocrystals (CNC-I) upon mercerization and conversion to CNC-II. **Carbohydrate Polymers**, v. 143, p. 327–335, 2016.
- JOFFRE, T. et al. A Method to Measure Moisture Induced Swelling Properties of a Single Wood Cell. **Experimental Mechanics**, v. 56, n. 5, p. 723–733, 2016.
- JONOBI, M. et al. Different preparation methods and properties of nanostructured cellulose from various natural resources and residues: a review. **Cellulose**, v. 22, n. 2, p. 935–969, 2015.
- JORDAN, J. H. et al. Lignin-containing cellulose nanofibers with gradient lignin content obtained from cotton gin motes and cotton gin trash. **Cellulose**, v. 28, n. 2, p. 757–773, 2021.
- JORFI, M.; FOSTER, E. J. Recent advances in nanocellulose for biomedical applications. **Journal of Applied Polymer Science**, v. 132, n. 14, p. 1–19, 2015.
- JOSSET, S. et al. Energy consumption of the nanofibrillation of bleached pulp, wheat straw and recycled newspaper through a grinding process. **Nord. Pulp. Pap. Res. J.**, v. 29, n. 1, p. 167–175, 2014.
- KAMEL, S. Nanotechnology and its applications in lignocellulosic composites, a mini review. **Express Polymer Letters**, v. 1, n. 9, p. 546–575, 2007.
- KARPPINEN, A. et al. Flocculation of microfibrillated cellulose in shear flow. **Cellulose**, v. 19, n. 6, p. 1807–1819, 2012.

- KIM, B.-Y. et al. Preparation and Properties of Cellulose Nanofiber Films with Various Chemical Compositions Impregnated by Ultraviolet-Curable Resin. **BioResources**, v. 12, n. 1, p. 1767–1778, 2017.
- KISHANI, S. et al. Solubility of Softwood Hemicelluloses. **Biomacromolecules**, v. 19, n. 4, p. 1245–1255, 2018.
- KLEMM, D. et al. Nanocelluloses as innovative polymers in research and application. **Advances in Polymer Science**, v. 205, n. 1, p. 49–96, 2006.
- KLEMM, D. et al. Nanocelluloses: A new family of nature-based materials. **Angewandte Chemie - International Edition**, v. 50, n. 24, p. 5438–5466, 2011.
- KOPONEN, A. I. The effect of consistency on the shear rheology of aqueous suspensions of cellulose micro- and nanofibrils: a review. **Cellulose**, v. 27, n. 4, p. 1879–1897, 2020.
- KROON-BATENBURG, L. M. J.; KROON, J. The crystal and molecular structures of cellulose I and II. **Glycoconjugate Journal**, v. 14, n. 5, p. 677–690, 1997.
- KRUYENISKI, J. et al. Physical and chemical characteristics of pretreated slash pine sawdust influence its enzymatic hydrolysis. **Industrial Crops and Products**, v. 130, n. July 2018, p. 528–536, 2019.
- KUMAR, A. K.; SHARMA, S. Recent updates on different methods of pretreatment of lignocellulosic feedstocks: a review. **Bioresources and Bioprocessing**, v. 4, n. 1, 2017.
- KUMAR, R.; WYMAN, C. E. Effects of Cellulase and Xylanase Enzymes on the Deconstruction of Solids from Pretreatment of Poplar by Leading Technologies. **Biotechnology Progress**, v. 25, n. 2, p. 302–314, 2009.
- KUMAR, V. et al. Rheology of microfibrillated cellulose suspensions in pressure-driven flow. **Applied Rheology**, v. 26, n. 4, p. 1–11, 2016.
- LAGO, R. C., DE OLIVEIRA A. L., DIAS, M. C., DE CARVALHO, E. E. N., TONOLI, G. H. D., BARROS VILAS BOAS, E. V. Obtaining cellulosic nano fibrils from oat straw for biocomposite reinforcement : Mechanical and barrier properties. **Industrial Crops & Products**, v. 148, n. December 2019, 2020.
- LAHTINEN, P. et al. A Comparative study of fibrillated fibers from different mechanical and chemical pulps. **BioResources**, v. 9, n. 2, p. 2115–2127, 2014.
- LASSEUGUETTE, E.; ROUX, D.; NISHIYAMA, Y. Rheological properties of microfibrillar suspension of TEMPO-oxidized pulp. **Cellulose**, v. 15, p. 425–433, 2008.
- LÊ, H. Q. et al. Effect of lignin on the morphology and rheological properties of nanofibrillated cellulose produced from  $\gamma$ -valerolactone/water fractionation process. **Cellulose**, v. 25, n. 1, p. 179–194, 2018.

- LEE, H. et al. Improved thermal stability of cellulose nanofibrils using low-concentration alkaline pretreatment. **Carbohydrate Polymers**, v. 181, p. 506–513, 2018a.
- LEE, H. et al. Improved thermal stability of cellulose nano fibrils using low-concentration alkaline pretreatment. **Carbohydrate Polymers**, v. 181, n. April 2017, p. 506–513, 2018b.
- LEE, S. H. et al. Increase in enzyme accessibility by generation of nanospace in cell wall supramolecular structure. **Bioresource Technology**, v. 101, n. 19, p. 7218–7223, 2010.
- LI, H. Y. et al. Structural characterization of hemicelluloses and topochemical changes in Eucalyptus cell wall during alkali ethanol treatment. **Carbohydrate Polymers**, v. 123, p. 17–26, 2015.
- LI, M. et al. Comparison of nonproductive adsorption of cellulase onto lignin isolated from pretreated lignocellulose. **Cellulose**, v. 27, n. 14, p. 7911–7927, 2020.
- LI, M.; PU, Y.; RAGAUSKAS, A. J. Current Understanding of the Correlation of Lignin Structure with Biomass Recalcitrance. **frontiers in chemistry**, v. 4, n. November, p. 1–8, 2016.
- LIN, D. et al. Food Hydrocolloids Viscoelastic properties of pectin / cellulose composites studied by QCM-D and oscillatory shear rheology. **Food hydrocolloids**, v. 79, p. 13–19, 2018.
- LING, Z. et al. Exploring crystalline-structural variations of cellulose during alkaline pretreatment for enhanced enzymatic hydrolysis. **Bioresource Technology**, v. 224, p. 611–617, 2017.
- LIU, C. et al. Properties of Nanocelluloses and Their Application as Rheology Modifier in Paper Coating. **Industrial and Engineering Chemistry Research**, v. 56, n. 29, p. 8264–8273, 2017.
- LIU, C. et al. Biopolymers Derived from Trees as Sustainable Multifunctional Materials: A Review. **Advanced Materials**, v. 33, n. 28, p. 1–27, 2021.
- LORENCI WOICIECHOWSKI, A. et al. Lignocellulosic biomass: Acid and alkaline pretreatments and their effects on biomass recalcitrance – Conventional processing and recent advances. **Bioresource Technology**, v. 304, n. January, p. 122848, 2020.
- LUND, K.; SJOSTRÖM, K.; BRELID, H. Alkali Extraction of Kraft Pulp Fibers: Influence on Fiber and Fluff Pulp Properties. **Journal of Engineered Fibers and Fabrics**, v. 7, n. 2, p. 30–39, 2012.
- LUO, X. L. et al. Effects of wet-pressing-induced fiber hornification on enzymatic saccharification of lignocelluloses. **Cellulose**, v. 18, n. 4, p. 1055–1062, 2011.
- MA, Y. et al. Porous lignin based poly (acrylic acid)/organo-montmorillonite

- nanocomposites: Swelling behaviors and rapid removal of Pb (II) ions. **Polymer**, v. 128, n. II, p. 12–23, 2017.
- MACRAE, C. F. et al. Mercury CSD 2.0 - New features for the visualization and investigation of crystal structures. **Journal of Applied Crystallography**, v. 41, n. 2, p. 466–470, 2008.
- MAHFOUDHI, N.; BOUFI, S. Nanocellulose as a novel nanostructured adsorbent for environmental remediation: a review. **Cellulose**, v. 24, n. 3, p. 1171–1197, 2017.
- MARCHESSAULT, R. H.; MOREHEAD, F. F.; KOCH, M. J. Some Hydrodynamic Properties of Neutral As Related To Size and Shape 1. **Journal of Colloid Science**, v. 344, p. 327–344, 1961.
- MARCHESSAULT, R. H.; SUNDARARAJAN, P. R. **Cellulose**. [s.l: s.n.].
- MARTIN-SAMPEDRO, R. et al. Lignin changes after steam explosion and laccase-mediator treatment of eucalyptus wood chips. **Journal of Agricultural and Food Chemistry**, v. 59, n. 16, p. 8761–8769, 2011.
- MIRMEHDI, S. et al. Spraying Cellulose Nanofibrils for Improvement of Tensile and Barrier Properties of Writing & Printing (W&P) Paper. **Journal of Wood Chemistry and Technology**, v. 3813, 2018.
- MISSOUM, K.; BELGACEM, M. N.; BRAS, J. Nanofibrillated cellulose surface modification: A review. **Materials**, v. 6, n. 5, p. 1745–1766, 2013.
- MOBERG, T. et al. Rheological properties of nanocellulose suspensions: effects of fibril/particle dimensions and surface characteristics. **Cellulose**, v. 24, n. 6, p. 2499–2510, 2017.
- MOHANTY, A. K.; MISRA, M.; HINRICHSEN, G. Biofibres, biodegradable polymers and biocomposites: An overview. **Macromolecular Materials and Engineering**, v. 276–277, p. 1–24, 2000.
- MOON, R. J. et al. **Cellulose nanomaterials review: Structure, properties and nanocomposites**. [s.l: s.n.]. v. 40
- MOONEY, C. A. et al. The effect of fiber characteristics on hydrolysis and cellulase accessibility to softwood substrates. **Enzyme and Microbial Technology**, v. 25, n. 8–9, p. 644–650, 1999.
- MORÁN, J. I. et al. Extraction of cellulose and preparation of nanocellulose from sisal fibers. **Cellulose**, v. 15, n. 1, p. 149–159, 2008.
- NADERI, A.; LINDSTRÖM, T. A comparative study of the rheological properties of three different nanofibrillated cellulose systems. v. 31, n. 3, 2016.

- NADERI, A.; LINDSTRÖM, T.; PETTERSSON, T. The state of carboxymethylated nanofibrils after homogenization-aided dilution from concentrated suspensions: A rheological perspective. **Cellulose**, v. 21, n. 4, p. 2357–2368, 2014.
- NAM, S. et al. Segal crystallinity index revisited by the simulation of X-ray diffraction patterns of cotton cellulose I $\beta$  and cellulose II. **Carbohydrate Polymers**, v. 135, p. 1–9, 2016.
- NECHYPORCHUK, O.; BELGACEM, M. N.; BRAS, J. Production of cellulose nanofibrils: A review of recent advances. **Industrial Crops and Products**, v. 93, p. 2–25, 2016.
- NECHYPORCHUK, O.; PIGNON, F.; BELGACEM, M. N. Morphological properties of nanofibrillated cellulose produced using wet grinding as an ultimate fibrillation process. **Journal of Materials Science**, v. 50, n. 2, p. 531–541, 2015.
- NISHIMURA, H. et al. Direct evidence for  $\alpha$  ether linkage between lignin and carbohydrates in wood cell walls. **Scientific Reports**, v. 8, n. 1, p. 1–11, 2018.
- NISHINO, T.; TAKANO, K.; NAKAMAE, K. Elastic modulus of the crystalline regions of cellulose polymorphs. **Journal of Polymer Science Part B: Polymer Physics**, v. 33, n. 11, p. 1647–1651, 1995.
- NISHIYAMA, Y.; LANGAN, P.; CHANZY, H. Crystal Structure and Hydrogen-Bonding System in Cellulose I $\beta$  from Synchrotron X-ray and Neutron Fiber Diffraction. **Journal of the American Chemical Society**, v. 124, n. 31, p. 9074–9082, ago. 2002.
- NLANDU, H. et al. Laccase-Mediated Grafting of Phenolic Compounds onto Lignocellulosic Flax Nanofibers. **Journal of Natural Fibers**, v. 00, n. 00, p. 1–10, 2020.
- OH, S. Y. et al. Crystalline structure analysis of cellulose treated with sodium hydroxide and carbon dioxide by means of X-ray diffraction and FTIR spectroscopy. **Carbohydrate Research**, v. 340, n. 15, p. 2376–2391, 2005.
- OKAHISA, Y. et al. Effects of delignification in the production of plant-based cellulose nanofibers for optically transparent nanocomposites. **Composites Science and Technology**, v. 71, n. 10, p. 1342–1347, 2011.
- OKSANEN, T.; BUCHERT, J.; VIKARI, L. The role of hemicelluloses in the hornification of bleached kraft pulps. **Holzforschung**, v. 51, n. 4, p. 355–360, 1997.
- OLEJNIK, K. et al. Swelling properties and generation of cellulose fines originating from bleached kraft pulp refined under different operating conditions. **Cellulose**, v. 24, n. 9, p. 3955–3967, 2017.
- OLIVEIRA, L. et al. Study of morphological properties and rheological parameters of cellulose nano fibrils of cocoa shell ( *Theobroma cacao* L .). **Carbohydrate Polymers**, v.

214, n. December 2018, p. 152–158, 2019.

ORNAGHI, H. L. et al. Correlation of the thermal stability and the decomposition kinetics of six different vegetal fibers. **Cellulose**, v. 21, n. 1, p. 177–188, 2014.

OSONG, S. H. et al. Qualitative evaluation of microfibrillated cellulose using the crill method and some aspects of microscopy. **Cellulose**, v. 23, n. 6, p. 3611–3624, 2016.

OSULLIVAN, A. C. Cellulose: the structure slowly unravels. **Cellulose**, v. 4, n. 3, p. 173–207, 1997.

OTTESEN, V. et al. Mechanical properties of cellulose nanofibril films : effects of crystallinity and its modification by treatment with liquid anhydrous ammonia. **Cellulose**, v. 26, n. 11, p. 6615–6627, 2019.

OUDIANI, A. EL et al. Crystal transition from cellulose I to cellulose II in NaOH treated *Agave americana* L. fibre. **Carbohydrate Polymers**, v. 86, n. 3, p. 1221–1229, 2011.

PÄÄKKO, M. et al. Enzymatic hydrolysis combined with mechanical shearing and high-pressure homogenization for nanoscale cellulose fibrils and strong gels. **Biomacromolecules**, v. 8, n. 6, p. 1934–1941, 2007.

PÄÄKKÖNEN, T. et al. Effect of xylan in hardwood pulp on the reaction rate of TEMPO-mediated oxidation and the rheology of the final nanofibrillated cellulose gel. **Cellulose**, v. 23, n. 1, p. 277–293, 2016.

PANTHAPULAKKAL, S.; SAIN, M. Isolation of Nano Fibres from Hemp and Flax and Their Thermoplastic Composites. **Plastic and Polymer Technology**, v. 2, n. 1, p. 9–16, 2013.

PARK, C. W. et al. Preparation and properties of holocellulose nanofibrils with different hemicellulose content. **BioResources**, v. 12, n. 3, p. 6298–6308, 2017.

PEDRAZZI, C. et al. Xylans on eucalyptus brown pulp propertie. **Ciencia Rural**, v. 45, n. 9, p. 1585–1591, 2015.

PELLEGRINI, V. DE O. A.; SEPULCHRO, A. G. V.; POLIKARPOV, I. Enzymes for lignocellulosic biomass polysaccharide valorization and production of nanomaterials. **Current Opinion in Green and Sustainable Chemistry**, v. 26, p. 100397, 2020.

PENG, F. et al. Rapid homogeneous lauroylation of wheat straw hemicelluloses under mild conditions. **Carbohydrate Research**, v. 343, n. 17, p. 2956–2962, 2008.

QIAN, R.; TANG, A.; CHEN, G. TEMPO-Mediated Oxidation of Cellulose and Preparation of Cellulose Nanofibrils. **Journal of Biobased Materials and Bioenergy**, v. 5, n. March, p. 253–257, 2011.

QIAO, C. et al. Structure and rheological properties of cellulose nanocrystals suspension. **Food Hydrocolloids**, v. 55, p. 19–25, 2016.

- RABINOVICH, M. L.; MELNICK, M. S.; BOLOBOVA, A. V. The structure and mechanism of action of cellulolytic enzymes. **Biochemistry (Moscow)**, v. 67, n. 8, p. 850–871, 2002.
- RAFSANJANI, A. et al. Hygroscopic swelling and shrinkage of latewood cell wall micropillars reveal ultrastructural anisotropy. **Journal of the Royal Society Interface**, v. 11, n. 95, 2014.
- RAJINIPRIYA, M. et al. Importance of Agricultural and Industrial Waste in the Field of Nanocellulose and Recent Industrial Developments of Wood Based Nanocellulose: A Review. **ACS Sustainable Chemistry and Engineering**, v. 6, n. 3, p. 2807–2828, 2018.
- RAMASAMY, J.; AMANULLAH, M. Nanocellulose for oil and gas field drilling and cementing applications. **Journal of Petroleum Science and Engineering**, v. 184, n. July 2018, 2020.
- RANTANEN, J. et al. Forming and dewatering of a microfibrillated cellulose composite paper. **BioResources**, v. 10, n. 2, p. 3492–3506, 2015.
- RODRIGUES, A. C. et al. Recycling of cellulases in lignocellulosic hydrolysates using alkaline elution. **Bioresource Technology**, v. 110, p. 526–533, 2012.
- RODRIGUES MOTA, T. et al. Plant cell wall composition and enzymatic deconstruction. **AIMS Bioengineering**, v. 5, n. 1, p. 63–77, 2018.
- ROL, F. et al. Pilot-Scale Twin Screw Extrusion and Chemical Pretreatment as an Energy-Efficient Method for the Production of Nanofibrillated Cellulose at High Solid Content. **ACS Sustainable Chemistry and Engineering**, v. 5, n. 8, p. 6524–6531, 2017.
- ROL, F. et al. Progress in Polymer Science Recent advances in surface-modified cellulose nanofibrils. **Progress in Polymer Science**, v. 88, p. 241–264, 2019.
- RUEDA, M. M. et al. Rheology and applications of highly filled polymers: A review of current understanding. **Progress in Polymer Science**, v. 66, p. 22–53, 2017.
- SAITO, T. et al. Homogeneous suspensions of individualized microfibrils from TEMPO-catalyzed oxidation of native cellulose. **Biomacromolecules**, v. 7, n. 6, p. 1687–1691, 2006.
- SAITO, T.; ISOGAI, A. TEMPO-mediated oxidation of native cellulose. The effect of oxidation conditions on chemical and crystal structures of the water-insoluble fractions. **Biomacromolecules**, v. 5, n. 5, p. 1983–1989, 2004.
- SANTOS, V. T. DE O. et al. Role of hemicellulose removal during dilute acid pretreatment on the cellulose accessibility and enzymatic hydrolysis of compositionally diverse sugarcane hybrids. **Industrial Crops and Products**, v. 111, n. December 2017, p. 722–730, 2018.
- SCATOLINO, M. V. et al. Impact of nanofibrillation degree of eucalyptus and Amazonian hardwood sawdust on physical properties of cellulose nanofibril films. **Wood Science and**

- Technology**, v. 51, n. 5, p. 1095–1115, 2017a.
- SCATOLINO, M. V. et al. Influence of cellulose viscosity and residual lignin on water absorption of nanofibril films. **Procedia Engineering**, v. 200, p. 155–161, 2017b.
- SCATOLINO, M. V. et al. Tannin-stabilized silver nanoparticles and citric acid added associated to cellulose nanofibrils: effect on film antimicrobial properties. **SN Applied Sciences**, v. 1, n. 10, 2019.
- SHELLER, H. V.; ULVSKOV, P. Hemicelluloses. **Annual Review of Plant Biology**, v. 61, n. 1, p. 263–289, 2010.
- SCHINDELIN, J. et al. Fiji: An open-source platform for biological-image analysis. **Nature Methods**, v. 9, n. 7, p. 676–682, 2012.
- SEHAQUI, H. et al. Wood cellulose biocomposites with fibrous structures at micro- and nanoscale. **Composites Science and Technology**, v. 71, n. 3, p. 382–387, 2011.
- SHARMA, S. et al. Characterization of micro fibrillation process of cellulose and mercerized cellulose pulp. **RSC Advances**, v. 5, n. 77, p. 63111–63122, 2015.
- SHOKRKAR, H.; EBRAHIMI, S.; ZAMANI, M. Enzymatic hydrolysis of microalgal cellulose for bioethanol production, modeling and sensitivity analysis. **Fuel**, v. 228, n. April 2017, p. 30–38, 2018.
- SILLS, D. L.; GOSSETT, J. M. Bioresource Technology Assessment of commercial hemicellulases for saccharification of alkaline pretreated perennial biomass. **Bioresource Technology**, v. 102, n. 2, p. 1389–1398, 2011.
- SILVA, L. E. et al. Redispersion and structural change evaluation of dried microfibrillated cellulose. **Carbohydrate Polymers**, v. 252, n. September 2020, 2021.
- SINGHANIA, R. R. et al. Role and significance of beta-glucosidases in the hydrolysis of cellulose for bioethanol production. **Bioresource Technology**, v. 127, p. 500–507, 2013.
- SIPPONEN, M. H. et al. Structural changes of lignin in biorefinery pretreatments and consequences to enzyme-lignin interactions. **Nordic Pulp and Paper Research Journal**, v. 32, n. 04, p. 550–571, 2017.
- SIQUEIRA, G. et al. Mechanical properties of natural rubber nanocomposites reinforced with cellulosic nanoparticles obtained from combined mechanical shearing, and enzymatic and acid hydrolysis of sisal fibers. **Cellulose**, v. 18, n. 1, p. 57–65, 2011.
- SIRÓ, I.; PLACKETT, D. Microfibrillated cellulose and new nanocomposite materials: A review. **Cellulose**, v. 17, n. 3, p. 459–494, 2010.
- SOARES, C. et al. Valorization of Jute Biomass : Performance of Fiber – Cement Composites Extruded with Hybrid Reinforcement ( Fibers and Nanofibrils ). **Waste and Biomass**



**Valorization**, 2021.

SOLALA, I.; IGLESIAS, M. C.; PERESIN, M. S. On the potential of lignin-containing cellulose nanofibrils ( LCNFs ): a review on properties and applications. **Cellulose**, v. 8, 2019.

SOUZA, L. O. et al. Study of morphological properties and rheological parameters of cellulose nanofibrils of cocoa shell (*Theobroma cacao* L.). **Carbohydrate Polymers**, v. 214, 2019.

SOVILJ, V.; PETROVIĆ, L. Interaction and phase separation in the system HPMC/NaCMC/SDS. **Colloids and Surfaces A: Physicochemical and Engineering Aspects**, v. 298, n. 1–2, p. 94–98, 2007.

SPENCE, K. L. et al. A comparative study of energy consumption and physical properties of microfibrillated cellulose produced by different processing methods. **Cellulose**, v. 18, n. 4, p. 1097–1111, 2011.

SPIESER, H. et al. Cellulose nanofibrils and silver nanowires active coatings for the development of antibacterial packaging surfaces. **Carbohydrate Polymers**, v. 240, n. April, p. 116305, 2020.

STEFFE, J. F. **Rheological methods in food process engineering**. Michigan: Freeman Press, 1996.

STEINMETZ, V. et al. In-situ extraction of depolymerization products by membrane filtration against lignin condensation. **Bioresource Technology**, v. 311, n. March, p. 123530, 2020.

STEWART, D. Lignin as a base material for materials applications: Chemistry, application and economics. **Industrial Crops and Products**, v. 27, n. 2, p. 202–207, 2008.

SUHAS; CARROTT, P. J. M.; RIBEIRO CARROTT, M. M. L. Lignin - from natural adsorbent to activated carbon: A review. **Bioresource Technology**, v. 98, n. 12, p. 2301–2312, 2007.

SUN, Q. et al. Comparison of changes in cellulose ultrastructure during different pretreatments of poplar. **Cellulose**, v. 21, n. 4, p. 2419–2431, 2014.

SUN, X. et al. Cellulose Nanofibers as a Modifier for Rheology, Curing and Mechanical Performance of Oil Well Cement. **Scientific Reports**, v. 6, p. 1–9, 2016.

SUN, X. et al. Rheology, curing temperature and mechanical performance of oil well cement: Combined effect of cellulose nanofibers and graphene nano-platelets. **Materials and Design**, v. 114, p. 92–101, 2017.

SYVERUD, K. et al. A comparative study of Eucalyptus and Pinus radiata pulp fibres as raw

- materials for production of cellulose nanofibrils. **Carbohydrate Polymers**, v. 84, n. 3, p. 1033–1038, 2011.
- TANG, Z. et al. Influence of cellulose nanoparticles on rheological behavior of oilwell cement-water slurries. **Materials**, v. 12, n. 2, p. 1–14, 2019.
- TARASOV, D.; LEITCH, M.; FATEHI, P. Lignin-carbohydrate complexes: Properties, applications, analyses, and methods of extraction: A review. **Biotechnology for Biofuels**, v. 11, n. 1, p. 1–28, 2018.
- TARRÉS, Q. et al. The suitability of banana leaf residue as raw material for the production of high lignin content micro/nano fibers: From residue to value-added products. **Industrial Crops and Products**, v. 99, p. 27–33, 2017.
- TAYEB, A. H.; TAJVIDI, M.; BOUSFIELD, D. Paper-based oil barrier packaging using lignin-containing cellulose nanofibrils. **Molecules**, v. 25, n. 6, 2020.
- TENHUNEN, T. M. et al. Significance of xylan on the stability and water interactions of cellulosic nanofibrils. **Reactive and Functional Polymers**, v. 85, p. 157–166, 2014.
- THOMSEN, S. T. et al. Water retention value predicts biomass recalcitrance for pretreated biomass: biomass water interactions vary based on pretreatment chemistry and reflect composition. **Cellulose**, v. 28, n. 1, p. 317–330, 2021.
- TONOLI, G. H. D. et al. Properties of cellulose micro/nanofibers obtained from eucalyptus pulp fiber treated with anaerobic digestate and high shear mixing. **Cellulose**, v. 23, n. 2, p. 1239–1256, 2016.
- TORRES, C. E. et al. Enzymatic approaches in paper industry for pulp refining and biofilm control. **Applied Microbiology and Biotechnology**, v. 96, n. 2, p. 327–344, 2012.
- TURBAK, A. F.; SNYDER, F. W.; SANDBERG, K. R. MICROFIBRILLATED CELLULOSE, A NEW CELLULOSE PRODUCT: PROPERTIES, USES, AND COMMERCIAL POTENTIAL. **Journal of Applied Polymer Science**, v. 37, p. 815–827, 1983.
- VASIĆ, K.; KNEZ, Ž.; LEITGEB, M. Bioethanol Production by Enzymatic Hydrolysis from Different Lignocellulosic Sources. **Molecules**, v. 26, n. 3, p. 753, 2021.
- VILA, C. et al. Use of thermogravimetric analysis to monitor the effects of natural laccase mediators on flax pulp. **Bioresource Technology**, v. 102, n. 11, p. 6554–6561, 2011.
- VIRK, A. P. et al. Combined Enzymatic and Physical Deinking Methodology for Efficient Eco-Friendly Recycling of Old Newsprint. **PLoS ONE**, v. 8, n. 8, 2013.
- WADA, M.; IKE, M.; TOKUYASU, K. Enzymatic hydrolysis of cellulose I is greatly accelerated via its conversion to the cellulose II hydrate form. **Polymer Degradation and**

**Stability**, v. 95, n. 4, p. 543–548, 2010.

WALLIS, A., WEARNE, R.H., WRIGHT, P. J. Chemical analysis of polysaccharides in plantation eucalypt woods and pulp. **Appita**, v. 49, p. 258–262, 1996.

WANG, H. et al. Preparation of tough cellulose II nanofibers with high thermal stability from wood. **Cellulose**, v. 21, n. 3, p. 1505–1515, 2014.

WANG, S.; YU, Y.; DI, M. Green modification of corn stalk lignin and preparation of environmentally friendly lignin-based wood adhesive. **Polymers**, v. 10, n. 6, 2018.

WANG, X. et al. Influence of the lignin content on the properties of poly(lactic acid)/lignin-containing cellulose nanofibrils composite films. **Polymers**, v. 10, n. 9, 2018.

WEI, W. B. et al. Chemical and structural characterization of alkaline-extractable hemicelluloses from various eucalyptus species. **Journal of Applied Polymer Science**, v. 130, n. 4, p. 2390–2398, 2013.

WEISS, N. D.; FELBY, C.; THYGESEN, L. G. Water retention value predicts biomass recalcitrance for pretreated lignocellulosic materials across feedstocks and pretreatment methods. **Cellulose**, v. 25, n. 6, p. 3423–3434, 2018.

WEN, Y. et al. Preparation and Characterization of Lignin-Containing Cellulose Nanofibril from Poplar High-Yield Pulp via TEMPO-Mediated Oxidation and Homogenization. **ACS Sustainable Chemistry and Engineering**, v. 7, n. 6, p. 6131–6139, 2019.

XU, Q. H. et al. Fiber surface characterization of old newsprint pulp deinked by combining hemicellulase with laccase-mediator system. **Bioresource Technology**, v. 102, n. 11, p. 6536–6540, 2011.

XU, X. et al. Cellulose Nanocrystals vs. Cellulose Nanofibrils: A Comparative Study on Their Microstructures and Effects as Polymer Reinforcing Agents. **ACS applied materials & interfaces**, v. 5, p. 2999–3009, 2013.

YAN, N. et al. Lignin as a key component in lignin-containing cellulose nanofibrils for enhancing the performance of polymeric diphenylmethane diisocyanate wood adhesives. **ACS Sustainable Chemistry and Engineering**, v. 8, n. 46, p. 17165–17176, 2020.

YE, W. et al. Lignin as a green reductant and morphology directing agent in the fabrication of 3D graphene-based composites for high-performance supercapacitors. **Industrial Crops and Products**, v. 109, n. August, p. 410–419, 2017.

YOO, C. G. et al. The critical role of lignin in lignocellulosic biomass conversion and recent pretreatment strategies: A comprehensive review. **Bioresource Technology**, v. 301, n. January, p. 122784, 2020.

YOU, T. T. et al. Structural elucidation of lignin-carbohydrate complex (LCC) preparations

- and lignin from *Arundo donax* Linn. **Industrial Crops and Products**, v. 71, p. 65–74, 2015.
- YOUSSEFIAN, S.; JAKES, J. E.; RAHBAR, N. Variation of Nanostructures , Molecular Interactions , and Anisotropic Elastic Moduli of Lignocellulosic Cell Walls with Moisture. **Scientific Reports**, n. March, p. 1–10, 2017.
- YOUSSEFIAN, S.; RAHBAR, N. Molecular origin of strength and stiffness in bamboo fibrils. **Scientific Reports**, v. 5, p. 1–13, 2015.
- ZHAO, Y. et al. Lignin-carbohydrate complexes (LCCs) and its role in biorefinery. **Journal of Cleaner Production**, v. 253, p. 120076, 2020.
- ZIDANES, U. L. et al. Preparation and characterization of tannin-based adhesives reinforced with cellulose nano fibrils for wood bonding. **Holzforschung**, v. 75, n. 2, p. 159–167, 2020.
- ZOGLAMI, A.; PAËS, G. Lignocellulosic Biomass: Understanding Recalcitrance and Predicting Hydrolysis. **Frontiers in Chemistry**, v. 7, n. December, 2019.
- ZULUAGA, R. et al. Cellulose microfibrils from banana rachis: Effect of alkaline treatments on structural and morphological features. **Carbohydrate Polymers**, v. 76, n. 1, p. 51–59, 2009.

## CHAPTER II: ARTICLE 1

Submitted and formatted according to the guidelines of the journal: International Journal of Biological Macromolecules

### INFLUENCE OF HEMICELLULOSE CONTENT AND CELLULOSE CRYSTAL CHANGE ON CELLULOSE NANOFIBERS PROPERTIES

**Matheus Cordazzo Dias<sup>1,4\*</sup>, Uasmim Lira Zidanes<sup>1</sup>, Caio Cesar Nemer Martins<sup>1</sup>, Ana Lázara Matos de Oliveira<sup>2</sup>, Renato Augusto Pereira Damásio<sup>3</sup>, Jaime Vilela de Resende<sup>2</sup>, Eduardo Valério de Barros Vilas Boas<sup>2</sup>, Mohamed Naceur Belgacem<sup>4</sup>, Gustavo Henrique Denzin Tonoli<sup>1</sup>, Saulo Rocha Ferreira<sup>5</sup>**

**\*Corresponding author: Matheus Cordazzo Dias**, Department of Forest Science, Federal University of Lavras, C.P. 3037, 37200-900 Lavras, MG, Brazil, e-mail: matheus.cordazzo@gmail.com <https://orcid.org/0000-0002-8154-2543>.

<sup>1</sup> Department of Forest Science, Federal University of Lavras, C.P. 3037, 37200-900 Lavras, MG, Brazil

<sup>2</sup> Department of Food Science, Federal University of Lavras, C.P. 3037, 37200-900 Lavras, MG, Brazil

<sup>3</sup> Klabin, Technology Center, Industrial R&D+I, Fazenda Monte Alegre, St. Harmonia, 84275-000 - Telêmaco Borba, PR, Brazil

<sup>4</sup> Université Grenoble Alpes, CNRS, Grenoble INP (Institute of Engineering Univ. Grenoble Alpes), LGP2, 38000, Grenoble, France

<sup>5</sup> Department of Engineering, Federal University of Lavras, C.P. 3037, 37200-900 Lavras, MG, Brazil

**Abstract:** This study aimed to evaluate the properties of cellulose nanofibers (CNFs) with different hemicellulose contents and cellulose II polymorphs. A link was found between these polysaccharides and the properties of CNFs. A decrease in crystallinity (from 69 to 63%) and changes in the crystalline structure of cellulose subjected to an alkaline environment were observed, promoting the partial conversion of cellulose I to cellulose II (from 2 to 42%) and preventing CNF production at NaOH concentrations higher than 5%. Most treatments showed pseudoplastic fluid behavior, except for the 10% NaOH treatment over 2 hours, which showed Newtonian fluid behavior. The quality index of the reference CNF (TEMPO-oxidized) was the highest ( $80 \pm 3$ ), followed by that of the 5% NaOH-treated ( $68 \pm 3$  and 22% energy savings compared to the untreated sample), and the untreated ( $63 \pm 3$ ) samples; and the 10% NaOH treatments had quality indices of  $51 \pm 3$  and  $32 \pm 1$ , respectively.

**Keywords:** Cellulose nanofibers; Cellulose polymorphs; Nanocellulose; Polyose; Shear rheology.

#### 1. Introduction

In recent years, there has been growing interest the production and application of cellulose nanofibers (CNFs). CNFs are usually obtained from fibers that have native cellulose polymorphs, known as cellulose I. There are three other types of cellulose polymorphs, cellulose II, III, and IV. Cellulose I and II are the most studied and most commonly used in industrial applications. Some works in the

literature report that the conversion of cellulose I to cellulose II hinders the nanofibrillation process [1,2].

Cellulose II can be obtained from native cellulose by mercerization and regeneration processes because it has a more stable structure. However, crystalline structure conversion through these processes results in materials with inferior mechanical properties [2].

One of the essential characteristics of nanocellulose-based materials is their complex rheology. Because of this characteristic, processing is challenging, especially finding the most suitable application according to its produced characteristics, which can vary [3] due to the source of the materials and the method by which the materials were obtained. The deformation of these suspensions at different shear rates is essential in various potential applications [3].

The rheology of an aqueous suspension of nanocellulose is influenced by hydrogen bonding between nanofibrils and water molecules [4], which is directly related to the efficiency and quality of nanofibrillation, where suspensions with high nanocellulose content have a gel-like appearance and consequently a higher viscosity. In comparison, less nanofibrillated materials have a more aqueous appearance and a lower viscosity. The viscosity of nanocellulose materials is an important factor that must be optimized to be low enough to enable the material's processing and high enough to improve the dispersion [5].

The morphological and chemical composition of the raw material affects the rheological and mechanical properties of the obtained cellulose nanomaterial and the quality of the final product [6–8].

The number of studies regarding CNF production and applications has increased progressively; hence, it is essential to extend the knowledge of its behavior and the relations between its chemical composition and the performance of derived materials. Therefore, this study aimed to evaluate the effects of the modifications on the properties of eucalyptus CNFs, especially the rheology of those containing different hemicellulose levels and cellulose I/cellulose II polymorph ratios.

## **2. Experimental**

### **2.1 Materials**

Once-dried BHKP (Bleached eucalyptus kraft pulp) donated by Klabin S.A. (Paraná/Brazil), was used throughout this work. All the materials and chemicals were used as received from the

manufacturers: deionized water; sodium hydroxide (NaOH) (ACS reagent,  $\geq 98\%$ , Sigma–Aldrich, Brazil); TEMPO (2,2,6,6-tetramethyl-1-piperidinyloxy free radical -  $C_9H_{18}NO$ ) (ACS reagent,  $\geq 98\%$ , Alfa Aesar, Germany); hydrochloric acid (HCl) (ACS reagent, 37%, Neon, Brazil); sodium bromide (NaBr) (ACS reagent, 99%, Synth, Brazil); sodium hypochlorite (NaClO) (ACS reagent,  $\geq 10\%$ , Dinâmica, Brazil); absolute ethyl alcohol ( $C_2H_6O$ ) (ACS reagent, 99%, Sigma–Aldrich, Brazil); 0.5 M cupriethylenediamine solution (ACS reagent, Dinâmica, Brazil) and sulfuric acid ( $H_2SO_4$ ) (ACS reagent, 99%, Sigma–Aldrich, Brazil).

## **2.2 Alkaline treatment of cellulose kraft pulp**

The alkaline treatment was performed under different concentration conditions and reaction times to achieve fibers with different hemicellulose contents. This step was carried out according to Dias et al. (2019)[9]. The pulp was treated with 5 and 10 wt% aqueous NaOH solution at 80 °C for 1 and 2 h under continuous stirring (800 rpm). After treatment, the fibers were filtered and repeatedly washed with deionized water until the pH reached neutrality. They were then dried in an air-circulating oven at 50 °C for 24 h.

## **2.3 TEMPO-mediated oxidation treatment of cellulose kraft pulp**

This treatment was also performed as a quality reference to compare the CNF properties obtained after the alkaline treatments. This step was based on the methodology of Fukuzumi et al. (2009)[10]. The fibers (1 g) were suspended in water (40 mL) containing TEMPO (0.016 g) and sodium bromide (0.1 g). The NaClO solution (10 mmol) was added to the slurry, and the mixture was stirred at room temperature for three hours, and a pH of 10 was maintained by adding drops of 0.5 M NaOH. Afterward, 100 mL of ethanol was added to quench the reaction, and the system pH was corrected to 7 by the addition of drops of 0.5 M hydrochloric acid (HCl).

## **2.4 Monosaccharide's quantification**

Monosaccharides (glucan, xylan, mannan and galactan) were determined after acid hydrolysis. The samples were hydrolyzed by adding 50 mg of fibers to 0.5 mL of 72 wt% sulfuric acid. The mixture was heated in a water bath at 30 °C for 1 h and then diluted to 4 wt% sulfuric acid concentrations with deionized water. The diluted mixture was then heated at 105 °C for 150 min before cooling on ice. An ion chromatography system (Dionex ICS 5000, USA) with a Dionex CarboPac PA1 column at 25 °C

with a flow rate of 1 mL min<sup>-1</sup> of MQ-water. The detector sensitivity was optimized by post column addition of 200 mM NaOH at a flow rate of 0.5 mL min<sup>-1</sup> to perform the analysis.

### **2.5 Cellulose nanofibers (CNF) production**

Eucalyptus cellulose fibers were immersed in distilled water at 2 wt% consistency for three days to guarantee fiber swelling. Then, they were nanofibrillated by passing the pulp through an ultrafine grinder Supermasscolloider (model MKCA6-2, stone model MKGA6-80, Masuko Sangyo Co., Ltd., Japan). The stone speed was fixed at 1,500 rpm [9]. Five passes through the equipment were necessary to obtain cellulose nanofibers.

### **2.6 Turbidity, visual inspection, and stability of the suspensions**

The turbidity, measured in Nephelometric Turbidity Units (NTU), of the CNF suspensions was measured with a portable turbidimeter (Aqualytic, AL-250, wavelength 860 nm) on a CNF suspension that was diluted to 0.1 wt% and stirred for 1 min with Ultra Turrax (IKA T-25) at 10,000 rpm. The suspensions were placed in the test locations for photo acquisition. Images were acquired at 0, 10, 30 min and 1, 2, 3, 4, 5, 6, 7, 8, and 24 h. Fiji software was used to estimate the CNF decantation in the suspensions, and then stability was calculated according to Eq. 1 proposed by Silva et al. (2021)[11]:

$$\text{Stability} = \left( \frac{\text{Dispersed}}{\text{Total}} \right) \times 100\% \quad (1)$$

where “Dispersed” is the height corresponding to suspended particles, and “Total” is the height of all the liquid in the recipient location.

### **2.6 Micro size area (μm<sup>2</sup>)**

The CNF suspensions were characterized using a light microscope (Zeiss Axio AX10, Germany). The suspensions were previously diluted to 0.1 wt%, stirred for 1 min with Ultra Turrax (IKA T-25) at 10,000 rpm, and sonicated for 5 min in an ultrasonic bath to obtain a better dispersion. Photographs were taken at 10x magnification and analyzed using Fiji software. The microsized area was obtained by following the methodology described elsewhere [12].

### **2.7 Transmission Electron Microscopy (TEM)**

The morphology of the CNFs was investigated using a Tecnai G2-12 (FEI company, USA) instrument with an accelerated voltage of 80 kV. Sample preparation and TEM configurations followed



recommendations described elsewhere [24]. Diameter measurements of CNFs were performed for at least 300 individual structures per image using Fiji software.

## 2.8 X-ray diffraction (XRD)

XRD analyses were performed using a PANalytical X'Pert PRO MPD X-ray diffractometer (Malvern Panalytical, UK) equipped with an X'celerator detector with a Cu-K $\alpha$  source ( $\lambda = 1.5406 \text{ \AA}$ ) in the  $2\theta$  range of  $10\text{-}40^\circ$ . A step rate of  $0.066^\circ$  was used. The equipment was operated at a tension of 45 kV and a current of 40 mA.

The theoretical coordinates of native cellulose I $\beta$  (full width at half maximum (FWHM) = 0.1) and cellulose II (FWHM = 0.1) were extracted from crystallography information data (.cif) using the software Mercury 2020.2.0 (CCDC, UK) obtained from the Supplementary Information accompanying the original work Nishiyama et al. (2002)[13].

The patterns were deconvoluted using the Gaussian function with Magic Plot 2.9 (Magicplot Systems, Russia). For the amorphous halo, the cellulose II pattern with full width at half maximum (FWHM = 9), only varying its intensity, was used, as suggested in the literature [14]. After deconvolution, the crystalline fraction (CF) was calculated from the ratio between the area below all the crystalline peaks and the total area below the curve, determined after deconvolution from Eq. 2:

$$CF(\%) = \frac{\sum \text{Area}_{\text{Crystalline Peaks}}}{\sum \text{Area}_{\text{Crystalline Peaks}} + \text{Area}_{\text{Amorphous Halo}}} \times 100 \quad (2)$$

For each NaOH-treated sample, the cellulose I (CI) and cellulose II (CII) contents were determined. From the sum of the peak area of the same crystal system ( $\sum$ area for cellulose I and  $\sum$ area for cellulose II), the CI and CII percentages were calculated using Eq. 3 and 4, which were proposed in a study by Oudiani et al. (2011)[15].

$$CI(\%) = \frac{\sum \text{Area}_{\text{CI}}}{\sum \text{Area}_{\text{CI}} + \text{Area}_{\text{CII}}} \times 100 \quad (3)$$

$$CII(\%) = \frac{\sum \text{Area}_{\text{CII}}}{\sum \text{Area}_{\text{CI}} + \text{Area}_{\text{CII}}} \times 100 \quad (4)$$

The crystallite size (CS) of the (200) plane peak was calculated according to Scherrer's equation (Eq. 5):

$$D = \frac{K \times \lambda}{\beta \times \cos\theta} \quad (5)$$

where  $D$  is crystallite size (Å),  $K$  (0.9) is a constant that refers to crystal shape,  $\lambda$  is the wavelength of the ray used (copper),  $\beta$  is the FWHM of the peak, in radians, and  $\theta$  is Bragg's angle of (200) plane diffraction.

## 2.9 Rheological behavior

The rheological behavior of CNF suspensions at a 1% wt concentration at 25 °C was studied on a HAAKE ReoStress 6000 (Thermo Scientific, Karlsruhe, Germany) rheometer coupled to a HAAKE A10 (Thermo Scientific) thermostatic bath and a universal temperature control system HAAKE UTM Controller (Thermo Scientific brand, Karlsruhe, Germany) using a CC25 DIN Ti concentric cylinder sensor ( $D = 25.0$  mm; Gap = 5.3 mm). The Newton law (Eq. 6), Power-law (Eq. 7), and Herschel-Bulkley (Eq. 8) models were adjusted to the data of the second increasing curve to determine the fluid flow profile and obtain the viscosity. The adjustment of the models was performed by the Statistical Analysis System 9.1.2 statistical package (SAS Institute Inc, USA) using three repetitions:

$$\tau = \mu \times \gamma \quad (6)$$

where  $\tau$  is the shear stress in (Pa),  $\mu$  is the dynamic viscosity (Pa.s), and  $\gamma$  is the shear rate ( $s^{-1}$ ).

$$\tau = K \times \gamma'^n \quad (7)$$

where  $\tau$  is the shear stress in (Pa),  $K$  is the consistency index ( $Pa \cdot s^n$ ),  $\gamma'$  is the deformation rate ( $s^{-1}$ ), and  $n$  is the flow behavior index (dimensionless).

$$\tau = \tau_0 + K \times \gamma'^n \quad (8)$$

where  $\tau$  is the shear stress in (Pa),  $\tau_0$  is the yield stress in (Pa),  $K$  is the consistency index ( $Pa \cdot s^n$ ),  $\gamma'$  is the deformation rate ( $s^{-1}$ ), and  $n$  is the flow behavior index (dimensionless).

The apparent viscosity values were evaluated at a shear rate of  $100 \text{ s}^{-1}$ , which, according to Souza et al. (2019)[16], corresponds to a deformation commonly suffered by fluids in industrial pipes due to processes such as pumping and agitation.

## 2.10 CNF films casting

Films were formed by casting, in which 60 mL of samples (1 wt%) was sonicated (Sonifier model QR500, Ecosonics, Brazil) at 40% power of the ultrasound for homogenization and later poured

onto 15 cm diameter acrylic Petri dishes. The samples were kept in an acclimatized room at  $23 \pm 2$  °C and a relative humidity of 50% until water evaporation. CNF films were formed after approximately seven days under those conditions.

### 2.11 Transparency at 550 nm (%)

The transmittance of the CNF films was measured at a wavelength of 550 nm using a UV spectrophotometer (SP 2000 UV, Bel photonics, Italy) in photometric mode. For each sample, five measurements were performed for samples from at least three different films. The transparency ( $T_{550}$ ) of the film samples was calculated according to Eq. 9 adapted from the work of Sothornvit et al. (2010)[17]:

$$T_{550} = \frac{(\log \%T)}{b} \quad (9)$$

where %T is the percent transmittance and b is the film thickness (mm).

### 2.12 Mechanical properties of CNF films

The tensile properties were measured with a tensile testing machine (Instron 3365, USA) equipped with a load cell of 5 kN capacity. The films with nominal dimensions of 100 mm x 15 mm were pulled at a speed of approximately 5 mm/min, starting with an initial separation of 50 mm between clamping jaws. The tensile properties of the samples were determined based on the ASTM Standard Method D 882–12. To measure the film thickness, a digital rapid advance micrometer (0–30 mm) with a resolution of 0.001 mm was used, and ten random measurements were made for each specimen. Six replicates of each film were tested.

### 2.13 Simplified quality index (\*Q.I.)

Distinct CNFs were evaluated according to the simplified quality index (\*Q.I.) adapted from the work of Desmaisons et al. (2017)[12]. In contrast with the original quality index, this adapted simplified version is based on four parameters (turbidity, transparency at 550 nm, Young's modulus, and area of microparticles), which are considered and used for the \*Q.I. calculation according to the Eq. 10:

$$\begin{aligned} * Q. I. = & (3 \times \text{turbidity mark}) + (3 \times \text{transparency mark}) + (3 \times \text{Young's modulus mark}) \\ & + (1 \times \text{micro size mark}) \end{aligned} \quad (10)$$

where the marks are calculated from the raw measured values as indicated in the original publication.

The resulting Eq. 11 including the raw test values was therefore:

$$* Q. I. = 0.3X_1 + 4.95 \ln(X_2) - 0.108 \times X_3^2 + 3.81 \times X_3 - 2.67 \ln(X_4) + 53.91 \quad (11)$$

where  $X_1$  is the turbidity (NTU),  $X_2$  is the transparency (%),  $X_3$  is Young's modulus (GPa), and  $X_4$  is the micro size area ( $\mu\text{m}^2$ ).

### 2.14 Statical analysis

Quantitative analyses that required repetition were submitted to statistical validation. Tukey's test at 95% significance was applied to investigate whether the averages were significantly different from those of the untreated sample. Statistical analyses were performed using the free software SISVAR version 5.6.

## 3. Results and discussion

To better communicate the results and facilitate the reading of the text, Table S1 summarizes each treatment carried out in this study, the materials and their respective identification codes.

### 3.1 Hemicellulose quantification

Table 1 gives the chemical composition of the eucalyptus fibers before and after the TEMPO and alkaline treatments. All treatments involved removing the hemicellulose from the pulp, although the alkaline treatment was more efficient than the TEMPO treatment.

**Table 1:** Average and standard deviation of the cellulose and hemicellulose contents of Eucalyptus fibers (F) before and after TEMPO and alkaline treatments. \* Different letters in the same column indicate significant ( $\rho \leq 0.05$ ) differences between the samples for Tukey's test. ND = Not detected.

Samples	Cellulose (%)	Xylan (%)	Mannan (%)	Galactan (%)	Total hemicellulose (%)
Untreated_F	83.52 ± 0.44 <sup>c</sup>	16.14 ± 0.20 <sup>a</sup>	0.10 ± 0.14 <sup>a</sup>	0.04 ± 0.06 <sup>a</sup>	16.28 ± 0.40 <sup>a</sup>
TOF	84.83 ± 0.45 <sup>c</sup>	14.85 ± 0.01 <sup>b</sup>	0.22 ± 0.30 <sup>a</sup>	ND	15.17 ± 0.45 <sup>b</sup>
Na5_2_F	89.82 ± 0.77 <sup>b</sup>	9.84 ± 0.52 <sup>c</sup>	0.11 ± 0.16 <sup>a</sup>	0.03 ± 0.04 <sup>a</sup>	9.98 ± 0.72 <sup>c</sup>
Na10_1_F	95.77 ± 1.35 <sup>a</sup>	4.06 ± 0.26 <sup>d</sup>	ND	ND	4.06 ± 0.26 <sup>d</sup>
Na10_2_F	96.58 ± 1.13 <sup>a</sup>	3.30 ± 0.11 <sup>e</sup>	ND	ND	3.30 ± 0.11 <sup>e</sup>

The hemicellulose content decreased from 16.28 ± 0.39 in Untreated\_F to 3.30 ± 0.11 in Na10\_2\_F. Higher NaOH concentrations and longer reaction times led to lower hemicellulose contents. Xylan was the major hemicellulosic compound in the fibers, despite treatment. Mannan and galactan

were also found in the hemicellulosic fraction, but at extremely low proportions, lower than 0.22%. In fact, neither was detected in Na10\_1\_F and Na10\_2\_F, and galactan was not found in TOF. Hardwood pulp fibers such as those from Eucalyptus contain xylan, which is mainly located on the fiber surface. The relative xylan content is higher than that in the corresponding inner layers after the kraft cooking process [18], where chemical attack is most efficient, which explains the effect of the treatments.

Hemicellulose presents a higher affinity for water than cellulose. Reducing the xylan content in the CNFs modifies the rheological behavior of the suspension, resulting in a weaker gel structure [19], which may affect the nanofibrillation efficiency.

### **3.2 Turbidity, visual inspection, and stability of the CNF suspensions**

As expected, TOCNF showed the lowest turbidity ( $83 \pm 5$  NTU). The Na5\_2\_N treatment promoted less turbidity ( $359 \pm 4$  NTU) than the Untreated\_N treatment ( $377 \pm 3$  NTU), suggesting that treatment with a solution of 5% NaOH can increase the degree of nanofibrillation of the material, while Na10\_1\_N and Na10\_2\_N showed the highest values ( $706 \pm 8$  and  $912 \pm 1$  NTU, respectively), indicating less nanofibrillation and aggregation of these CNFs. The turbidity is linked to the material's size; if the suspension is only composed of nanoscale materials, the turbidity value is close to zero. However, the presence of non-nanofibrillated material in the suspension tends to increase the turbidity. These results demonstrate the importance of maintaining certain hemicellulose levels to avoid coalescence between the cellulose micro/nanofibrils.

The sedimentation analysis and the percentage stability over time allowed evaluation of the general stability of the aqueous CNF suspensions (Fig. 1).

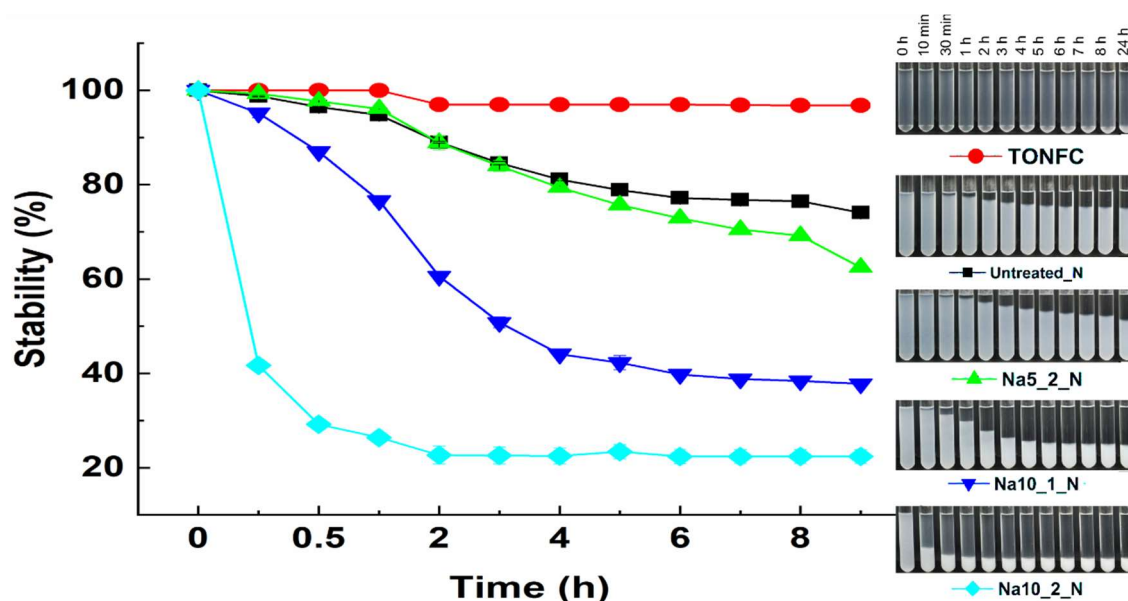


**Fig. 1.** A) Dispersion states of the 0.1 wt.% CNF suspensions at 0, 10, 30 min, 1, 2, 3, 4, 5, 6, 7, 8, and 24 h. Influence of time on CNF suspension stability in water.

TOCNF showed the most stable behavior (97% after 24 h compared to 74% Untreated\_N) among all the samples, corroborating the previous results. Nanoscale cellulose particles are stable due to Brownian motion, which maintains the suspended particles through the interaction of repelling forces, according to Silva et al. (2021)[20].

The sedimentation results show a tendency of NaOH to strongly affect the stability of the suspension. After 24 h, the CNF Na5\_2\_N showed a stability of approximately 62%, followed by Na10\_1\_N and Na10\_2\_N with 38% and 22% stability, respectively. The stability decrease may be related to two factors: (i) the removal of hemicellulose with the increase in alkali concentration and (ii) partial conversion of cellulose I to cellulose II. Hemicellulose acts as an inhibitor of cellulose coalescence. Therefore, as the removal of hemicellulose increases, the cellulose fibrils tend to agglomerate more, consequently decreasing the suspension stability.

During alkali treatment, cellulose microfibrils agglomerate via interdigitation. According to Lee et al. (2018)[21], the polarities of the cellulose II nanofibrils are the opposites of those of the adjacent nanofibrils; thus, neighboring nanofibrils intermingle into irregular aggregates.

### 3.3 CNF morphology

Fig. 2 shows the CNF networks of Untreated\_N (Fig. 2a), TOCNF (Fig. 2b), Na5\_2\_N (Fig. 2c), Na10\_1\_N (Fig. 2d) and Na10\_2\_N (Fig. 2e).

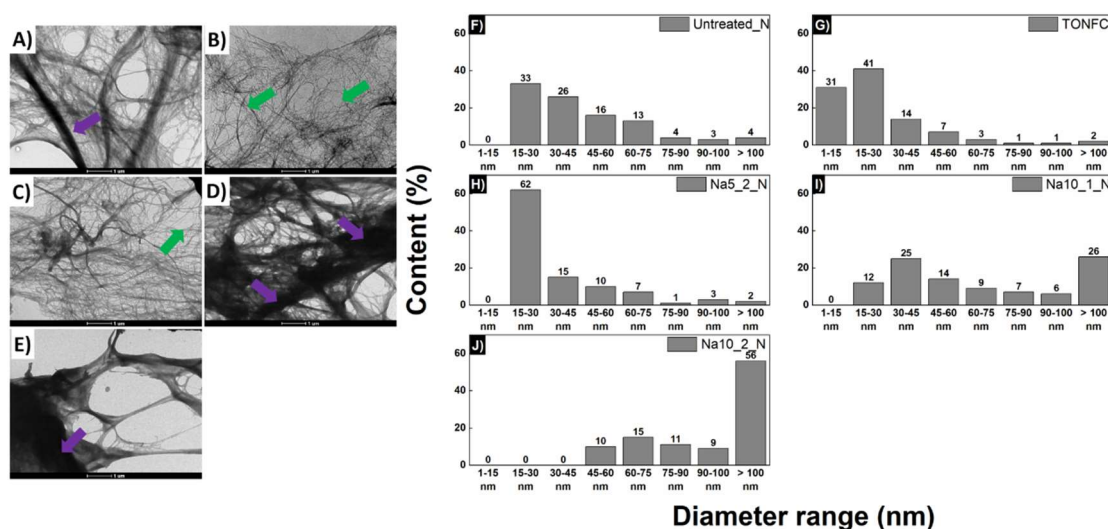


**Fig. 2.** Typical transmission electron microscopy (TEM) and diameter distribution of CNFs and images from (A and F) Untreated\_N; (B and G) TOCNF; (C and H) Na5\_2\_N; (D and I) Na10\_1\_N; and (E and J) Na10\_2\_N. The green arrows indicate more individualized CNFs, while purple arrows indicate more electrodense regions and consequently less individualized CNFs.

Note that as expected, TOCNF produced more individualized CNFs (indicated by green arrows) with smaller diameters ( $26 \pm 20$  nm), followed by Na5\_2\_N with an average diameter of approximately  $34 \pm 22$  nm, while Untreated\_N led to CNFs with an average diameter of approximately  $45 \pm 23$  nm. Na10\_1\_N showed nanofibril structures with an average diameter of  $77 \pm 48$  nm, and Na10\_2\_N showed structures with an average diameter greater than 100 nm (approximately  $194 \pm 171$  nm). These results are associated with the results obtained in the turbidity analysis, in which the treatments with smaller diameters were also those with lower turbidity values (Table 2).

With the excessive decrease in the hemicellulose content before the CNF is obtained (Figs. 2d and 2e), the products have larger diameters, indicating less fibril individualization, evidencing, once again, the role of these noncellulosic polysaccharides as regulators of the morphological properties of the CNF.

More intense alkaline treatments led to a higher degradation of hemicellulose (xylan) from the fiber structure, forming aggregates of cellulose fibrils and affecting the CNF network structure (Figs. 2d and 2e). Furthermore, surface xylan played a significant role as an electrostatic stabilizer in the CNF dispersions by reducing the cohesion energy between the fibrils, whereas the removal of xylan drastically changed the CNF dispersion properties [22,23].

Fig. 2 also shows the diameter distribution of CNFs produced under different conditions. With average diameters lower than 30 nm, which make the CNFs potentially useful as reinforcing agents in composites [24], the content of CNFs was approximately 33%, 72%, and 62% for Untreated\_N, TOCNF, and Na5\_2\_N, respectively, and approximately 12% and 0% for Na10\_1\_N and Na10\_2\_N, respectively. These results indicate that the alkali-treated sample containing approximately 10% hemicellulose (Na5\_2) was the only one that led to better nanofibrillation and individualization of the fibrils. This treatment presented more homogeneous nanofibrils, with 62% of the elements measured within the class of diameter of 15-30 nm, surpassing even the TOCNF treatment that presented 41% of the elements measured within the same class. Dias et al. (2019) stated that hemicellulose content in the range of approximately 9 to 12% facilitates cell wall deconstruction.

TOCNF showed a slight reduction in hemicellulose content (from ~16% to ~15%), and it was the treatment with the best level of nanofibrillation. However, it is essential to note that, unlike other treatments, TEMPO-mediated oxidation promotes cellulose chemical modification through the selective oxidation of C6 hydroxyl groups by inserting carbonyl and aldehyde groups [10].

The darker regions in Figs 2d and 2e overlap, showing less individualization in these samples. The darker color (purple arrows) indicates a more electrodense region. The beam electrons cannot be transmitted in these regions, meaning that they are thicker than in Figs. 2a, 2b, and 2c.

Figs. 2a (Untreated\_N), 2b (TOCNF), and 2c (Na5\_2\_N) more prominently show that these samples had better-structured CNF networks (mainly in Figs. 2b and 2c) compared to the others. The more efficient the fibrils' individualization was, the greater the surface area of the material, allowing it to have more sites available to bind with water molecules, contributing to its final gel consistency. As previously shown in the WRV analysis, the partial removal of xylan to a certain point facilitates the penetration of water molecules into the cellulose fibrils, improving the CNF network's swelling. According to Pääkkönen et al. (2016) [19], the swelling level has a considerable contribution to the gel network's quality, rheological behavior, and dewatering behavior of CNF suspensions.

### 3.5 X-ray diffraction (XRD)

Fig. 3 shows that samples Untreated\_N and TOCNF present the typical parallel crystalline structure of cellulose I $\beta$  with peaks at  $2\theta = 14.9^\circ, 16.4^\circ, 20.5^\circ, 22.6^\circ$  and  $34.7^\circ$ , corresponding to lattice



planes (1-10), (110), (102), (200) and (004), respectively [25]. Sample Na5\_2\_N presents all the mentioned peaks related to cellulose I $\beta$ . However, a displacement of the peak at  $2\theta = 22.6^\circ$  can be attributed to the beginning of the formation of an additional peak at  $2\theta = 22^\circ$ . It corresponds to the lattice plane (020) of cellulose II, which may indicate the beginning of cellulose mercerization [15].

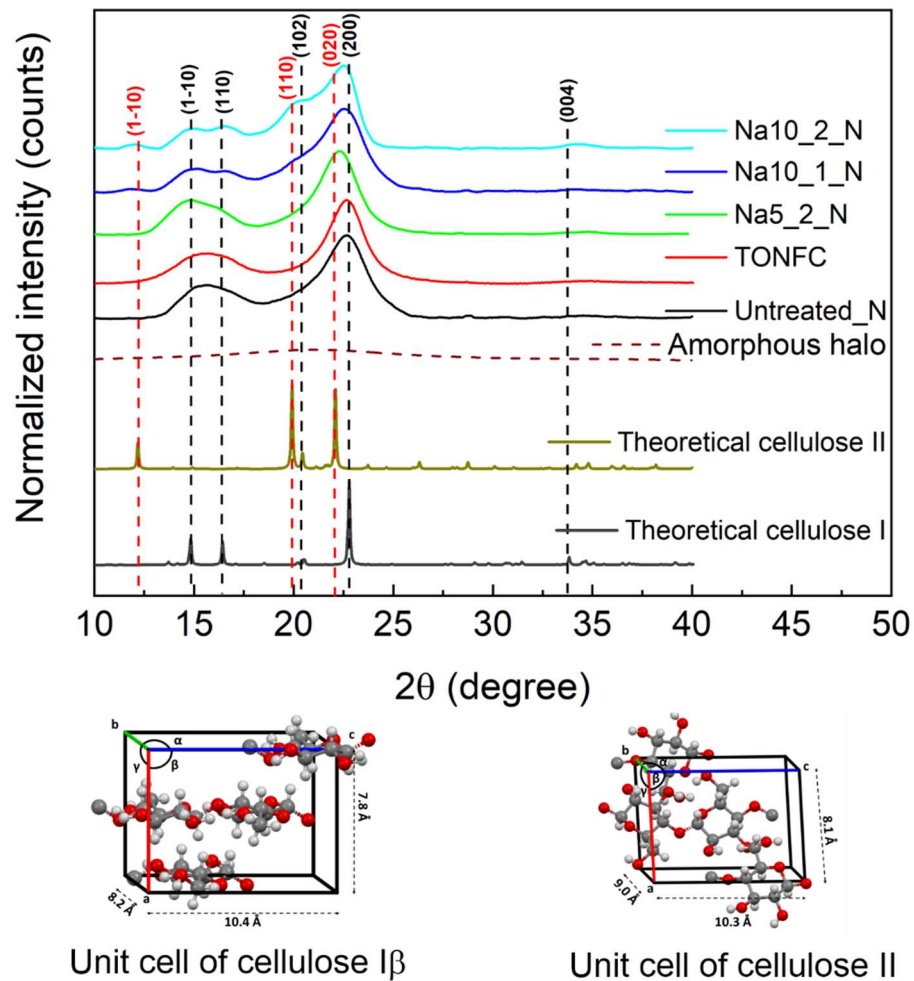


**Fig. 3.** Typical X-ray patterns of Eucalyptus CNF samples obtained from fiber pulps before and after TEMPO and alkaline treatments. Characteristic peaks and the associated lattice planes are indicated for Cellulose I $\beta$  (black dashed lines) and Cellulose II (red dashed lines), respectively. An amorphous halo of cellulose II with an FWHM of 9 is used as a reference for crystalline fraction calculation.

Fig. 3 also shows the partial conversion from native cellulose I $\beta$  to cellulose II on fibers treated with an alkali concentration of 10% (Na10\_1\_N and Na10\_2\_N). The diffraction peaks observed at  $2\theta = 12.2^\circ$ ,  $20.1^\circ$  and  $22.1^\circ$  correspond to the (1-1 0), (110) and (020) lattice planes of cellulose II, respectively [25].

The crystalline fractions (CFs) were calculated using peak deconvolution and an area-based method because the amorphous component used in the Segal method is substantially influenced by the

overlap of crystalline peaks [14]. Table 2 shows the modifications that occurred in the samples after the respective treatments. A higher CF average was found in Untreated\_N, followed by TOCNF and the alkaline treatments Na5\_2\_N, Na10\_1\_N and Na10\_2\_N.

**Table 2:** Average and standard deviation values of the crystalline fraction (CF) and crystallite size (CS) for Eucalyptus CNFs produced under different conditions. Different letters in the same column indicate significant ( $p \leq 0.05$ ) differences between the samples for Tukey's test.

Samples	Crystalline fraction (CF%)	Cellulose I (%)	Cellulose II (%)	Crystallite size (CS nm)
Untreated_N	69 ± 1 <sup>a</sup>	100	0	3.23 ± 0.02 <sup>c</sup>
TOCNF	67 ± 1 <sup>a</sup>	100	0	3.63 ± 0.03 <sup>a</sup>
Na5_2_N	67 ± 1 <sup>a</sup>	98	2	3.49 ± 0.04 <sup>b</sup>
Na10_1_N	63 ± 2 <sup>b</sup>	73	23	2.78 ± 0.01 <sup>d</sup>
Na10_2_N	63 ± 1 <sup>b</sup>	58	42	2.31 ± 0.01 <sup>c</sup>

All the treatments impacted the crystallinity of the cellulose. TEMPO-mediated oxidation preserved the native cellulose I structure of the sample. A slight (nonsignificant) decrease in TOCNF crystallinity was observed. This decrease in crystallinity may indicate that decrystallization of crystalline cellulose presumably occurred to some extent under oxidation [26].

The NaOH concentration also influenced the CF of the samples. As the NaOH concentration increased, CF decreased, probably due to the beginning of cellulose mercerization, inducing irreversible transformation of the native crystalline structure into cellulose II. According to Banvillet et al. (2021) [27], the formation of the cellulose II crystalline structure was globally less organized, leading to a decrease in crystallinity.

In Na10\_1\_N and Na10\_2\_N, cellulose II formation with antiparallel chains (Fig. 3) resulted in a gradual decrease in the cellulose I crystalline regions to soda cellulose I crystallites (Table 3). Cellulose I with antiparallel chains could absorb more alkaline solution, and then it was converted into cellulose II [15]. Furthermore, the conversion to cellulose II by the alkaline solution made fibrillation more complicated because of the aggregation via the interdigitation of micro/nanofibrils in the fiber's secondary cell wall [1].

The untreated sample had a crystallite size of 3.23 ± 0.05 nm (Table 3). The following TEMPO treatment led to an increase in CS (3.63 ± 0.03 nm). The explanation for this increase is that during TEMPO-mediated oxidation, the intra- and intermolecular repulsion increases with the selective

oxidation of hydroxyl groups at C6, leading to an increase in crystallite size. TEMPO-mediated oxidation is known to insert negative charges to form strong electrostatic repulsion between cellulose chains in water [28].

Na5\_2\_N also led to an increase in the CS ( $3.49 \pm 0.04$  nm). This increase may be due to the rearrangement in the crystal orientation and formation of some interstitial coalescence during the conversion of the (200) plane to the (020) plane [29]. In contrast, Na10\_1\_N and Na10\_2\_N showed decreased CS,  $2.78 \pm 0.01$  nm, and  $2.31 \pm 0.01$  nm, respectively. The stronger alkali solution could penetrate the crystalline regions, resulting in a disorder in the fiber crystallites, leading to decreased sizes.

### 3.6 Rheological behavior

The rheological behavior of the Eucalyptus CNF suspensions was investigated at 25 °C. The curves of apparent viscosity as a function of shear rate are shown in Fig. 4.

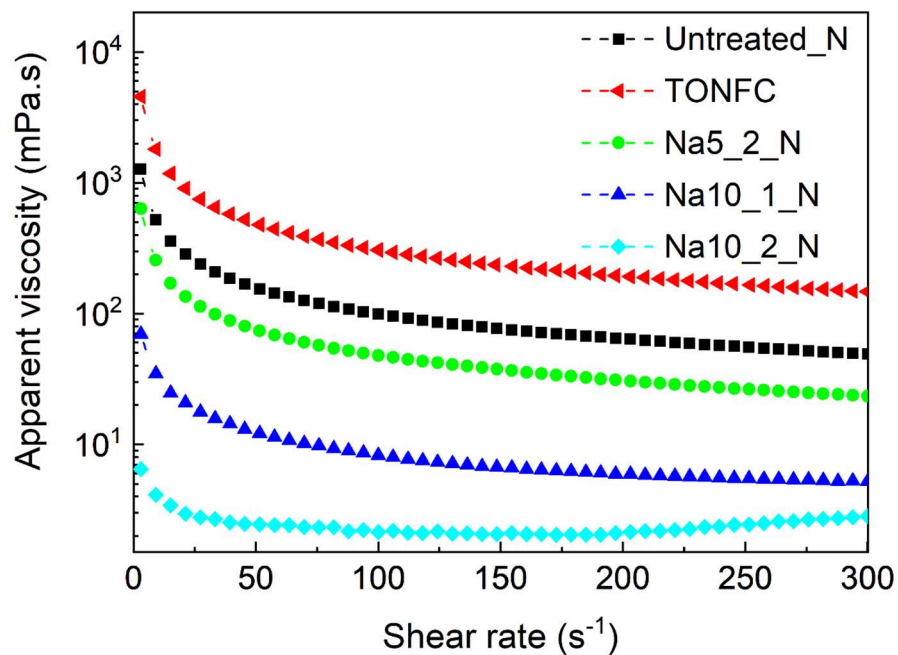


**Fig. 4.** Apparent viscosity vs. shear rate for the CNF suspensions under different conditions.

In Table 3, Newton's Law was adequately adjusted for Na10\_2\_N ( $R^2 \geq 0.9544$ ), while the Power law and Herschel-Bulkley models were adjusted for Untreated ( $R^2 \geq 0.9963$  and  $0.9984$ , respectively), TOCNF ( $R^2 \geq 0.9975$  and  $0.9983$ , respectively), Na5\_2\_N ( $R^2 \geq 0.9941$  and  $0.9957$ , respectively) and Na10\_1\_N ( $R^2 \geq 0.9883$  and  $0.9963$ , respectively). All the samples presented low square root mean square error (RMSE) values ( $\leq 0.17$ ).

**Table 3:** Parameters of the Newton model for EUC10% 2H and power law and Herschel-Bulkley models for Untreated\_N, TOCNF\_N, Na5\_2\_N, and N10\_1\_N.

Newton's Law								
Sample	$\mu$	Pr > t	R <sup>2</sup>	RMSE	$\eta_{\text{initial}}$ (mPa.s)	$\eta_{100}$ (mPa.s)		
Na10_2_N	0.0024	<.0001	0.9544	0.05	6.0 ± 2	2.0 ± 0.1		
Power law								
Sample	k (Pa.s <sup>n</sup> )	n (-)	Pr > t	R <sup>2</sup>	RMSE	$\eta_{\text{initial}}$ (mPa.s)	$\eta_{100}$ (mPa.s)	
Untreated_N	2.08	0.34	<.0001	0.9963	0.17	1265 ± 26	99.0 ± 1.0	
TOCNF_N	11.65	0.26	<.0001	0.9975	0.11	4450 ± 131	307.0 ± 5.0	
Na5_2_N	1.01	0.34	<.0001	0.9941	0.10	635 ± 34	48.0 ± 0.7	
Na10_1_N	0.08	0.52	<.0001	0.9883	0.04	70 ± 4	8.0 ± 0.1	
Herschel-Bulkley								
Sample	t	k (Pa.s <sup>n</sup> )	n (-)	Pr > t	R <sup>2</sup>	RMSE	$\eta_{\text{initial}}$ (mPa.s)	$\eta_{100}$ (mPa.s)
Untreated_N	1.95	1.10	0.43	<.0001	0.9984	0.11	1265 ± 26	99.0 ± 1.0
TOCNF_N	3.89	9.10	0.29	<.0001	0.9983	0.10	4450 ± 131	307.0 ± 5.0
Na5_2_N	0.81	0.59	0.41	<.0001	0.9957	0.09	635 ± 34	48.0 ± 0.7
Na10_1_N	0.24	0.02	0.73	<.0001	0.9963	0.02	70 ± 4	8.0 ± 0.1

It was observed that the consistency index (K) was higher for TOCNF. A higher value of the (K) factor may indicate suspensions containing CNFs with a higher aspect ratio, which is expected for TEMPO-oxidized CNFs. The (K) and apparent viscosity seem to be strongly influenced by the hemicellulose content. It can be observed that the value decreases clearly from Untreated\_N to Na5\_2\_N and almost reaches zero to Na10\_1\_N. According to Pääkkönen et al. (2016), hemicellulose (especially xylan) is responsible for linking a significant amount of water to the fiber/CNF structure, conferring higher viscosity to the suspensions, thereby increasing the (K) value.

The morphology of the material (each fibril) may be related to the (K) value. Poor nanofibrillated material (Na10\_1\_N and Na10\_2\_N) containing particles with larger dimensions leads to a weak fiber network with lower stiffness, facilitating its breaking and ordering when subjected to shear, thereby decreasing the viscosity [16].

Untreated\_N presented flow index values of 0.34 (Power law) and 0.43 (Herschel-Bulkley), while TOCNF presented the lowest values (0.26 and 0.29 for Power Law and Herschel-Bulkley, respectively). Na5\_2\_N presented flow index values of 0.34 and 0.41 (Power Law and Herschel-

Bulkley, respectively), and Na10\_1\_N presented ( $n$ ) values of 0.52 and 0.73 (Power Law and Herschel-Bulkley, respectively).

The flow index ( $n$ ) depends on the structural properties of the entire suspension (Koponen, 2019) and indicates the degree of non-Newtonian characteristics of the material. The values for all CNF samples (except Na10\_2\_N) in the Power law and Hershel-Bulkley models point to pseudoplastic fluid behavior, presenting values lower than 1. Similar behavior was reported by Naderi et al. (2014) [30] when investigating the viscosity of softwood pulp and reported by Souza et al. (2019) [16] when studying the rheological behavior of Pinus, Eucalyptus, and cocoa shell CNFs. The decrease in viscosity is characteristic of pseudoplastic fluids as the shear rate applied to the fluid increases (Fig. 4). This phenomenon is due to the state of order of the material present in the stable solution, which is disordered, and, as shear is applied, it starts to become organized, decreasing the viscosity.

The ( $K$ ) values can also be linked as an indicator of the viscosity of the suspension, while the ( $n$ ) values can be related to the shear-thinning behavior of the suspension. Thus, highly viscous suspensions would yield larger ( $K$ ) values, while ( $n$ ) values would decrease as the suspensions become more thinning [31].

The rheology of nanocellulose suspensions is dependent on the structure, degree of dispersion, degree of nanofibrillation, and interactions between the nanocellulose and the solvent or matrix material [32]. The presence of a significant amount of surface hydroxyl groups makes them easily dispersed in water and provides fluids with shear-thinning rheology and thixotropy, even at low concentrations [33]. Rheological behavior characterization is essential for understanding nanocellulose applicability to the use of nanocellulose-containing products and processing issues related to coating, extrusion, molding, etc. [6].

Na10\_2\_N presented almost Newtonian flow, and the difference from the other treatments may be due to the low efficiency of nanofibrillation. Fig. 2 shows that there was no good deconstruction of the fiber cell wall in Na10\_2\_N, so there was no efficient individualization of nanoscale fibrils, leading to the absence of a gel-like aspect. Geng et al. (2018) [34] found that without reaching the gel-like point, the behavior of CNF suspensions is almost Newtonian.

The majoritarian presence of large particles may have contributed to this behavior, as observed by Marchessault et al. (1961) [35], who studied the viscosity of cellulose microcrystal suspensions and found that particle size influenced the rheological behavior of suspensions, showing Newtonian behavior. The low concentration (1%) of this suspension (Na10\_2\_N) also contributed to this behavior.

Due to its gel-like behavior, CNFs can be applied in the paper industry as a coating layer on paper and paperboards. Coating processes such as bars and extrusion have the advantages of high flexibility, absence of adhesive, and low production cost compared to a laminated system [36].

The rheological behavior of the CNFs may be correlated to the efficiency of nanofibrillation and the morphology of the material, which explains the lower viscosity of the CNFs of Na10\_2\_N; they have more non-nanofibrillated fibers than other CNFs. This discrepancy may result in the lack of a web-like network, which could facilitate breaking and ordering when the CNFs are exposed to shear force [16]. When nanofibrillation is effective, the surface area increases, and therefore, more interactions between fibril aggregates occur, leading to higher flow resistance of the suspension [37,38].

Two different types of behaviors can be observed in cellulose fiber suspensions: at lower shear rates, the pulp suspension is a Newtonian fluid, and at higher shear rates, pulp behavior is a non-Newtonian fluid [39].

Fig. 5 shows the apparent viscosity of CNFs at  $100 \text{ s}^{-1}$  under different conditions as a function of hemicellulose content. When the hemicellulose content in the CNFs increased, the apparent viscosity also increased, demonstrating a direct correlation ( $R^2 = 0.9966$ ) between these two parameters. The hemicellulose content of Na5\_2\_N decreased by approximately 39% compared with that of Untreated\_N, and the apparent viscosity decreased by approximately 52% at a shear rate of  $100 \text{ s}^{-1}$ . The hemicellulose content of Na10\_1\_N and Na10\_2\_N decreased by 75% and 80%, respectively, whereas the apparent viscosity at shear rate at  $100 \text{ s}^{-1}$  decreased 92% and 98%, respectively.

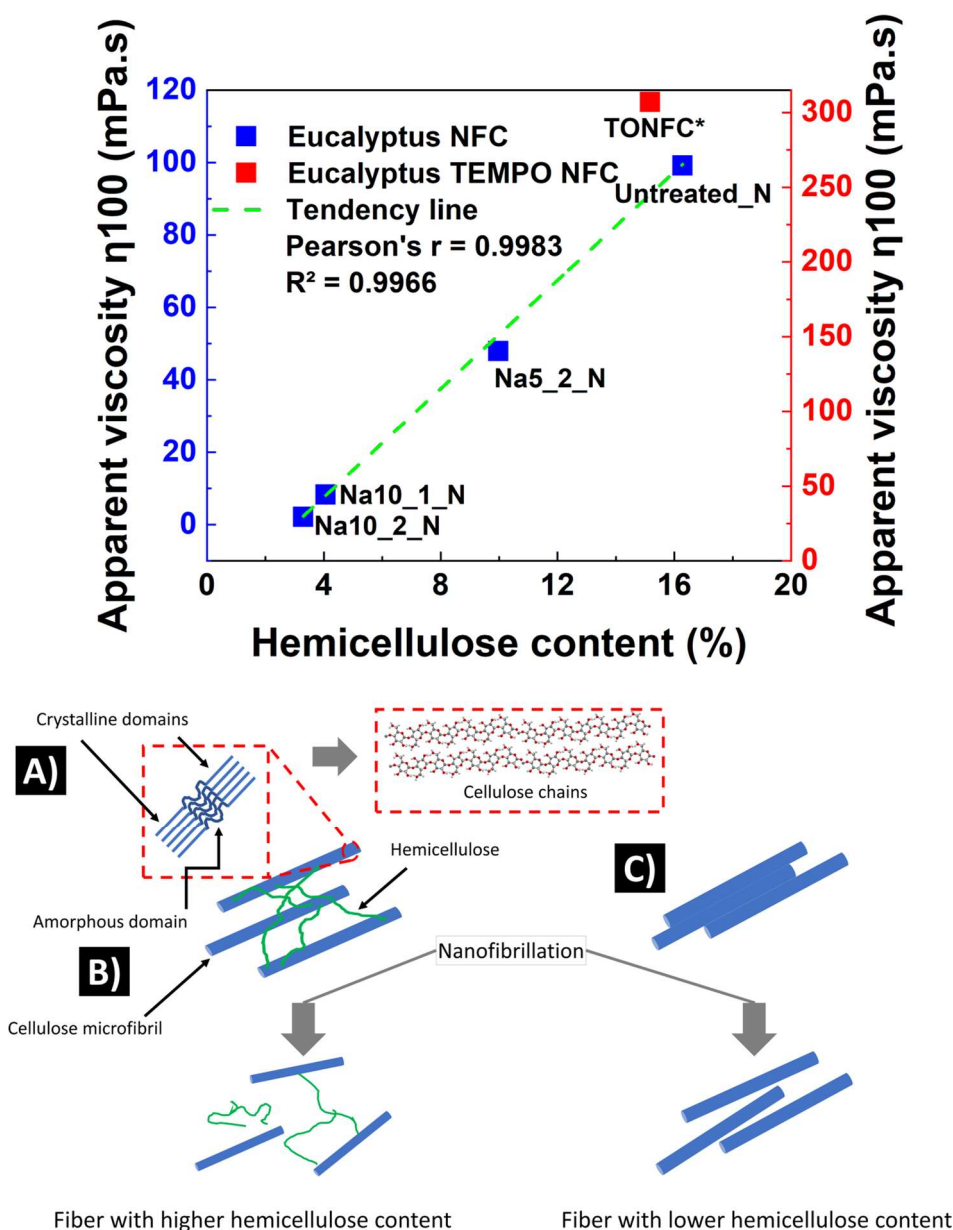


**Fig. 5.** The relationship between apparent viscosity and hemicellulose contents in the different CNFs after nanofibrillation. \* EUC TEMPO was not considered in the correlation because, unlike the other fibers, it was a chemically modified fiber. Schematic representation showing how hemicellulose influences the separation of cellulose microfibrils. A) Representation of cellulose nanofibrils composed of crystalline and amorphous domains, both formed by ordered and disordered regions of cellulose chains; B) fibers with higher hemicellulose content being cut during nanofibrillation and being easily individualized; and C) nanofibrils from fibers with a low hemicellulose content are more difficult to individualize due to the coalescence between microfibrils.

However, in TOCNF, substitution by aldehyde and carboxyl groups in C6 caused the nanofibrils to create strong electrostatic repulsions with each other, allowing a greater number of bonds with water molecules. This bonding resulted in a significant increase in the viscosity of the suspension (210%), despite the slight loss of hemicellulose (~7%) due to oxidation in an alkaline environment.

Hemicellulose plays an essential role in the nanofibrillation of wood pulp because its presence impedes microfibril coalescence due to its ability to bind directly to cellulose microfibrils through

hydrogen bonds [40]. These results indicate that a higher hemicellulose content supports CNF individualization (as shown in Fig. 5) because of the increase in viscosity, implying the formation of a complex network of CNFs. In contrast to cellulose, which is more rigid than the other cell wall components, the behavior of hemicellulose is more plastic, and hemicellulose can be plasticized, reducing the cohesion forces between the microfibrils [41].

The viscosity of polymers and their solutions and suspensions is an essential transport property that involves their process and applications. The rheological behavior of Untreated\_N, TOCNF, and Na5\_2\_N suspensions indicates that these can be applied in processes where viscosity is a determinant, such as coating on the paper surface.

During the coating process, the viscosity of the paper coating is relatively low at high shear rates. After being transferred to the paper surface, CNFs in the coating form a highly viscous layer when the shear force ends [42]. Na10\_1\_N and Na10\_2\_N, due to their low viscosity, may be applied as reinforcement agents, where the viscosity is not a limiting factor.

The viscosities of the Na10\_1\_N and Na10\_2\_N samples at a shear rate of  $100 \text{ s}^{-1}$  are extremely low (8 mPa.s and 2 mPa.s, respectively), indicating that they would not be effective as rheological modifiers in the present conditions. The WRV of these samples was also lower (3.41 g/g and 3.25 g/g, respectively), indicating that they have more free water in the suspension. This free water in greater quantities can harm the healing process of a cement system.

### 3.7 Mechanical performance of the CNF films

Table 4 shows the average and standard deviation values of the mechanical properties of different CNF films.

**Table 4:** Average and standard deviation values of tensile strength, Young's modulus, and elongation at break of the nanostructured films from CNFs under different conditions. \*It was impossible to perform the test on EUC10% 2H because it was not possible to form films for this treatment. Different letters in the same column indicate significant ( $\rho \leq 0.05$ ) differences between the samples for Tukey's test.

Samples	Tensile strength (MPa)	Young's modulus (GPa)	Elongation at break (%)
Untreated_N	41.5 ± 5.5 <sup>b</sup>	3.8 ± 0.8 <sup>bc</sup>	1.8 ± 0.4 <sup>a</sup>
TOCNF	54.5 ± 5.5 <sup>a</sup>	8.5 ± 0.9 <sup>a</sup>	1.2 ± 0.3 <sup>b</sup>
Na5_2_N	45.9 ± 6.5 <sup>ab</sup>	4.2 ± 0.5 <sup>b</sup>	1.7 ± 0.3 <sup>a</sup>
Na10_1_N	24.9 ± 6.4 <sup>c</sup>	3.0 ± 0.6 <sup>c</sup>	1.1 ± 0.2 <sup>b</sup>
Na10_2_N*	-	-	-



TOCNF had higher averages of tensile strength and Young's modulus, whereas Na10\_1\_N had lower averages. Untreated\_N and Na5\_2\_N presented intermediate averages and did not differ from each other. This result can be attributed to the reduction of empty spaces in the interfaces between nanofibrils, promoted by the increase in the highly individualized nanofibril surface area. However, CNF Na10\_1\_N ( $24.9 \pm 6.4$  MPa) exhibited lower nanofibrillation efficiency. A higher free volume between fibrils may have resulted in a reduction in the crystallinity index, thereby decreasing the tensile strength and Young's modulus (3.0 GPa) of fibrils themselves [43].

Another factor that explains the decrease in the mechanical properties of the CNF Na10\_1\_N films is the partial conversion of cellulose I to cellulose II. In the literature, cellulose II has a lower Young's modulus than cellulose I [44].

The hemicellulose content can also influence the mechanical properties of films, as shown in the previous section. Na10\_1 demonstrated a lower hemicellulose content (~4%) than Untreated (~16%), TOCNF (~15%), and Na5\_2 (~10%). When the hemicellulose content declined drastically, the mechanical properties of the Na10\_1 sample film may have decreased. The superiority of samples with a higher hemicellulose content on mechanical properties may be due to many hydroxyl groups that increase the hydrogen bond energy density [45]. Furthermore, the presence of more xylan contributes to the adhesion between CNFs in the dried state, leading to an improvement in the strength of the CNF films [46].

The elongation at break averages of Untreated\_N and Na5\_2\_N were similar. Na10\_1\_N presented a lower average, although it was similar to TOCNF. In the case of Na10\_1\_N ( $1.1 \pm 0.2\%$ ), the decrease may indicate that hemicellulose is essential for plastic deformation of CNF films because of their amorphous nature [47].

Excessive removal of hemicellulose caused coalescence between fibrils, impeding the formation of an interconnected network resulting in low nanofibrillation (Fig. 2D). As already reported, these polymers inhibit the coalescence between microfibrils, facilitating cell wall delamination.

### **3.8 Effect of modifications on quality of cellulose nanofibers**

The CNFs produced after the different treatments were evaluated by the simplified quality index (\*Q.I.) proposed by Desmaisons et al. (2017) [12], obtaining the values shown in Table 5.

**Table 5:** Simplified quality indices of CNFs produced by different treatments. Different letters in the same column indicate significant ( $p \leq 0.05$ ) differences between the samples for Tukey's test.

Sample	Turbidity (NTU)	Transparency (%)	Young's modulus (GPa)	Microsize area ( $\mu\text{m}^2$ )	*Q.I.
Untreated_N	$377 \pm 3^c$	$29 \pm 4^c$	$3.8 \pm 0.8^{bc}$	$32.8 \pm 1^{bc}$	$63 \pm 3^b$
TOCNF	$83 \pm 5^e$	$77 \pm 9^a$	$8.5 \pm 0.9^a$	$22.8 \pm 1^c$	$80 \pm 3^a$
Na5_2_N	$359 \pm 4^d$	$51 \pm 4^b$	$4.2 \pm 0.5^b$	$28.7 \pm 7^c$	$68 \pm 3^b$
Na10_1_N	$706 \pm 8^b$	$46 \pm 8^b$	$3.0 \pm 0.6^c$	$52.5 \pm 13^b$	$51 \pm 3^c$
Na10_2_N	$912 \pm 1^a$	$43 \pm 1^{bc}$	-	$121.2 \pm 22^a$	$32 \pm 1^d$

The TOCNF treatment obtained the highest score in the quality index. It was observed that the Na5\_2\_N treatment obtained a quality index score statistically equal to that of the Untreated\_N sample. However, it promoted economical energy consumption during nanofibrillation, reflecting the efficiency of this treatment in reducing the recalcitrance of the fibers, facilitating its deconstruction into smaller structures. The quality index score for the Untreated\_N sample was similar to those obtained by [48] ( $59.5 \pm 5.5$ ), while the Na10\_1\_N treatment obtained a lower value than that found by [27] ( $54.0 \pm 2.8$ ).

The Na10\_2\_N treatment resulted in the lowest score, demonstrating the influence of the reaction time of the alkaline treatment. As already discussed in previous sections, this behavior may be associated with the hemicellulose content in the samples, which facilitates the deconstruction of the fiber cell wall, as shown in the results of the microsize area, where the treatment with less hemicellulose showed a larger area of non-nanofibrillated particles.

The NaOH treatments, in general, promoted increased transparency of the samples compared to Untreated\_N, which can be attributed to the disorder caused by the alkaline treatment in the cellulose structure during the conversion from the native form to cellulose II and to the increased presence of amorphous structures [49].

#### 4 Conclusions

NaOH treatments under different conditions promoted changes in fiber properties and the crystalline structure of cellulose. The partial removal of hemicellulose to a range close to 10% and the coexistence of cellulose I and cellulose II polymorphs (in low quantity) facilitated the production of CNFs. Hemicellulose influenced the rheological behavior of the CNFs because its removal reduced the

formation of complex networks between nanofibrils because it has free hydrogen bonding sites that allow for cross-linking between cellulose chains. It also influenced their mechanical performance; the higher removal impaired the entanglement of the nanofibrils, weakening the structure of the films. The present paper contributes with valuable information about deconstruction of lignocellulosic biomass and provides data support for further theoretical research.

### **Supporting information**

Supplementary data of this work can be found in the online version of the paper.

### **Acknowledgments**

The authors thank the Research Support Foundation of Minas Gerais (FAPEMIG), the National Council for Scientific and Technological Development (CNPq), the Brazilian Federal Agency for the Support and Evaluation of Graduate Education (CAPES; Funding Code 001), and the Wood Science and Technology graduate program from Federal University of Lavras for providing equipment and financial support. We also thank the Laboratoire Génie des Procédés Papetiers (LGP2) as a part of the LabEx Tec 21 (Investissements d'Avenir—grant agreement no. ANR-11-LABX- 0030) and of the Energies du Futur and PolyNat Carnot Institutes. The Center of Microscopy at the Federal University of Minas Gerais (<http://www.microscopia.ufmg.br>) for providing the equipment and technical support for experiments involving TEM and Thierry Encinas from CMTC - Grenoble for the XRD analysis.

### **Conflict of interest**

The authors declare that they have no conflicts of interest.

## **5 References**

- [1] H. Wang, D. Li, H. Yano, K. Abe, Preparation of tough cellulose II nanofibers with high thermal stability from wood, *Cellulose*. 21 (2014) 1505–1515. doi:10.1007/s10570-014-0222-6.
- [2] S. Sharma, S.S. Nair, Z. Zhang, A.J. Ragauskas, Y. Deng, Characterization of micro fibrillation process of cellulose and mercerized cellulose pulp, *RSC Adv.* 5 (2015) 63111–63122. doi:10.1039/c5ra09068g.
- [3] V. Kumar, B. Nazari, D. Bousfield, M. Toivakka, Rheology of microfibrillated cellulose suspensions in pressure-driven flow, *Appl. Rheol.* 26 (2016) 1–11. doi:10.3933/ApplRheol-26-43534.
- [4] M.A. Hubbe, P. Tayeb, M. Joyce, P. Tyagi, M. Kehoe, K. Dimic-Misic, L. Pal, Rheology of nanocellulose-rich aqueous suspensions: A review, *BioResources*. 12 (2017) 9556–9661. doi:10.15376/biores.12.4.Hubbe.
- [5] M.M. Rueda, M.C. Auscher, R. Fulchiron, T. Périé, G. Martin, P. Sonntag, P. Cassagnau,

- Rheology and applications of highly filled polymers: A review of current understanding, *Prog. Polym. Sci.* 66 (2017) 22–53. doi:10.1016/j.progpolymsci.2016.12.007.
- [6] T. Moberg, K. Sahlin, K. Yao, S. Geng, G. Westman, Q. Zhou, K. Oksman, M. Rigdahl, Rheological properties of nanocellulose suspensions: effects of fibril/particle dimensions and surface characteristics, *Cellulose*. 24 (2017) 2499–2510. doi:10.1007/s10570-017-1283-0.
- [7] O. Nechyporchuk, M.N. Belgacem, J. Bras, Production of cellulose nanofibrils: A review of recent advances, *Ind. Crops Prod.* 93 (2016) 2–25. doi:10.1016/j.indcrop.2016.02.016.
- [8] N. V. Ehman, A.F. Lourenço, B.H. McDonagh, M.E. Vallejos, F.E. Felissia, P.J.T. Ferreira, G. Chinga-Carrasco, M.C. Area, Influence of initial chemical composition and characteristics of pulps on the production and properties of lignocellulosic nanofibers, *Int. J. Biol. Macromol.* 143 (2020) 453–461. doi:10.1016/j.ijbiomac.2019.10.165.
- [9] M.C. Dias, M.C. Mendonça, R.A.P. Damásio, Influence of hemicellulose content of Eucalyptus and Pinus fibers on the grinding process for obtaining cellulose micro / nanofibrils, *Holzforschung*. 73 (2019) 1035–1046.
- [10] H. Fukuzumi, T. Saito, T. Iwata, Y. Kumamoto, A. Isogai, Transparent and high gas barrier films of cellulose nanofibers prepared by TEMPO-mediated oxidation, *Biomacromolecules*. 10 (2009) 162–165. doi:10.1021/bm801065u.
- [11] L.E. Silva, A. de A. dos Santos, L. Torres, Z. McCaffrey, A. Klamczynski, G. Glenn, A.R. de Sena Neto, D. Wood, T. Williams, W. Orts, R.A.P. Damásio, G.H.D. Tonoli, Redisperison and structural change evaluation of dried microfibrillated cellulose, *Carbohydr. Polym.* 252 (2021). doi:10.1016/j.carbpol.2020.117165.
- [12] J. Desmaisons, E. Boutonnet, M. Rueff, A. Dufresne, J. Bras, A new quality index for benchmarking of different cellulose nanofibrils, *Carbohydr. Polym.* 174 (2017) 318–329. doi:10.1016/j.carbpol.2017.06.032.
- [13] Y. Nishiyama, P. Langan, H. Chanzy, Crystal Structure and Hydrogen-Bonding System in Cellulose I $\beta$  from Synchrotron X-ray and Neutron Fiber Diffraction, *J. Am. Chem. Soc.* 124 (2002) 9074–9082. doi:10.1021/ja0257319.
- [14] A.D. French, Increment in evolution of cellulose crystallinity analysis, *Cellulose*. 27 (2020) 5445–5448. doi:10.1007/s10570-020-03172-z.
- [15] A. El Oudiani, Y. Chaabouni, S. Msahli, F. Sakli, Crystal transition from cellulose I to cellulose II in NaOH treated Agave americana L. fibre, *Carbohydr. Polym.* 86 (2011) 1221–1229. doi:10.1016/j.carbpol.2011.06.037.
- [16] L.O. Souza, O.A. Lessa, M.C. Dias, G.H.D. Tonoli, D.V.B. Rezende, M.A. Martins, I.C.O. Neves, J.V. de Resende, E.E.N. Carvalho, E.V. de Barros Vilas Boas, J.R. de Oliveira, M. Franco, Study of morphological properties and rheological parameters of cellulose nanofibrils of cocoa shell (*Theobroma cacao* L.), *Carbohydr. Polym.* 214 (2019). doi:10.1016/j.carbpol.2019.03.037.
- [17] R. Sothornvit, S.I. Hong, D.J. An, J.W. Rhim, Effect of clay content on the physical and antimicrobial properties of whey protein isolate/organo-clay composite films, *LWT - Food Sci. Technol.* 43 (2010) 279–284. doi:10.1016/j.lwt.2009.08.010.
- [18] M.C. Li, Q. Wu, K. Song, S. Lee, Y. Qing, Y. Wu, Cellulose Nanoparticles: Structure-Morphology-Rheology Relationships, *ACS Sustain. Chem. Eng.* 3 (2015) 821–832. doi:10.1021/acssuschemeng.5b00144.
- [19] T. Pääkkönen, K. Dimic-Misic, H. Orelma, R. Pönni, T. Vuorinen, T. Maloney, Effect of xylan in

- hardwood pulp on the reaction rate of TEMPO-mediated oxidation and the rheology of the final nanofibrillated cellulose gel, *Cellulose*. 23 (2016) 277–293. doi:10.1007/s10570-015-0824-7.
- [20] C. Soares, F. Mário, V. Scatolino, L. Eduardo, S. Maria, A. Martins, M. Guimarães, J. Gustavo, H. Denzin, Valorization of Jute Biomass : Performance of Fiber – Cement Composites Extruded with Hybrid Reinforcement ( Fibers and Nanofibrils ), *Waste and Biomass Valorization*. (2021). doi:10.1007/s12649-021-01394-1.
- [21] H. Lee, J. Sundaram, L. Zhu, Y. Zhao, S. Mani, Improved thermal stability of cellulose nano fibrils using low-concentration alkaline pretreatment, *Carbohydr. Polym.* 181 (2018) 506–513. doi:10.1016/j.carbpol.2017.08.119.
- [22] T.M. Tenhunen, M.S. Peresin, P.A. Penttilä, J. Pere, R. Serimaa, T. Tammelin, Significance of xylan on the stability and water interactions of cellulosic nanofibrils, *React. Funct. Polym.* 85 (2014) 157–166. doi:10.1016/j.reactfunctpolym.2014.08.011.
- [23] E. Jin, J. Guo, F. Yang, Y. Zhu, J. Song, Y. Jin, O.J. Rojas, On the polymorphic and morphological changes of cellulose nanocrystals (CNC-I) upon mercerization and conversion to CNC-II, *Carbohydr. Polym.* 143 (2016) 327–335. doi:10.1016/j.carbpol.2016.01.048.
- [24] G.H.D. Tonoli, K.M. Holtman, G. Glenn, A.S. Fonseca, D. Wood, T. Williams, V.A. Sa, L. Torres, A. Klamczynski, W.J. Orts, Properties of cellulose micro/nanofibers obtained from eucalyptus pulp fiber treated with anaerobic digestate and high shear mixing, *Cellulose*. 23 (2016) 1239–1256. doi:10.1007/s10570-016-0890-5.
- [25] S. Nam, A.D. French, B.D. Condon, M. Concha, Segal crystallinity index revisited by the simulation of X-ray diffraction patterns of cotton cellulose I $\beta$  and cellulose II, *Carbohydr. Polym.* 135 (2016) 1–9. doi:10.1016/j.carbpol.2015.08.035.
- [26] Y. Chen, B. Geng, J. Ru, C. Tong, H. Liu, J. Chen, Correction to: Comparative characteristics of TEMPO-oxidized cellulose nanofibers and resulting nanopapers from bamboo, softwood, and hardwood pulps, *Cellulose*. 25 (2018) 895. doi:10.1007/s10570-017-1553-x.
- [27] G. Banvillet, G. Depres, N. Belgacem, J. Bras, Alkaline treatment combined with enzymatic hydrolysis for efficient cellulose nanofibrils production, *Carbohydr. Polym.* 255 (2021). doi:10.1016/j.carbpol.2020.117383.
- [28] A. Isogai, T. Saito, H. Fukuzumi, TEMPO-oxidized cellulose nanofibers, *Nanoscale*. 3 (2011) 71–85. doi:10.1039/c0nr00583e.
- [29] Z. Ling, S. Chen, X. Zhang, F. Xu, Exploring crystalline-structural variations of cellulose during alkaline pretreatment for enhanced enzymatic hydrolysis, *Bioresour. Technol.* 224 (2017) 611–617. doi:10.1016/j.biortech.2016.10.064.
- [30] A. Naderi, T. Lindström, T. Pettersson, The state of carboxymethylated nanofibrils after homogenization-aided dilution from concentrated suspensions: A rheological perspective, *Cellulose*. 21 (2014) 2357–2368. doi:10.1007/s10570-014-0329-9.
- [31] F. Serra-Parareda, Q. Tarrés, P. Mutjé, A. Balea, C. Campano, J.L. Sánchez-Salvador, C. Negro, M. Delgado-Aguilar, Correlation between rheological measurements and morphological features of lignocellulosic micro/nanofibers from different softwood sources, *Int. J. Biol. Macromol.* 187 (2021) 789–799. doi:10.1016/j.ijbiomac.2021.07.195.
- [32] E.J. Foster, R.J. Moon, U.P. Agarwal, M.J. Bortner, J. Bras, S. Camarero-Espinosa, K.J. Chan, M.J.D. Clift, E.D. Cranston, S.J. Eichhorn, D.M. Fox, W.Y. Hamad, L. Heux, B. Jean, M. Korey, W. Nieh, K.J. Ong, M.S. Reid, S. Renneckar, R. Roberts, J.A. Shatkin, J. Simonsen, K. Stinson-Bagby,

- N. Wanasekara, J. Youngblood, Current characterization methods for cellulose nanomaterials, *Chem. Soc. Rev.* 47 (2018) 2609–2679. doi:10.1039/c6cs00895j.
- [33] J. Ramasamy, M. Amanullah, Nanocellulose for oil and gas field drilling and cementing applications, *J. Pet. Sci. Eng.* 184 (2020). doi:10.1016/j.petrol.2019.106292.
- [34] L. Geng, A. Naderi, Y. Mao, C. Zhan, P. Sharma, X. Peng, B.S. Hsiao, Rheological Properties of Jute-Based Cellulose Nanofibers under Different Ionic Conditions, Umesh A, Rajai A, Akira I Nanocelluloses Their Prep. Prop. Appl. ACS Symp. Ser. (2018) 113–132. doi:10.1021/bk-2017-1251.ch006.
- [35] R.H. Marchessault, F.F. Morehead, M.J. Koch, Some Hydrodynamic Properties of Neutral As Related To Size and Shape 1, *J. Colloid Sci.* 344 (1961) 327–344.
- [36] M. Iotti, Ø.W. Gregersen, S. Moe, M. Lenes, Rheological Studies of Microfibrillar Cellulose Water Dispersions, *J. Polym. Environ.* 19 (2011) 137–145. doi:10.1007/s10924-010-0248-2.
- [37] F. Grüneberger, T. Künniger, T. Zimmermann, M. Arnold, Rheology of nanofibrillated cellulose/acrylate systems for coating applications, *Cellulose.* 21 (2014) 1313–1326. doi:10.1007/s10570-014-0248-9.
- [38] K. Pakutsah, D. Aht-ong, Facile isolation of cellulose nanofibers from water hyacinth using water- based mechanical de fi brillation : Insights into morphological , physical , and rheological properties, *Int. J. Biol. Macromol.* 145 (2020) 64–76. doi:10.1016/j.ijbiomac.2019.12.172.
- [39] D. Chaussy, C. Martin, J.C. Roux, Rheological behavior of cellulose fiber suspensions: Application to paper-making processing, *Ind. Eng. Chem. Res.* 50 (2011) 3524–3533. doi:10.1021/ie101591s.
- [40] D. Lin, P. Lopez-sanchez, N. Selway, M.J. Gidley, Food Hydrocolloids Viscoelastic properties of pectin / cellulose composites studied by QCM-D and oscillatory shear rheology, *Food Hydrocoll.* 79 (2018) 13–19. doi:10.1016/j.foodhyd.2017.12.019.
- [41] D.M. de Carvalho, C. Moser, M.E. Lindström, O. Sevastyanova, Impact of the chemical composition of cellulosic materials on the nanofibrillation process and nanopaper properties, *Ind. Crops Prod.* 127 (2019) 203–211. doi:10.1016/j.indcrop.2018.10.052.
- [42] C. Liu, H. Du, L. Dong, X. Wang, Y. Zhang, G. Yu, B. Li, X. Mu, H. Peng, H. Liu, Properties of Nanocelluloses and Their Application as Rheology Modifier in Paper Coating, *Ind. Eng. Chem. Res.* 56 (2017) 8264–8273. doi:10.1021/acs.iecr.7b01804.
- [43] S. Youssefian, J.E. Jakes, N. Rahbar, Variation of Nanostructures , Molecular Interactions , and Anisotropic Elastic Moduli of Lignocellulosic Cell Walls with Moisture, *Sci. Rep.* (2017) 1–10. doi:10.1038/s41598-017-02288-w.
- [44] T. Nishino, K. Takano, K. Nakamae, Elastic modulus of the crystalline regions of cellulose polymorphs, *J. Polym. Sci. Part B Polym. Phys.* 33 (1995) 1647–1651. doi:10.1002/polb.1995.090331110.
- [45] S. Youssefian, N. Rahbar, Molecular origin of strength and stiffness in bamboo fibrils, *Sci. Rep.* 5 (2015) 1–13. doi:10.1038/srep11116.
- [46] M. He, G. Yang, J. Chen, X. Ji, Q. Wang, Production and Characterization of Cellulose Nanofibrils from Different Chemical and Mechanical Pulps, *J. Wood Chem. Technol.* 38 (2018) 149–158. doi:10.1080/02773813.2017.1411368.
- [47] F. Ceccon, M. Matos, C. Jordão, F. Avelino, D. Lomonaco, W. Luiz, E. Magalhães, Enhanced

- micro fibrillated cellulose-based film by controlling the hemicellulose content and MFC rheology, 218 (2019) 307–314. doi:10.1016/j.carbpol.2019.04.089.
- [48] E. Espinosa, F. Rol, J. Bras, A. Rodríguez, Use of multi-factorial analysis to determine the quality of cellulose nanofibers: effect of nanofibrillation treatment and residual lignin content, *Cellulose*. 3 (2020). doi:10.1007/s10570-020-03136-3.
- [49] W. Wang, T. Liang, H. Bai, W. Dong, X. Liu, All cellulose composites based on cellulose diacetate and nano fibrillated cellulose prepared by alkali treatment, *Carbohydr. Polym.* 179 (2018) 297–304. doi:10.1016/j.carbpol.2017.09.098.

## CHAPTER III: ARTICLE 2

Submitted and formatted according to the guidelines of the journal: International Journal of Biological Macromolecules

# ECO-FRIENDLY LACCASE AND CELLULASE ENZYMES PRETREATMENT FOR OPTIMIZED PRODUCTION OF HIGH CONTENT LIGNIN-CELLULOSE NANOFIBRILS

Matheus Cordazzo Dias<sup>1,2\*</sup>, Mohamed Naceur Belgacem<sup>2</sup>, Jaime Vilela de Resende<sup>3</sup>, Maria Alice Martins<sup>4</sup>, Renato Augusto Pereira Damásio<sup>5</sup>, Gustavo Henrique Denzin Tonoli<sup>1</sup>, Saulo Rocha Ferreira<sup>6</sup>

\*Corresponding author: **Matheus Cordazzo Dias**, Department of Forest Science, Federal University of Lavras, C.P. 3037, 37200-900, Lavras, MG, Brazil, e-mail: matheus.cordazzo@gmail.com. <https://orcid.org/0000-0002-8154-2543>

<sup>1</sup> Department of Forest Science, Federal University of Lavras, C.P. 3037, 37200-900, Lavras, MG, Brazil

<sup>2</sup> Université Grenoble Alpes, CNRS, Grenoble INP (Institute of Engineering Univ. Grenoble Alpes), LGP2, 38000, Grenoble, France

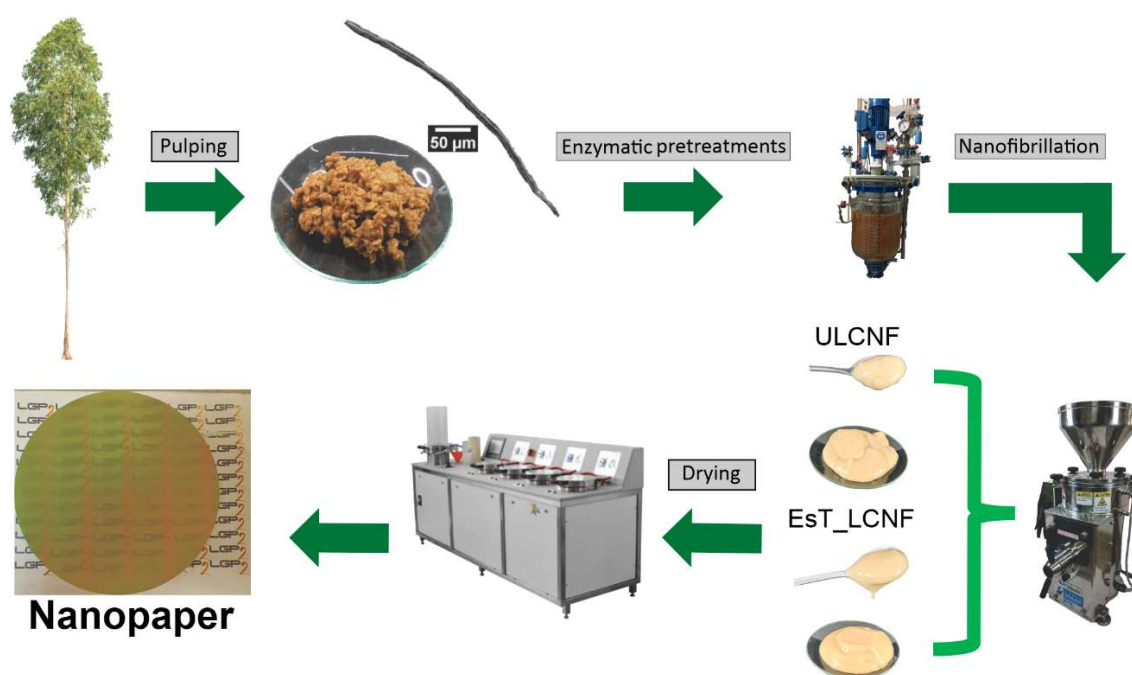
<sup>3</sup> Department of Food Science, Federal University of Lavras, C.P. 3037, 37200-900 Lavras, MG, Brazil

<sup>4</sup> Nanotechnology National Laboratory for Agriculture, Embrapa Instrumentation, 13560-970, São Carlos, SP, Brazil

<sup>5</sup> Klabin, Technology Center, Industrial R&D+I, Fazenda Monte Alegre, St. Harmonia, 84275-000 - Telêmaco Borba, PR, Brazil

<sup>6</sup> Department of Engineering, Federal University of Lavras, C.P. 3037, 37200-900 Lavras, MG, Brazil

### Graphical abstract:





**Abstract:** The objective of this study was to evaluate the impact of a combined enzymatic pretreatment of laccase and endoglucanase for LCNF production. The laccase enzyme loading used was efficient in modifying the lignin to facilitate the action of the endoglucanase enzyme on cellulose without causing the removal of this macromolecule. This pretreatment improved the quality of LCNF ( $61 \pm 3$  to  $71 \pm 2$  points) and, therefore, can be used to produce LCNF for a variety of applications. The LCNF obtained after the enzymatic treatments improved mechanical strength in 24% and exhibited good water vapor ( $2.42 \text{ g.mm/m}^2 \cdot \text{kPa.day}$ ) and grease barrier properties (kit n° 12), being attractive for its use in the packaging industry. The rheology of the LCNF suspensions corroborates this potential application because they exhibited non-Newtonian behavior and can return to the original resting state after the application of a shear force, a typical characteristic of materials of thixotropic nature, playing a key role in the consolidation of the coating during the paper coating process. Finally, this pretreatment could be suitable for industrial production due to reduced energy requirements.

**Keywords:** Cell wall. Cellulose nanofibers. Enzymatic hydrolysis. Lignin. Nanofibrillated cellulose.

## 1. Introduction

Cellulose nanofibrils have been widely studied for the most diverse applications as substitutes for synthetic and non-biodegradable polymers, and almost always, the raw source to produce of this material has been bleached cellulosic pulps, as it is reported that lignin is considered an obstacle in the nanofibrillation process (Wen et al., 2019).

The presence of lignin in the nanofibrils matrix improves the hydrophobicity and thermal stability of cellulose nanofibrils, benefitting the compatibility with various hydrophobic polymers (Gupta et al., 2017). Recently, studies have incorporated lignin-containing cellulose nanofibrils (LCNF) in different applications, like composites films (Wang et al., 2018), additives in papermaking and packaging industries (Tayeb et al., 2020), and as a reinforcement agent in wood adhesives (Yan et al., 2020).

Lignin is linked to hemicellulose through covalent bonds, at the carbon- $\alpha$  and C-4 positions on the benzene ring. Presumably, small-scale intermolecular chemical bonds of lignin-carbohydrates exist natively between lignin, hemicellulose, and cellulose (Zhao et al., 2020). Its monomers' properties and the inter polymer interactions cause this structure to present biological, chemical, and mechanical resistance, hindering separation and recovery of its three main components, characterizing recalcitrance.(Lorenci Woiciechowski et al., 2020).

Thus, for the most effective use of this plant biomass, it is essential to carry out pre-treatments to make cellulose more accessible by modifying its physical and chemical structure, facilitating the conversion of plant fibers into several by-products. (Kumar and Sharma, 2017).

Lignin is the third major component that forms the plant cell wall and the most abundant non-carbohydrate component (Yoo et al., 2020). It is widely accepted that lignin's structure differs considerably due to different conditions of extraction, isolation, and among the most diverse types of plants (Guo et al., 2017).

Researches have described that lignin is highly relevant for the recalcitrance of lignocellulosic biomass (Li et al., 2016). Its structure can inhibit the action of enzymes in cellulose through physical barriers, such as hydrophobicity, surface charges, electrostatic interactions, and interactions between hydrogen bonds, limiting the accessibility of enzymes, decreasing enzyme yield (Li et al., 2020).

Cellulose enzymatic hydrolysis requires physical contact between glycosidic hydrolases and their substrates, which can be obstructed by lignin in several ways (Sipponen et al., 2017). In unbleached pulps, insoluble lignin can block enzyme access to carbohydrate surfaces, or it can irreversibly bind enzymes and prevent enzymes from accessing their substrate. The fate of the catalytic activity of the adsorbed cellulases is under debate since there are reports of cellulases linked to lignin retaining most of their activity (Rodrigues et al., 2012). It is challenging to develop new pretreatments that selectively attack the other compounds to make the cellulose isolation more effective.

Laccase enzymes have emerged as important biotechnological catalysts for their ecological nature and mild working conditions. They are multi-copper enzymes capable of catalyzing the direct oxidation of a wide range of aromatic compounds, such as lignin monomers, of generating reactive radicals, and using molecular oxygen as an oxidizer (Nlandu et al., 2020). However, Steinmetz et al. (2020) demonstrated the potential of laccase as a depolymerizing agent of lignin in a semi-continuous process in mild conditions.

This study aims to evaluate the effectiveness of two sequential enzyme pre-steps in the cellulose nanofibrillation quality and energy consumption: 1) laccase enzyme to depolymerize lignin; and 2) cellulase enzymes to facilitate mechanical shearing actions and investigate if it may be a viable alternative to increase the yield and quality of lignin-cellulose nanofibrils.

## 2. Experimental section

### 2.1 Materials

Unbleached Eucalyptus kraft liner pulp donated by Klabin S.A. (Paraná/Brazil) was used. All the materials were used as received from the producers: acetic acid (CH<sub>3</sub>COOH) (ACS reagent, ≥99.7%, Sigma-Aldrich, France); deionized water; endoglucanase FiberCare 4890 ECU/g enzyme solution (Novozymes, Denmark); laccase Novozym ≥1000 LAMU/g enzyme solution (Sigma-Aldrich, France); sodium acetate trihydrate (CH<sub>3</sub>COONa·3H<sub>2</sub>O) (ReagentPlus, ≥99.0%, Sigma-Aldrich, France).

### 2.2 Characterization of the pulp fibers

The morphological properties of the fiber's suspensions were measured using a MorFi fiber and shive analyzer (TECHPAP, France). This equipment consists of a charge-coupled device (CCD) camera that captures the images of the fibers suspension and records them for further analysis with a software that conducts the measurements and statistical corrections. The software discriminates between fibers and fines by size criteria. A fine element was considered as any detected object present in the pulp with dimensions lower than those of fibers, in this case, length under 80 μm or width under 5 μm.

The samples of fibers suspensions were diluted in deionized water to about 0.400 g/L, and 1 L of this suspension was poured into the MorFi and measured for five minutes. Three repetitions were performed, and the obtained results averaged. The length values are calculated from the framework of the fiber following the course of each segment. It is consequently the real developed length of the fiber. The length weighted in length ( $L_{wl}$ ) is given by Eq. (1):

$$L_{wl} = \frac{\sum_{i=1}^n (L_i \times L_i)}{\sum_{i=1}^n L_i} \quad (1)$$

Where n is the number of fibers and  $L_i$  is the length of each individual fiber ( $1 < i < n$ ).

Soluble lignin and carbohydrates content were determined. Acid-insoluble lignin was determined following the standard TAPPI T222-15 and acid-soluble lignin content was evaluated following the standard TAPPI UM 250-76. Carbohydrates were determined according to the standard TAPPI T249-09. An Dionex ICS 5000 ion chromatography system (ThermoFisher, USA) was used.

## 2.3 Enzymatic pretreatments

### 2.3.1 Laccase mediated enzymatic hydrolysis

Laccase mediated enzymatic pretreatment using a laccase commercial enzyme Novozym 51003 was performed with a concentration of 60 LAMU/g of cellulose. 200 g of refined pulp with a Schopper-Riegler degree of 70-80° were introduced at 2 wt% in a reactor pre-heated at 40°C under continuous mechanical agitation with a 300-rpm rotation speed. A pH of 4.5 was adjusted by adding an acetate buffer composed of acetic acid and sodium trihydrate. Once the temperature (40°C) and pH stabilized, an enzyme solution was poured into the reactor and left for a reaction time of 2 h. To stop the enzymatic activity, the reactor was heated to 80°C for 10 min, then cooled to 25°C. Finally, the suspension was recovered, filtered using a 1 µm nylon sieve, and rinsed with deionized water.

### 2.3.2 Endoglucanase mediated enzymatic hydrolysis

Previously laccase pretreated pulp was pretreated using an endoglucanase commercial enzyme FiberCare was performed with a concentration of 300 ECU/g of cellulose. The pulp was introduced at 2 wt% in a reactor pre-heated at 50°C under continuous mechanical agitation with a 300-rpm rotation speed. A pH of 5 was adjusted by adding an acetate buffer composed of acetic acid and sodium trihydrate. Once the temperature and pH stabilized, the enzyme solution was poured into the reactor and left for a reaction time of 2 h. To stop the enzymatic activity, the reactor was heated to 80°C for 10 min, then cooled to 25°C. Finally, the same procedure as the previous pre-treatment was used to recover the material.

All pretreatments were coded to be easily assessed throughout the work (Table 1).

**Table 1:** Experimental design and coding of samples.

Fiber	Condition	Pretreatment	Code
Unbleached Eucalyptus Kraft Pulp	Before nanofibrillation	Not pretreated	UEKP
		Laccase treated	LT_UEKP
		Laccase-cellulase treated	LCT_UEKP
	After nanofibrillation	Not pretreated	ULCNF
		-	-
		Laccase-cellulase treated	EsT_LCNF

## 2.4 LCNF production by mechanical nanofibrillation

Refined cellulose pulps were immersed for three days in deionized water at 2 wt% to guarantee fiber swelling. Then, they were nanofibrillated by passing the pulp through an ultra-fine grinder Supermasscolloider (model MKCA6-2, disk model MKGA6-80, Masuko Sangyo Co., Ltd., Japan). The disks speed was fixed at 1,500 rpm (Dias et al., 2019). A three-phase wattmeter was introduced on the Masuko device to measure the total active power.

The energy used during nanofibrillation was determined with a three-phase wattmeter, which can measure total input energy using the Eq. (2):

$$TEC_{(kWh/kg)} = \frac{TIE (kWh)}{m (kg)} \quad (2)$$

TEC is the total energy consumption (kWh/kg), TIE is the total energy input, and m is the mass of cellulose pulp (kg).

## 2.5 Turbidity, visual inspection, stability, and Zeta potential of LCNF suspensions

The turbidity (NTU) of the LCNF suspensions was measured with a portable turbidimeter (Aqualytic, AL-250, wavelength 860 nm) on an LCNF suspension that was diluted to 0.1 wt% and stirred for 1 min with Ultra Turrax (IKA T-25). The unity NTU refers to Nephelometric Turbidity Units.

The suspensions were diluted to 0.1 wt%, and 100 mL was placed in test recipients for photos acquisition. Images were acquired at 0, 10, 30 min, 1, 2, 3, 4, 5, 6, 7, 8, and 24 h. Fiji software was used to estimate NFC decantation in the suspensions, and then stability was calculated according to Eq. 3 proposed by Silva et al., (2021):

$$\text{Stability} = \left( \frac{\text{Dispersed}}{\text{Total}} \right) \times 100\% \quad (3)$$

Where “Dispersed” is the height corresponding to suspended particles, and “Total” is the height of all the liquid in the recipient.

The zeta potential test was conducted with a Dynamic Zetasizer (Zetasizer Nano ZS 90, Malvern Panalytical Instruments, UK) at 25°C to evaluate the stabilization of LCNF suspensions (0.1 wt%).

## 2.6 Light Microscopy (LM)

The LCNF suspensions were characterized using a light microscope (Zeiss Axio AX10, Germany). The suspensions were previously diluted to 0.1 wt%, stirred for 1 min with Ultra Turrax

(IKA T-25) at 10,000 rpm, and plunged for five minutes in an ultrasonic bath to obtain a better dispersion. Pictures were taken at 10x magnification and analyzed using Fiji software. The images were transformed to an 8-byte format and thresholded to perform the analysis. Then, the average size of the visible particles was extracted corresponding to the average surface of the particle. The micro size is obtained by divided the total surface by the number of particles. Ten images by sample were used in this step.

## 2.7 Transmission Electron Microscopy (TEM)

Transmission Electron Microscopy of the LCNF was investigated using a Tecnai G2-12 (FEI company, USA) instrument with an accelerated voltage of 80 kV. A drop of dilute LCNF suspensions (0.001%) were deposited onto a carbon-coated electron microscopy copper grid.

The excess liquid suspension was absorbed by a piece of filter paper, and a drop of 2% uranyl acetate negative stain was added before drying. The liquid in excess was blotted, and the remaining film of stain was taken to dry at room temperature. Images were post-processed using Fiji.

## 2.8 Nano-structured papers preparation

LCNF nano-structured papers, also called “nanopapers” were prepared with a sheet former (Xell Rapid Kothen, ISO 5269-2, PTE, Austria) from 2 g of LCNF (dry content) diluted to 0.5% in deionized water. First, the suspension was filtered in a 1  $\mu\text{m}$  nylon sieve under vacuum at  $-600$  mbar during a specific time until removing of water supernatant. Then, the sheet was dried at  $85^\circ\text{C}$  under 0.8 bar pressure between two 1  $\mu\text{m}$  nylon sieves (one on each side) to prevent adherence and two cardboards (one on each side) for 20 min. All the nanopapers were stored for 48 h in a conditioned room at  $23 \pm 2^\circ\text{C}$  and  $50 \pm 2\%$  RH before characterization.

## 2.9 Porosity (%)

The porosity of the nanopapers was calculated from the basis weight of each nanopaper ( $\text{kg}/\text{m}^2$ ) and its thickness ( $\mu\text{m}$ ), using the following Eq. (4) described by Desmaisons et al. (2017). The samples were cut at  $(50 \times 50)$   $\text{mm}^2$  dimensions.

$$P(\%) = 1 - \left( \frac{BW}{e \times \rho c} \right) \times 100 \quad (4)$$

where  $BW$  is the basis weight ( $\text{kg/m}^2$ ),  $e$  is the thickness (m), and  $\rho c$  is the density of cellulose ( $1540 \text{ kg/m}^3$ ). At least five replicates were performed.

### 2.10 X-Ray diffraction (XRD)

The XRD analyses were performed using a PANalytical X'Pert PRO MPD X-ray diffractometer (Malvern Panalytical, UK), equipped with an X'celerator detector with a Cu-K $\alpha$  source ( $\lambda = 1.5406 \text{ \AA}$ ) in the  $2\theta$  range of  $10 - 40^\circ$ . A step rate of  $0.066^\circ$  was used. The equipment was operated at a tension of 45 kV and a current of 40 mA.

The theoretical coordinates of native cellulose I $\beta$  (FWHM = 0.1) were extracted from crystallography information data (.cif) using the software Mercury 2020.2.0 (CCDC, UK) obtained from the Supplementary Information accompanying the original work (Nishiyama et al., 2002).

The patterns were deconvoluted using the Gaussian function with Magic Plot 2.9 (Magicplot Systems, Russia). For the amorphous halo, cellulose II pattern with peak width at half maximum (FWHM = 9), only varying its intensity, was used as suggested in the literature (French, 2020). After deconvolution, the crystalline fraction (CF) was calculated from the ratio between the area below all the crystalline peaks and the total area below the whole curve, determined after deconvolution following Eq. (5):

$$CF(\%) = \frac{\sum \text{Area}_{\text{Crystalline Peaks}}}{\sum \text{Area}_{\text{Crystalline Peaks}} + \text{Area}_{\text{Amorphous Halo}}} \quad (5)$$

The crystallite size of the (200) plane peak was calculated according to Scherrer's equation (Eq. 6):

$$D = \frac{K \times \lambda}{\beta \times \cos\theta} \quad (6)$$

Where  $D$  is crystallite size ( $\text{\AA}$ ),  $K$  (0.9) is a constant that refers to crystal shape,  $\lambda$  is the wavelength of the ray used (Copper),  $\beta$  is the FWHM of the peak, in radians, and  $\theta$  is the Bragg's angle of (200) plane diffraction.

### 2.11 Rheological parameters

This step was performed according to Souza et al. (2019). The study of the rheological behavior of LCNF suspensions at 1% wt concentration was performed on a Physica MCR 301 (Anton Paar, Austria) rheometer coupled to an AWC100 (Julabo, Germany) thermostatic bath using the PP25 DIN Ti

parallel plate sensor ( $D = 25$  mm; Gap = 1 mm). The samples were submitted to flow curves using three continuous ramps (ascending, decreasing, and ascending) with a deformation rate ranging from 0 to 300  $s^{-1}$  for 2 min for each curve at 25 °C. The Herschel-Bulkley (Eq. 7) model was adjusted to the data of the second increasing curve to determine the fluid flow profile and obtain the viscosity. The model was adjusted by the software Origin 2022 (OriginLab, USA), using three repetitions.

$$\tau = \tau_0 + K \times \dot{\gamma}^n \quad (7)$$

Where  $\tau$  is the shear stress in (Pa),  $\tau_0$  is the yield stress in (Pa),  $K$  is the consistency index (Pa  $s^n$ ),  $\dot{\gamma}$  is the deformation rate ( $s^{-1}$ ), and  $n$  is the flow behavior index (dimensionless).

The apparent viscosity values were evaluated at a shear rate of 100  $s^{-1}$ , which, according to (Steffe, 1996), corresponds to a deformation commonly suffered by fluids in industrial pipes concerning processes as pumping and agitation.

### ***2.11.1 Viscoelastic properties***

Dynamic viscoelastic moduli, storage modulus ( $G'$ ) and loss modulus ( $G''$ ), were measured as a function of angular frequency ( $\omega = 0.1$  to 100  $s^{-1}$ ) using oscillatory tests. The linear viscoelastic range of the sample (LVE) was obtained from an amplitude sweep using constant angular frequency ( $\omega = 1$   $s^{-1}$ ) with varying strain amplitude between 0.01 and 100% to perform the frequency sweep test.

### ***2.11.2 3 Interval thixotropy test recovery measurements (3ITT)***

This step was according to the work of Rantanen et al. (2015). The purpose of the 3ITT measurement was to determine the structural recovery of the dynamic elastic network structure after the removal of high shear. Initially, samples were subjected to low shear rate (0.1  $s^{-1}$ ), then subsequently high shear rate (1000  $s^{-1}$ ), and finally once again low shear rate, the recovery stage (0.1  $s^{-1}$ ). Structure recovery was traced in respect to recovery of dynamic transient viscosity ( $\eta^+$ ) in the third interval, expressed as a percentage (%) of ratio  $\eta^+ / \eta_0$  after 250 s of measurements, where  $\eta_0$  is the low shear viscosity at the beginning of the first interval.

## **2.12 Mechanical properties**

The tensile properties were measured with a tensile testing machine (Instron 3365, USA) equipped with a load cell of 5 kN capacity, following the NF Q03-004 standard. The weight basis of the



nanopaper specimens was measured using an analytical balance, and the thickness of the specimens was measured using a Lhomargy micrometer. These values were then reported into the tensile device to obtain the Young's Modulus. The grips have been selected to limit the slipping of samples. Tensile tests were performed at 5 mm/min, and an initial distance of 100 mm between the clamping jaws. The dimensions of the samples were 150 mm for the length and 15 mm for the width. For each sample, the minimal number of repetitions was seven and the average value was used for further calculations. The tear resistance was measured using a tear tester (Noviprofibre, Elmendorf pendulum 4000mN, France). Samples were cut at (65×50) mm<sup>2</sup> dimensions, and the measurement corresponds to the force (mN) needed for tear propagation after a primer.

### **2.13 Contact angle, surface wettability and surface free energy of nanopapers**

The contact angle and surface wettability of the nanopapers was determined following the standard TAPPI T458-14. This analysis was conducted using a Drop Shape Analyzer model DSA25B (Krüss, Germany) and the software ADVANCE version 1.4.1.2. The dispersive and polar components of the surface free energy of the LCNF nanopapers samples were determined according to Owens and Wendt (1969) using deionized water, glycerol, and ethylene glycol as polar solvents, and diiodomethane and 1-bromonaphthalene as apolar solvents.

### **2.14 Barrier properties**

The water vapor transmission rate (WVTR) and water vapor permeability (WVP) were determined following the standard TAPPI T464 om-18. The nanopapers were sealed on glass containers which were placed in a controlled chamber at around 38°C and a 90% RH and weighted at separate times intervals to calculate the mass gain. The grease resistance of the nanopapers was determined according the standard TAPPI T559 cm-12.

### **2.15 Simplified quality index (Q.I\*)**

A quality index adapted from the work of Desmaisons et al. (2017) was used for the comparison of LCNF suspensions together. Although the quality index (Q.I\*) was developed for the analysis of enzymatic bleached CNF and not for lignin-containing CNF, it was used to obtain a broad view of the quality of the produced material. This value regroups 6 tests assessing LCNF optical and mechanical

properties (Turbidity, tear resistance, Young's modulus, porosity, and macro size,), and is representative of the global quality of LCNF suspensions.

The equation (Eq. 8) that was adapted for quality index calculation was:

$$\begin{aligned} Q.I^* = & 2 \times \text{Turbidity mark} + 2 \times \text{tear resistance mark} + 3 \times \text{Young's modulus mark} \\ & + 2 \times \text{porosity mark} \\ & + 1 \times \text{micro size mark} \end{aligned} \quad (8)$$

where marks are calculated from raw test values as indicated in the original publication. The resulting equation (Eq. 9) including the raw test values was therefore:

$$\begin{aligned} Q.I^* = & -0.02 \times X_1 - 7.18 \times \ln(X_2) - 0.108 \times X_3^2 + 3.81 \times X_3 - 0.32 \times X_4 - 5.35 \ln(X_5) \\ & + 57.2 \end{aligned} \quad (9)$$

with  $X_1$  representing the turbidity (NTU),  $X_2$  the tear resistance (mN),  $X_3$  the Young's modulus (GPa),  $X_4$  the porosity (%), and  $X_5$  the micro-size ( $\mu\text{m}^2$ ).

## 2.16 Statical analysis

Quantitative analyses that required repetition were submitted to statistical validation. The Tukey's test at 95% significance, was applied to investigate if the averages were statistically different from the Untreated sample. Statistical analyzes were performed using the free software SISVAR version 5.6.

## 3. Results and discussion

### 3.1 Effect of enzymatic treatments on fiber properties

The MorFi system was used to understand the modifications on fibers' structure before and after the enzymatic hydrolyses. The considered traits were mean length of fibers, mean fiber width; the proportion of fines based on the length of fines (total length of fines to the total length of the elements present in the suspension) below  $80 \mu\text{m}$ , the fibrillation index, and the fiber coarseness (Table 2).

**Table 2:** Effect of laccase and cellulase mediated enzymatic hydrolysis treatments of unbleached eucalyptus kraft pulp on fibers' morphological properties. \*Different letters in the same column indicate significant ( $\rho \leq 0.05$ ) differences between the samples for the Tukey's test.

Sample	Mean length-weighted length ( $\mu\text{m}$ )	Mean fiber width ( $\mu\text{m}$ )	Fine's content (%)	Fibrillation index (%)	Mean fiber coarseness (mg/m)
UEKP	$620 \pm 4^c$	$18.5^a$	$65 \pm 1^a$	$3.01 \pm 0.01^c$	$0.0938^a$
LT_UEKP	$669 \pm 3^a$	$18.3^b$	$55 \pm 1^c$	$2.86 \pm 0.01^b$	$0.0819^b$
LCT_UEKP	$643 \pm 5^b$	$18.6^a$	$62 \pm 1^b$	$3.14 \pm 0.03^a$	$0.0804^b$

UEKP = Unbleached eucalyptus kraft pulp without any treatment; LT\_UEKP = Laccase treated unbleached eucalyptus kraft pulp and LCT\_UEKP = Laccase and cellulase treated unbleached eucalyptus kraft pulp.

Comparing the untreated sample (UEKP) with the one that underwent treatment only with the laccase enzyme (LT\_UEKP), there was an increase in the average length of the fibers (from  $620 \pm 4 \mu\text{m}$  to  $669 \pm 3 \mu\text{m}$ ). Besides, there was a slight decrease in their average width (from  $18.5 \mu\text{m}$  to  $18.3 \mu\text{m}$ ). Thus, it supports that the laccase enzyme prefers attacking smaller structures present in the suspension, represented by the fines. As shown in Table 1, there was a considerable reduction in the content of fines after laccase-mediated enzymatic hydrolysis. Additionally, according to Chen et al. (2021), this behavior, along with the fibrillation indexes, which decreased from  $3.01 \pm 0.01$  to  $2.86 \pm 0.01\%$  after treatment with laccase, suggests that the enzyme acts more on the surface of the fibers instead of inside. The fact that the enzyme attacked the smaller structures caused the average fiber length to increase.

The decrease in coarseness after laccase-mediated enzymatic hydrolysis (from  $0.0938$  to  $0.0819$  mg/m) can also be observed. The fiber's coarseness measures the amount of fiber per length of fiber, and this parameter indicates the fiber's cell wall thickness, besides how the fiber is being hydrolyzed (Mooney et al., 1999). From this result, it can be suggested that the first treatment with the laccase enzyme will already facilitate the action of the cellulase enzyme in the subsequent treatment.

Analyzing the LCT\_UEKP sample, the average length of the fibers increased relative to UEKP, but when compared to the LT\_UEKP sample, it decreased in the average length of the same (from  $669 \pm 3$  to  $643 \pm 5 \mu\text{m}$ ), which indicates that even with the presence of lignin, the cellulase enzyme was able to attack cellulose in the fiber structure. Lignin typically inhibits cellulase enzyme action in cellulose through physical barriers, such as hydrophobicity, surface charges, electrostatic interactions, and interactions between hydrogen bonds (Li et al., 2020).

Concerning the average fiber width, after the enzymatic treatment using cellulase, the fiber width slightly increased from 18.5 to 18.6  $\mu\text{m}$ , compared to UEKP, and 18.3 to 18.6  $\mu\text{m}$  compared to LT\_UEKP. The fines content increased from  $55 \pm 1\%$  after laccase treatment to  $62 \pm 1\%$  after cellulase treatment. These results indicate that cellulases induce the fibers to swell by attacking the surface and the inner of the fibers, allowing more significant amounts of water molecules into the fibers. Moreover, according to Beyene et al. (2018), during cellulase mediated hydrolysis, the fibers swelling by the action of carbohydrate-binding modules and non-hydrolytic enzymes, which induce amorphogenesis.

The increase in fibrillation index (from  $2.86 \pm 0.01\%$  to  $3.14 \pm 0.03\%$ ) corroborates the earlier discussion in this section; it indicates that microfibrils are individualized in the fiber cell wall once again because of the cellulase enzyme action. The value of coarseness for LCT\_UEKP also decreased after cellulase hydrolysis (from 0.0819 to 0.0804 mg/m), which agree with the fiber length change, since the longer fibers largely determine the coarseness of a fiber population, and it is more sensitive to changes in the weight of that fraction (Mooney et al., 1999). According to Azevedo et al. (2020), fibers presenting lower coarseness provide a more wettable surface, facilitating water molecules penetration into the fiber structure.

Table 3 gives the chemical composition of the Eucalyptus fibers before and after the enzymatic treatments. Xylan was the main non-cellulosic carbohydrate compound found in the samples. Arabinan and Galactan were also found in the hemicellulosic fraction, but in extremely low proportions, while the presence of Mannan was not detected in the analysis. Eucalyptus pulp fibers contain mostly Xylan, which is mainly located on the fiber surface (Ehman et al., 2020).

**Table 3:** Average and standard deviation of the chemical components content of Eucalyptus fibers before and after enzymatic treatments. \*Different letters in the same column indicate significant ( $p \leq 0.05$ ) differences between the samples for the Tukey's test. ND = Not detected.

Chemical composition (%)							
Samples	Glu	Hemicellulose				ILig	SLig
		Xyl	Man	Ara	Gal		
UEKP	64 ± 0.1 <sup>a</sup>	10 ± 0.01 <sup>a</sup>	ND	0.2 ± 0.01 <sup>a</sup>	0.5 ± 0.01 <sup>a</sup>	17 ± 0.3 <sup>a</sup>	3 ± 0.06 <sup>a</sup>
LT_UEKP	65 ± 0.2 <sup>a</sup>	9 ± 0.07 <sup>b</sup>	ND	0.1 ± 0.02 <sup>a</sup>	0.4 ± 0.01 <sup>a</sup>	17 ± 0.1 <sup>a</sup>	3 ± 0.05 <sup>a</sup>
LCT_UEKP	63 ± 0.4 <sup>b</sup>	10 ± 0.05 <sup>a</sup>	ND	0.1 ± 0.00 <sup>a</sup>	0.5 ± 0.00 <sup>a</sup>	17 ± 0.1 <sup>a</sup>	3 ± 0.10 <sup>a</sup>

Glu = glucan; Xyl = Xylan; Man = Mannan; Ara = Arabinan; Gal = Galactan; ILig = Insoluble lignin; and SLig = Soluble lignin.

A slight increase (not significant) in the Glucan content was observed in the material treated with the laccase enzyme. This apparent increase is related to the decrease in the content of Xylan in the constitution of the material. The significant reduction in Glucan content after hydrolysis with the endoglucanase enzyme demonstrates that the previous treatment with laccase was effective in modifying the lignin and leaving the cellulose more exposed to the cellulase attack. According to Li et al. (2020), the structure of lignin can inhibit the action of enzymes on cellulose through physical barriers, limiting the accessibility of enzymes, inhibiting their hydrolysis.

The content of hemicellulose ranged from approximately 11% for UEKP and LCT\_UEKP to 9% for LT\_UEKP. Dias et al. (2019) stated that hemicellulose content in the range of 9 to 12% facilitates cell wall deconstruction. The presence of hemicellulose and its carboxylic groups act to regulate the extent of microfibril aggregation through electrostatic repulsion forces. This acts to facilitate the mechanical nanofibrillation of the fibers.

Regarding the content of insoluble and soluble lignin, no change was observed in its content, showing that the enzymatic load used was able to modify the lignin present in the fiber structure but was not enough to remove it, thus preserving the original content of this macromolecule in the fibers and LCNF obtained.

### 3.2 Turbidity, visual inspection, stability, and Zeta potential of LCNF suspensions

The turbidity and sedimentation analysis and the percentage stability over time allowed evaluating the general stability of the aqueous NFC suspensions (Figure 1).

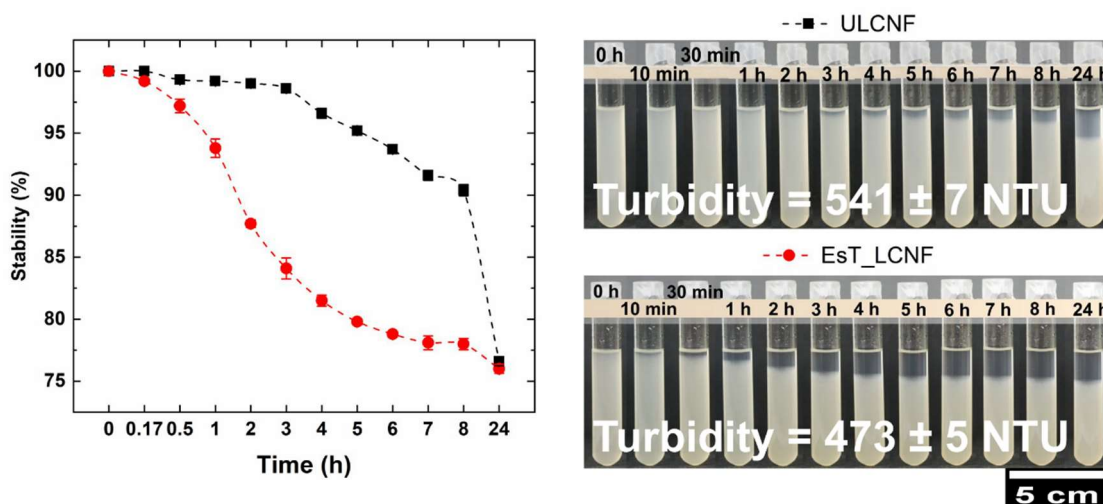


**Figure 1:** Dispersion states of the 0.1 wt.% ULCNF and EsT\_LCNF suspensions at 0, 10, 30 min, 1, 2, 3, 4, 5, 6, 7, 8, and 24 h. Influence of time on LCNF suspensions stability in water.

The turbidity is an indirect indicator of the nanofibrillation yield due to the light scattering produced by large particles in a suspension (Espinosa et al., 2020). The enzyme pretreatments promoted a decrease in turbidity in the LCNF suspension ( $473 \pm 5$  NTU compared to  $541 \pm 7$  NTU of the untreated sample, a first indication that the material has more nanoscale and less aggregated particles. When cellulose particles are in nanoscale, they are stable due to Brownian motion, which keeps the particles in suspension caused by the interaction of repelling forces (Silva et al., 2021).

The turbidity measures the light that is dispersed by the material in suspension. As the material becomes smaller, the visible light is not dispersed in the material and the turbidity value tends to approach zero. The opposite happens when the material is composed mostly of particles with larger dimensions in which visible light ends up being dispersed, increasing the turbidity value. According to Foster et al. (2018), although turbidity of NFC suspensions is complex due to the number of scatterers per unit volume, size distribution, and optical properties of the light-scattering bodies, it is consistent method for estimating the quality of nanofibrils.

Since the existence correlation between particles shapes and sizes, particle agglomerates, and stability, sedimentation analysis has been widely used to evaluate cellulose nanoparticles quality (Silva

et al., 2021). The sedimentation shows a tendency of enzymes to affect the stability of the suspension during the first 24 h. As can be seen in Figure 1, the ULCNF remains highly stable after the first three hours of analysis, showing a stability of 98.6%. On the other hand, the EsT\_LCNF starts to suffer a decrease in stability after only 30 min and after three hours shows a stability of 84.1%.

After the fourth hour the ULCNF started to show a tendency to decrease the suspension stability and at the end of 8 h, it showed 90% stability while the EsT\_LCNF after 8 h showed 78% stability. Interestingly, after 24 h of analysis, both suspensions showed similar stability (77% for ULCNF versus 76% for EsT\_LCNF). These results indicate that the ULCNF suspension keeps the dispersed particles in Brownian motion in the suspension longer than the EsT\_LCNF. Due to the latter having more repulsion charges as is shown in the Zeta potential values that will be discussed below. Brownian motion tends to randomize the orientation of fibrils when the dispersion is diluted enough, which keeps them dispersed (Silva et al., 2021).

The surface charges of nanofibrils are an important parameter for the use of this material as a reinforcement agent. Nanoparticles must have high Zeta potential, so that the colloidal suspension can resist aggregation, to increase its degree of dispersion in the matrix (Tibolla et al., 2014), but, according to Bhattacharjee (2016), higher Zeta potential values are not always a guarantee of greater stability in colloidal suspensions, because Van der Waals forces that act between particles can promote their agglomeration.

The Zeta potential values found for the ULCNF sample was  $-21.3 \pm 0.6$  mV and for EsT\_LCNF sample was  $-19.1 \pm 0.4$  mV, similar to the value that was found by Bardet et al. (2015) which was  $-18 \pm 3$  mV. The Zeta potential of the EsT\_LCNF sample was still close to the values found by Lee et al. (2018) for NFC obtained after different sodium hydroxide treatments. The values found in this study were higher than those obtained for LCNF found by Imani et al. (2020), these authors obtained a Zeta potential of  $-28.1 \pm 1.5$  mV.

These results indicate that the two suspensions are moderately stable due to the presence of negatively charged carboxyl groups present in the hemicellulose (Bardet et al., 2015). Zeta-potential measurements give an indication of the stability of the colloidal suspensions. It is assumed that

suspensions with a zeta-potential higher than +30mV or lower than -30mV are stable (Herrera et al., 2018).

### 3.3 Morphological properties of LCNF

The morphology of the obtained LCNF was studied using transmission electron microscopy (Figure 2). The enzymatic treatments did not cause significant changes in the average diameter of the nanofibrils, but there was a differentiation in the distribution of the diameter ranges of the nanofibrils, as well as in the overall appearance of the nanofibril network of the two samples.

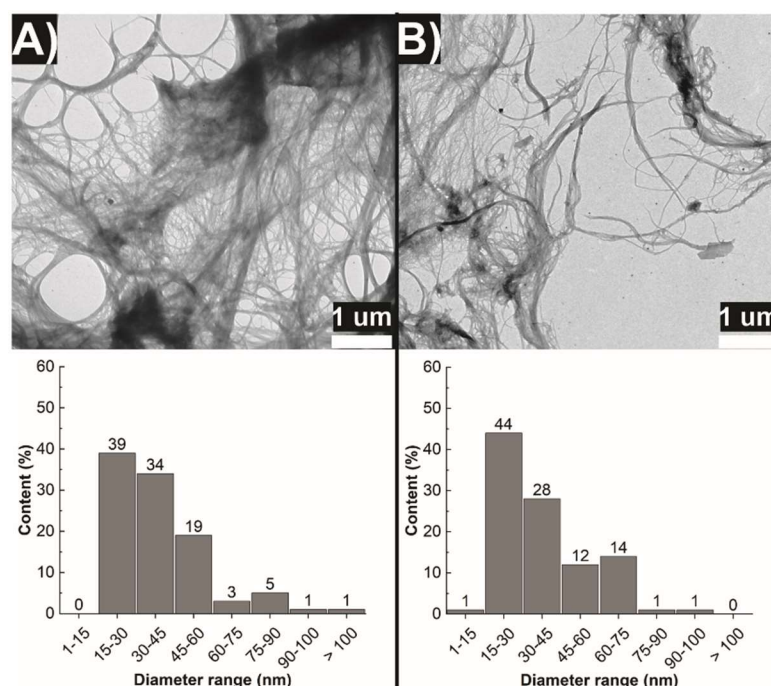


**Figure 2:** Typical transmission electron microscope (TEM) images and diameter distribution of CNF from: A) Untreated Lignin-cellulose nanofibrils (ULCNF), and B) Enzymes treated Lignin-cellulose nanofibrils (EsT\_LCNF).

Both treatments lead to an efficient fibrillation into micro- and nano-scale elements, the analysis of TEM images enables to determine that these LCNF are composed of bundles of elementary fibrils, with widths between  $39 \pm 17$  nm (ULCNF) and  $38 \pm 16$  nm (EsT\_LCNF) and lengths over to  $3 \mu\text{m}$  leading to a high aspect ratio, making this material suitable for polymer reinforcement (Zhou et al., 2012). Dimensions of these nanofibrils were similar to those reported elsewhere for samples treated by mechanical nanofibrillation (Dias et al., 2019; Tonoli et al., 2016).

Figure 2 also shows the diameter distribution of LCNF produced in different conditions, with average diameters lower than 30 nm that makes them potentially useful as reinforcing agents in



composites (Tonoli et al., 2016), the content of LCNF was around 39%, and 45% for ULCNF and EsT\_LCNF respectively. These results indicate that the enzyme-treated pulp led to better nanofibrillation and individualization of the fibrils, being the treatment that presented more homogeneous nanofibrils, with 44% of the elements measured within the class of diameter of 15-30 nm. TEM images enable to observe that EsT\_LCNF (Fig. 4B) shows less nanofibril aggregates compared to ULCNF (Fig. 4A). A lower level of aggregation of LCNF allows them to better interact with polymer matrices via hydrogen bonds. This enhances their mechanical and barrier properties and is attractive in the production of bio nanocomposites (do Lago et al., 2020; Guimarães et al., 2016).

### 3.4 Crystallographic characterization

The crystalline structure of LCNF was assessed with X-ray diffraction (XRD) before and after the treatments. Figure 3 shows that both LCNF presents the typical parallel crystalline structure of cellulose I $\beta$  with peaks at  $2\theta = 14.9^\circ$ ,  $16.4^\circ$ ,  $20.5^\circ$ ,  $22.6^\circ$  and  $34.7^\circ$ , corresponding to the lattice planes (1-10), (110), (102), (200) and (004) respectively (French, 2014).

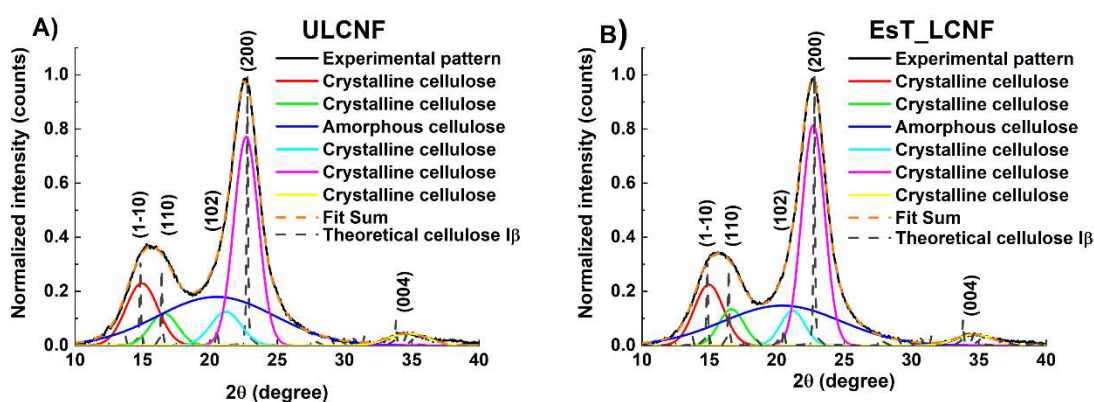


**Figure 3:** Typical X-ray diffraction (XRD) patterns of Eucalyptus LCNF samples obtained from fiber pulps a) before and b) after enzymatic pretreatments.

The enzymatic hydrolysis resulted in a considerable increase of CF, from  $59.6 \pm 1.7\%$  to  $64.6 \pm 1.5\%$  for EsT\_LCNF. This result may indicate that the laccase enzyme was able to partially depolymerize the lignin (Steinmetz et al., 2020), weakening its structure and avoiding the known inhibitory effect that lignin has on enzymes in cellulosic fibers (Li et al., 2020).

The increase of crystallinity means that the endoglucanase enzyme was able to attack the amorphous domains of cellulose. It is already reported in several studies that endoglucanase has a preferential action of disordered regions of cellulose than crystalline cellulose (Hakeem et al., 2015;

Nechyporchuk et al., 2015). This can be confirmed in Table 3 with the decrease in Glucan content in the material treated with the cellulase enzyme. The decrease in Glucan indicates that this polysaccharide molecules were hydrolyzed into Glucose due to the action of the enzyme.

Concerning the crystallites size, it was observed that enzymatic hydrolysis led to an increase of crystallites' dimension at the plane (200) from  $3.12 \pm 0.01$  nm to  $3.22 \pm 0.05$  nm. It is expected that after the attack of the amorphous domains of cellulose, enzymes begin to attack the small crystallites (Tonoli et al., 2016).

### 3.5 Rheological behavior

The behavior of the viscosity of the LCNF suspensions was investigated at 25°C. The flow curves and oscillatory tests are shown in Figure 4.

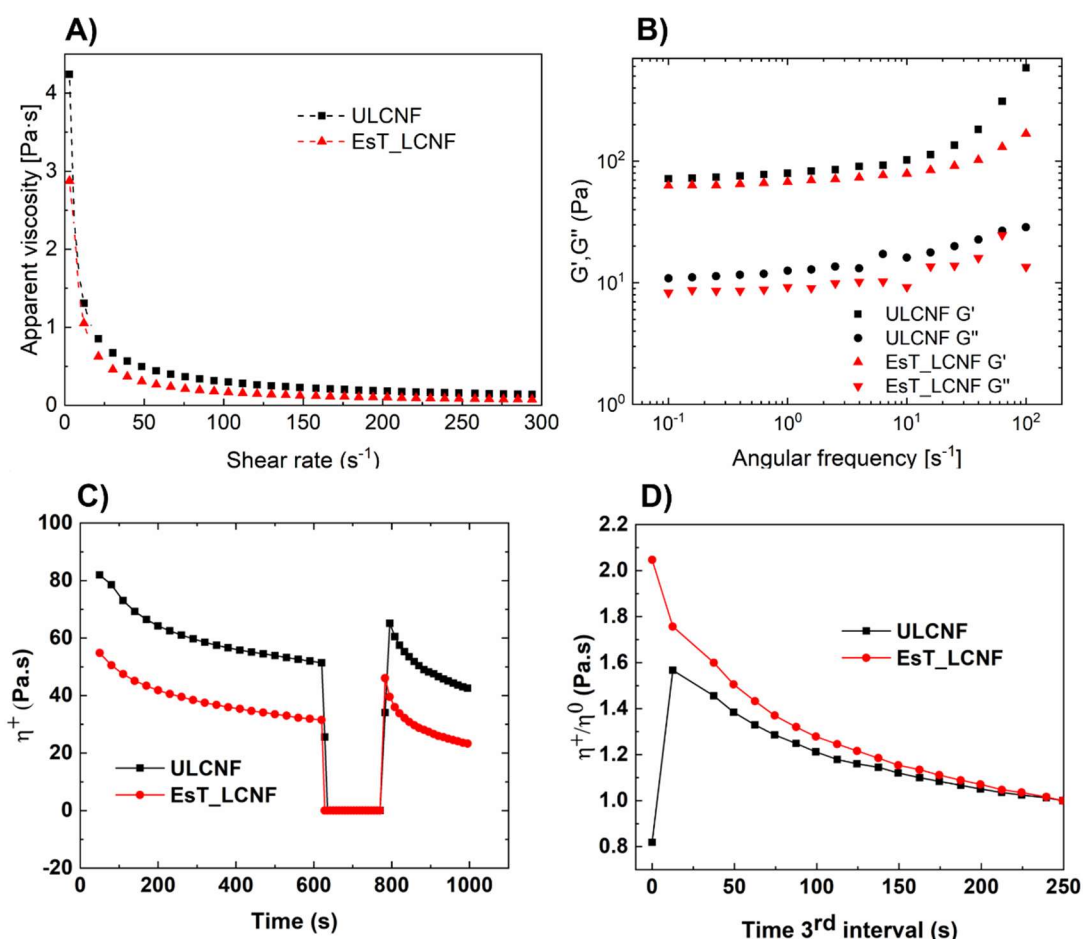


**Figure 4:** Rheological behavior of LCNF suspensions. A) Apparent viscosity vs. shear rate for the LCNF suspensions, and B) Storage ( $G'$ ) and loss ( $G''$ ) moduli of suspensions with 1.0% (w/w) LCNF as a function of frequency for: Lignin-cellulose nanofibrils obtained from control) and laccase and cellulase enzymes treated and structural recovery in 3ITT experiments plotted as C) transient viscosity recovery in rotational test, and D) Transient viscosity recovery in rotational test with normalized transient viscosity ( $\eta^+/\eta^0$ ).

The Herschel-Bulkley model was adjusted appropriately for the data of the flow curve ( $p < 0.001$ ), presenting high values of the coefficient of determination ( $R^2 \geq 0.9834$  and  $R^2 \geq 0.9932$  for ULCNF and EsT\_LCNF respectively). The rheological parameters of the model, as well as the apparent viscosity at  $100 \text{ s}^{-1}$ , are presented in Table 4.

**Table 4:** Parameters of the Herschel-Bulkley model and initial apparent viscosity and at  $100 \text{ s}^{-1}$  ( $\eta_{100}$ ) for ULCNF and EsT\_LCNF.

Herschel-Bulkley						
Sample	$\tau_0$ (Pa)	$k$ (Pa.s <sup>n</sup> )	$n$ (-)	Pr > t	$R^2$	$\eta_{100}$ (mPa.s)
ULCNF	0.90	7.19	0.30	< 0.001	0.9834	$303.3 \pm 7.6$
EsT_LCNF	6.0	2.12	0.36	< 0.001	0.9932	$172.3 \pm 4.9$

ULCNF presented higher value for the consistency index (K) than EsT\_LCNF, indicating that this suspension has a higher aspect ratio. The morphology of the material is related to the (K) value, which also explains the lower viscosity of the Est\_LCNF (along with the degree of polymerization), since they present nanofibrils shorter than the ULCNF. Shorter nanofibrils results in a lower stiffness of the network, facilitating its breaking and ordering when subjected to shear, thereby decreasing viscosity (Souza et al., 2019).

ULCNF presented flow index values of 0.30 while EsT\_LCNF presented 0.36. The flow index (n) suggests the entire suspensions' structural property (Koponen, 2020) and indicates the degree of non-Newtonian characteristics of the material. All the LCNF in the Herschel-Bulkley model point to pseudoplastic fluids' behavior presenting (n) values lower than 1. Similar behavior was reported by Czaikoski et al. (2020) when investigating the rheological behavior of cellulose nanofibrils obtained from cassava peel and reported by Souza et al., (2019) studying rheological behavior of Pinus, Eucalyptus, and cocoa shell NFC. The decay of viscosity characterizes pseudoplastic fluids as the shear rate applied to the fluid increases (Figure 4A). It is due to the ordination of the material present in the stable suspension, which is disordered, and, as shear is applied, it starts to become organized, decreasing the system viscosity (Steffe, 1996).

Oscillatory shear measurements were performed to identify the response of the viscoelastic properties of the LCNF suspensions. In Figure 4B, both  $G'$  and  $G''$  were presented as the functions of frequency at a fixed strain of 0.2% within the linear viscoelastic region.  $G'$  increased with the frequency

and it was much larger than  $G''$ , which showed a viscoelastic solid-like feature (gel-like properties), indicating that the elastic properties were dominant compared to the viscous properties. Usually,  $G'$  is an in-phase elastic modulus associated with energy storage and release in the periodic deformation, and  $G''$  is an out of-phase elastic modulus associated with the dissipation of energy (Qiao et al., 2016).

The results show that EsT\_LCNF had lower values for  $G'$  and  $G''$  than ULCNF, which may be related to the action of both enzymes that partially depolymerized both lignin and cellulose, making their rheological properties smaller when compared to the Control. Jordan et al. (2021) found similar behavior studying the variations of the degree of polymerization in rheological properties of lignin-containing cellulose nanofibrils from cotton gin notes and cotton gin trash containing high lignin content and after bleaching with  $\text{NaOCl}_2$  for reduced lignin content. For an ideal gel that behaves elastically, the storage modulus is expected to be independent of frequency and  $G' > G''$  (Qiao et al., 2016). Table 5 shows the storage modulus ( $G'$ ), gel stiffness ( $G'/G''$ ) and the loss tangent value ( $\tan \delta$ ) of LCNF suspensions.

**Table 5:** Values of storage modulus ( $G'$ ), gel stiffness ( $G'/G''$ ) and loss tangent value ( $\tan \delta(G''/G')$ ) obtained from the mechanical spectra at  $25^\circ\text{C}$  and  $0.1 \text{ rad s}^{-1}$  for LCNF suspensions at concentrations of 1 wt%.

Samples	Suspension concentration		
	1 wt%		
	$G'$ (Pa)	$G'/G''$	$\tan \delta$
ULCNF	71.9	6.61	0.15
EsT_LCNF	62.9	7.58	0.13

The EsT\_LCNF showed a higher value of  $G'/G''$  (7.58) compared to ULCNF (6.61), revealing an increase of the ionic strength of the suspension. According to Naderi and Lindström (2016), the stiffening effect might imply a more intimate contact between the nanofibrils, however, the exact mechanism behind this notion is not clear. This behavior may explain the higher value of  $\tau_0$  for EsT\_LCNF when compared to ULCNF. Figure 4 also shows the dependency of the behavior of  $G'$  and  $G''$  in relation to the frequency applied for both LCNF investigated. Furthermore,  $G'/G''$  values are between 1 and 10, indicating that the materials present gel-like characteristics (Dimic-Misic et al., 2013; Souza et al., 2019). In this situation, the classic structure is related to the existence of a three-dimensional

organization of the molecules that are broken under shear, causing the flow of the material, distinct of true gels, that break under shearing (Souza et al., 2019).

The transition from liquid-like to solid-like behavior for a viscoelastic coating material during immobilization has been described as the maximum slope of the loss factor, which is the ratio of the viscous to elastic modulus (Dimic-Misic et al., 2013). The loss tangent value ( $\tan \delta$ ), ( $G''/G'$ ) ratio, was of the order of 0.1 ( $\tan \delta < 1$ ) for all the samples investigated. This means that the medium is structured in the same way, leading to a gel-like structure. A similar result also was found by Agoda-Tandjawa et al. (2010) and Jordan et al. (2021).

Figures 4C and 4D show the time-dependent structure regeneration after the removal of a high shear rate. This analysis shows the deformation and recovery of structure through the regeneration of dynamic transient viscosity ( $\eta^+$ ) after applying a high shear period. This is an important test because it simulates a practical application of LCNF. The high shear rate in the test reflects the shear rate during a practical application (Dimic-Misic et al., 2013).

It can be noted that after the breakdown of elastic gel-like structure at high shear during the second interval, both LCNF presented a facility to reorganize and recovery the initial state, even presenting low viscosity than at the beginning of the first interval at a low shear rate. In both cases, the accumulation forces related to the thixotropic behavior of the suspensions and the shear forces compete with each other, causing the interruption of the accumulation structure in progress, resulting in an oscillatory behavior of the recovery curve (Lê et al., 2018).

Lê et al. (2018) obtained related results by studying the rheological behavior of suspensions of cellulosic nanofibrils with different lignin levels. They concluded that lignin's presence influences the level of aggregation and elasticity within the nanocellulose gel network, improving the water release properties and increasing the elasticity of the structure. As can be observed in Figure 4D, EsT\_LCNF showed a slightly faster recovery than ULCNF. This result may be due to the laccase enzyme caused the lignin in the fibrils to be made more available on its surfaces or accessible in the aqueous phase. It facilitated flocculation and aggregation of particles making recovery of the initial characteristics of the suspension faster after the end of the high shear rate, as shows the higher values of ( $\eta^+/\eta^0$ ) (Imani et al., 2020). Moreover, it means that the faster the recuperation of the viscosity, the better is the sagging

resistance after application on a rough surface (Dimic-Misic et al., 2013). Understanding the recuperation of the viscosity of LCNF suspensions is essential for the basis of selecting a proper coating procedure.

### 3.6 Contact angle, wettability, free surface energy and barrier properties

Figure 5A shows the contact angle (CA) and wettability for the studied LCNF nanopapers.

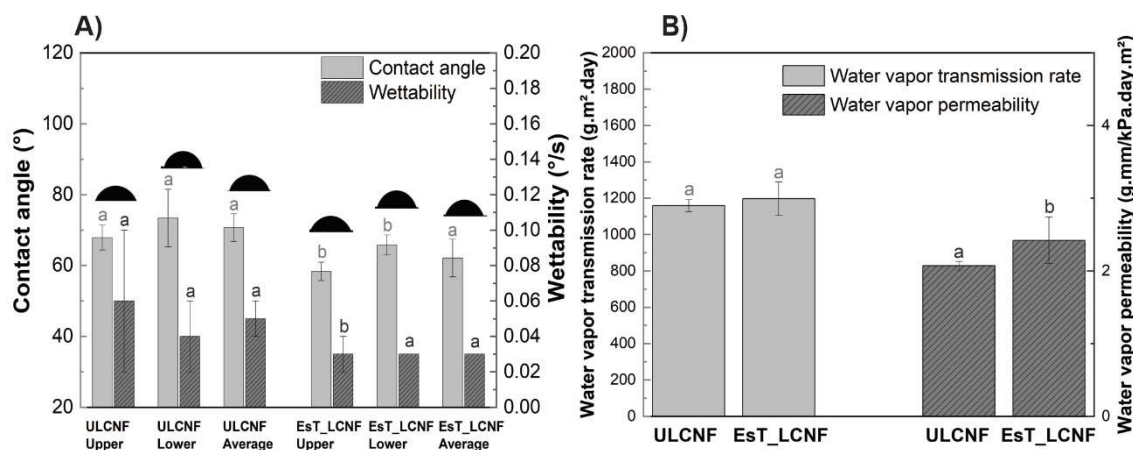


**Figure 5:** Average contact angle and wettability values (A) and WVTR and WPA values (B) for untreated and enzymes treated lignin-cellulose nanopapers.

The average contact angles of LCNF nanopapers were  $71 \pm 4^\circ$  and  $62 \pm 5^\circ$  for ULCNF and EsT\_LCNF, respectively. Concerning the wettability properties of the nanopapers, the ULCNF sample reached a value of  $0.05 \pm 0.01$  (°/s) while EsT\_LCNF obtained  $0.03 \pm 0$  (°/s). These values were much higher than those found by Nlandu et al. (2020), who for LCNF, these authors found a CA of 30, and similar to the result found by (Yook et al., 2020). This difference may be due to how the substrates (LCNF) were prepared. In the study by Nlandu and co-workers, these authors prepared films in Petri dishes by the casting method and allowed them to dry overnight at a milder temperature ( $40^\circ\text{C}$ ). Whereas in this study, nanopapers were prepared under vacuum filtration and drying under pressure and elevated temperature, which leads to the formation of a denser and more compact structure with a smaller volume of voids. This causes a more hydrophobic surface, caused by the flow of lignin, which can be more evenly distributed over the surface due to possible plasticization of the lignin under the temperature and humidity conditions used during the nanopaper drying process (Herrera et al., 2018).

On the other hand, the AC results obtained in this study were lower than those found by (Herrera et al., 2018; Wen et al., 2019), This can be explained by the fact that these authors have used high yield

pulps (Thermo Chemi-mechanical) with higher lignin contents than the material used in this study. However, the values obtained in this work are higher than those found in literature for conventional (lignin-free) nanofibrillated cellulose (NFC). Tayeb et al. (2020) found a CA value of  $59.4^\circ$  for NFC, while Solala et al. (2018) found  $\sim 25^\circ$  as result for CA, and Wang et al. (2021) found a CA of  $12^\circ$  for microfibrillated cellulose (MFC).

Statistically, the use of laccase enzyme as a pre-treatment step did not result in interference with the contact angle and wettability properties of the nanopapers. As it acts depolymerizing the lignin, the enzyme could decrease the hydrophobicity of nanopapers, which was not confirmed. We suspect that the endoglucanase enzyme, by preferentially attacking the amorphous regions of cellulose, leaving the material with more crystalline regions, where fewer sites are available for binding with water molecules, when compared to the amorphous regions of cellulose, may have assisted to compensate for the depolymerization of lignin.

The barrier properties of the lignin-cellulose nanopapers were analyzed in terms of water vapor transmission rate (WVTR) and water vapor permeability (WVP) and the results are shown in Figure 5B and in the Table 4.

The values for WVTR were 1159 and 1197  $\text{g}\cdot\text{m}^2\cdot\text{day}$  for ULCNF and EsT\_LCNF nanopapers respectively, the samples showed no statistical difference between each other. The EsT\_LCNF showed higher WVP property ( $2.42 \text{ g}\cdot\text{mm}/\text{m}^2\cdot\text{kPa}\cdot\text{day}$ ) compared to the ULCNF sample that showed a value of  $2.07 \text{ g}\cdot\text{mm}/\text{m}^2\cdot\text{kPa}\cdot\text{day}$ . These values are in agreement with the values reported by other authors for different raw materials (Espinosa et al., 2020; Tayeb et al., 2020). The increase of WVP in EsT\_LCNF is since the enzyme laccase, when attacking lignin, ends up decreasing its hydrophobic nature. The presence of lignin reduces the absorption of water molecules during the initial stage of diffusion of water molecules in LCNF nanopapers (Espinosa et al., 2020).

On the other hand, some authors in the literature studying the barrier properties (WVTR and WVP) of films from different nanofibrillated cellulose sources with diverse chemical compositions, observed an increase in WVTR for the films containing lignin, which according to the same authors may be due to the lower quality of hydrogen bonds in the films (Spence et al., 2011). In addition, the barrier

properties of LCNF nanopapers are the result of the combination of their crystalline structure as well as their ability to form dense networks with low porosity (Espinosa et al., 2020).

The grease resistance was measured according to the kit test, based on 12 different grease solutions numbered from 1 to 12. The material that achieves oil kit number of 12 is the one that shows the highest grease resistance during the test. According Lavoine et al. (2014), a paper is considered grease resistant when it reaches the kit number of 8 or higher. Table 6 report the grease resistance obtained by the LCNF samples.

**Table 6:** Grease resistance (oil kit number) and surface free energy (SFE) for the nanopapers of ULCNF and EsT\_LCNF. \*Different letters in the same row indicate significant ( $p \leq 0.05$ ) differences between the samples for the Tukey's test.

Characteristic	ULCNF	EsT_LCNF
Oil kit number	12 <sup>a</sup>	12 <sup>a</sup>
SFE (mN/m)	43 ± 3 <sup>b</sup>	47 ± 1 <sup>a</sup>
Disperse (mN/m)	37 ± 5 <sup>a</sup>	37 ± 1 <sup>a</sup>
Polar (mN/m)	6 ± 2 <sup>b</sup>	10 ± 1 <sup>a</sup>

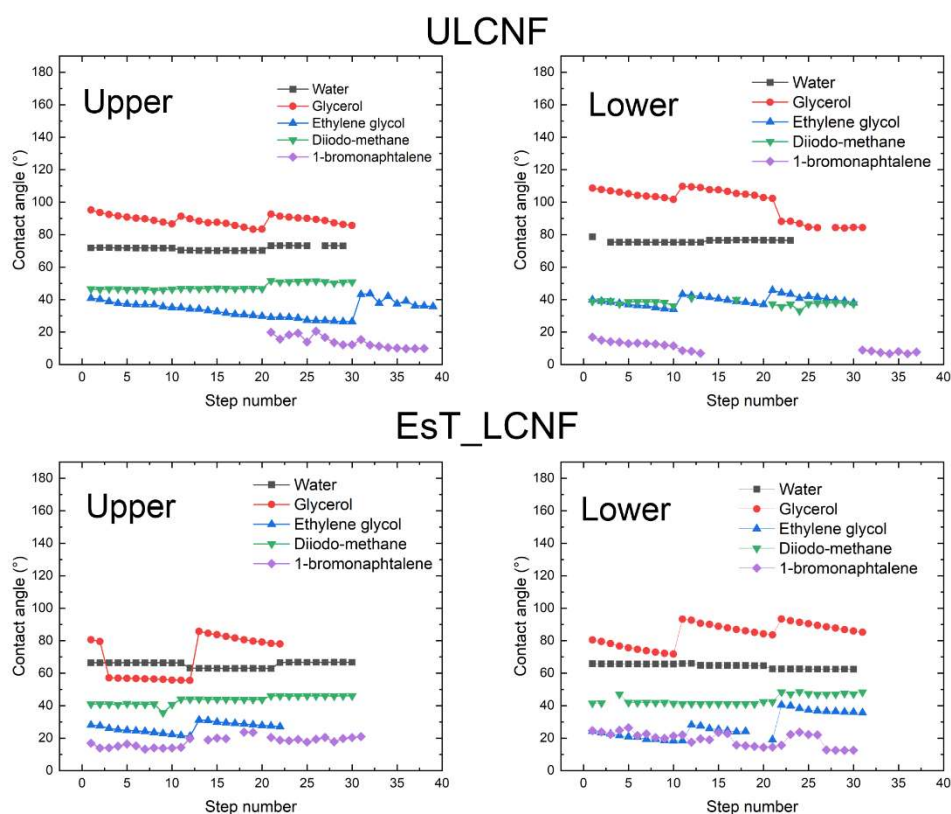
Both samples reached the oil kit number of 12, the same result found by Tayeb et al. (2020), indicating that they have the potential to be applied as coating agent in paper and packaging. his result is still indicative of a satisfactory level of nanofibrillation, since the more nanofibrillated the material is, the smaller the pore size in the nanopaper structure makes it more effective at blocking grease and water molecules (Wang et al., 2021).

Table 6 also show the total surface free energy distinguishing the dispersive and polar contributions. Surface free energy can provide more detailed information about the lignin-cellulose matrix, and it can be calculated from the OWRK model that uses polar and dispersive elements (Balasubramaniam et al., 2020). The surface free energy predicts how well a given solvent wets the surface of a polymer matrix. The increase of the polar component in EsT\_LCNF indicates an improvement of their hydrophilic character due to the degradation of non-carbohydrates constituents, more specifically the lignin from the fiber surface. It is known that oxidizing agents react mainly with lignin, breaking unsaturated bonds and producing final carbonyl and carboxyl structures, thus increasing the hydrophilic character of the fibers (Tonoli et al., 2012). In this same context, Steinmetz et al. (2020)



demonstrated the potential of laccase as a depolymerizing agent of lignin in a continuous depolymerization process in mild conditions.

Although both samples achieved oil kit number of 12 in the grease resistance test, and the dispersive components of surface free energies remain the same for both samples, behavior that was also observed by Hossain et al. (2021), the control sample (ULCNF) seems to be more suitable for application for oil barrier purposes, since it has a lower polar contribution than EsT\_LCNF, this means that its surface contains molecules that interact with liquids mainly through dispersive forces, such as Van der Waals interactions (Balasubramaniam et al., 2020). The influence of surface energy in grease resistance was mentioned in recent works by (Sheng et al., 2019; Tayeb et al., 2020). Figure 6 show ULCNF presented higher contact angles with polar liquids (water, glycerol, and ethylene-glycol) when compared with EsT\_LCNF, leading to lower surface free energy, and a lower surface free energy indicates that fewer solvents can wet the sample surface.



**Figure 6.** Dynamic nanopaper contact angles for the upper and lower sides of untreated lignin-cellulose nanofibrils (ULCNF) and Enzyme-treated lignin-cellulose nanofibrils (EsT\_LCNF). Polar solvents (Deionized water, Glycerol and Ethylene glycol) and apolar solvents (Diiodomethane and 1-bromonaphtalene) were used.

### 3.7 Energy consumption

The use of enzymatic pretreatments influenced the energy consumption for producing LCNF suspensions. In comparison to ULCNF, EsT\_LCNF promoted a reduction of 42% in energy requirements to produce the nanofibrils, decreasing the consumption of 10.5 kWh/kg to 6.1 kWh/kg. The necessary energy to produce nanocellulose materials is a crucial factor to allow competitive industrial production commercialization of these materials and their derivatives so that they can compete with polymers of petroleum origin. According to Desmaisons et al. (2017), since 2008, studies have shown that the use of pretreatments reduces the energy demand for nanofibrillation from 20-30 kWh/kg to 1.0 kWh/kg.

Figure 6A shows for both samples, energy consumption for mechanical nanofibrillation increases with the extending of grinding passes. The time spent for each pass through the grinder, for all the samples are shown in Figure 7B. The time for each pass tended to increase during the nanofibrillation process for all treatments.

It is interesting to note that the specific nanofibrillation energy for each passage through the grinder of the EsT\_LCNF sample is greater than that of the ULCNF. Furthermore, the two energy consumption evolution curves (Figure 7A) follow a similar trend. In Figure 7B, the time per passage for the sample treated with the enzymes is also longer compared to the one without treatment. However, even with higher specific energy and nanofibrillation time per pass, the EsT\_LCNF sample needed fewer passes (6 against 21 passes) and less time to reach the gel point than the ULCNF sample, making it consume less overall energy when compared to the control sample.

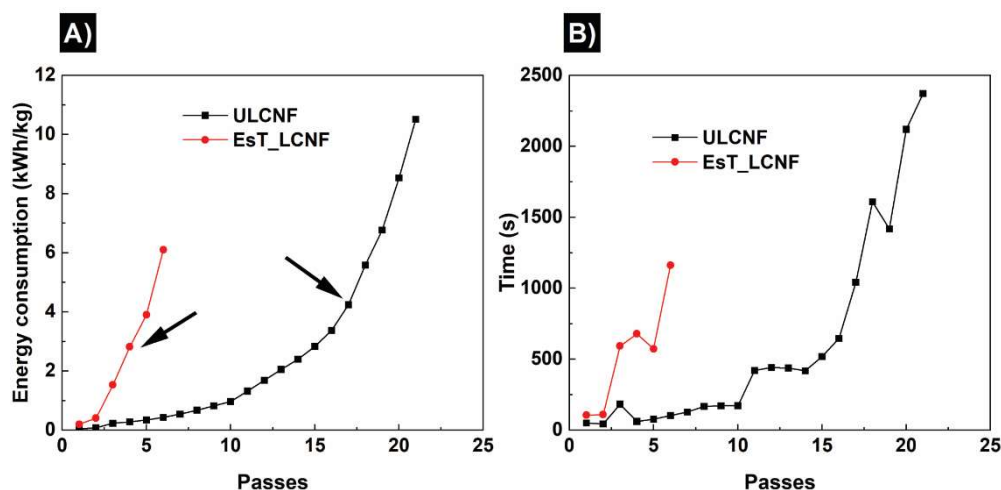


**Figure 7:** A) Evolution of energy consumption for each pass and B) Time spent vs. nanofibrillation pass for ULCNF and EsT\_LCNF. The black arrows indicate the point at which it was observed that the suspensions acquired a consistent gel appearance.

One factor that can explain this behavior is that in EsT\_LCNF, the fibers' cell wall was delaminated more quickly, making the microfibrils more easily individualized, increasing the water retention capacity of the suspension and, consequently, increasing its viscosity. Furthermore, increasing the nanofibrillation time of the material with each pass through the grinder. This is due to the ability of the cellulose nanoparticles to retain a large amount of water. The increase of viscosity along the nanofibrillation process is a consequence of the disintegration of fibrils, showing a stronger network formation as is typical of cellulose nanoparticles and forming a strong gel structure (Lahtinen et al., 2014).

Literature reports that lignin is one of the most significant factors in the recalcitrance of lignocellulosic biomass (Li et al., 2016), a fact that is widely observed during the nanofibrillation of mechanical pulps (He et al., 2018; Lahtinen et al., 2014). On the other hand, in the case of chemical pulps, there are reports that the presence of residual lignin can decrease the energy consumption of nanofibrillation (Spence et al., 2011). This different behavior between these two types of pulp may be related to the sulfonation of lignin in the compound pulps that allow a more extensive swelling of the fibers by water, accompanied by a more extensive softening of the material (Solala et al., 2019).

### 3.8 Quality of lignin-cellulose nanofibrils

The lignin-cellulose nanofibrils produced without and after enzymatic pretreatments were characterized and had their quality evaluated based on the index proposed by Desmaisons et al. (2017) obtaining the values shown in Table 7.

**Table7:** Quality indexes of lignin-cellulose nanofibrils produced by different conditions. Different letters in the same column indicate significant ( $p \leq 0.05$ ) differences between the samples for the Tukey's test.

Quality index of Lignin-cellulose nanofibrils						
Samples	Turbidity (NTU)	Tear resistance (mN)	Young's modulus (GPa)	Porosity (%)	Micro-size area ( $\mu\text{m}^2$ )	Q.I*
ULCNF	$541 \pm 7^a$	$49 \pm 3^a$	$7.2 \pm 0.3^b$	$29.8 \pm 1.7^a$	$73 \pm 8^a$	$61 \pm 3^b$
EsT_LCNF	$473 \pm 5^b$	$41 \pm 3^b$	$9.5 \pm 0.4^a$	$25.5 \pm 1.9^b$	$54 \pm 9^b$	$71 \pm 2^a$

As already discussed in the previous section, the decrease of turbidity values obtained by the EsT\_LCNF treatment already shows the efficiency of the enzymes as a facilitator of nanofibrillation of the unbleached fibers. The mechanical tests results show significance differences on nanopapers properties. The tear resistance result decrease from  $49 \pm 3$  to  $41 \pm 3$  mN after enzymatic hydrolysis, showing the effectiveness of these pre-treatments to facilitate the action of the enzyme endoglucanase on the fiber structure that still contains lignin after the action of the enzyme laccase that weakened the lignin structure allowing the effective cutting of fibers and generation of fine elements.

These results present the same tendency as the work of Banvillet et al. (2021), where after the use of enzyme hydrolysis, the authors reported decrease of the values of tear resistance. The tear resistance of the nanopapers is related to interactions and dimensions of the LCNF; the more homogeneous the structures are at the nanoscale, more cohesive the material is, facilitating the propagation of the tear by the absence of empty spaces (Desmaisons et al., 2017). The Young's modulus was positively affected by the enzymes, the value increased from  $7.2 \pm 0.3$  to  $9.5 \pm 0.4$  GPa where this property is directly influenced by the aspect ratio and interactions of lignin-cellulose nanofibrils. This increase is due to the hydrolysis of the amorphous cellulose in the fibers by the enzymatic action that caused the relative increase of crystalline domains that led to the increase of the stiffness of the material. The decrease of porosity of the nanopapers (from 29.8% to 25.5%) corroborates with the increase of Young's Modulus after the enzymatic treatments. According to Benítez and Walther (2017), this occurs

because materials with lower porosity contain more mechanically resistant nanostructures while materials with higher porosity contain air instead of a LCNF network with high mechanical strength. Also according to the same authors and Banvillet et al. (2021) with an enzymatic pretreatment, nanopapers with porosities less than 20% and Young's modulus between 8 and 15 GPa are usually obtained.

Regarding the micro-size area ( $\mu\text{m}^2$ ), the residual non-nanofibrillated fibers was lower for EsT\_LCNF ( $54 \pm 9 \mu\text{m}^2$ ), indicating that in this case there was a greater delamination of the cell wall. The pretreatment facilitates the nanofibrillation and leads to the decrease of energy demand. As shown in the previous section, the energy consumption along the nanofibrillation process decreased by 42% after the enzymatic hydrolysis. After determining the quality index for each material, the EsT\_LCNF sample achieved a higher value ( $71 \pm 2$ ), with a 10-point advantage over the untreated sample ( $61 \pm 3$ ). Besides the quality of LCNF, an essential factor to produce this material in industrial scale is the energy consumption required for the deconstruction of the lignocellulosic fiber from the macro to the nanoscale. In this study, it was evidenced the effectiveness of the pre-treatments presented as a viable alternative to produce lignocellulosic nanofibrils.

#### **4. Conclusions**

This study confirms the positive impact of a combined enzymatic pretreatment of laccase and endoglucanase for LCNF production. The laccase enzyme proved effective in attacking the lignin helping to decrease the recalcitrance of the fiber cell wall and making the cellulose more exposed to physical contact for the action of the endoglucanase enzyme. The effectiveness of the enzymatic activity during pretreatment was proven, with the increase of IC and positive effect on morphological and mechanical parameters of LCNF. The pretreatment led to the production of LCNF with lower aggregation of nanofibers, evidenced by lower turbidity and by electron microscopy image. The enzymes also led to LCNF with superior mechanical properties, evidenced by Young's modulus that varied from 7.2 to 9.5 GPa of the control sample compared to the one treated with the enzymes, respectively. LCNF production confirmed the positive influence of the combined pretreatment compared to the untreated sample, with an increase in the quality index and a decrease in energy demand.

The shear viscosity data were fitted with the Herschel-Bulkley equation, and the flow rates varied little between the control sample and the one pretreated with enzymes, ranging from 0.30 to 0.36 indicating that both present non-Newtonian fluid behavior, being necessary the application of an initial force to flow them. The results also showed that both suspensions can return to their original state, with a greater ease for EsT\_LCNF to return to the original resting state after application of a shear force, a typical characteristic of materials of thixotropic nature, and thixotropy plays a key role in the consolidation of the coating during the paper coating process. The contact angle, wettability and barrier properties tests showed that the enzyme laccase did not negatively affect the hydrophobic properties of the material, as this enzyme attacks the lignin it could cause increased interaction of the material with water molecules.

This new pretreatment could therefore be used to produce LCNF in various applications, being attractive for its use in the packaging industry, or for high value-added applications such as substrates for printed electronics. Finally, this pretreatment could be suitable for industrial production (due to the decreased energy requirements) and experiments in the present paper provide data support for additional theoretical research.

### **Acknowledgments**

The authors thank the Research Support Foundation of Minas Gerais (FAPEMIG), the National Council for Scientific and Technological Development (CNPq), the Brazilian Federal Agency for the Support and Evaluation of Graduate Education (CAPES; Funding Code 001) and the Wood Science and Technology graduate program from Federal University of Lavras for supplying equipment and financial support. We also thank the Laboratoire Génie des Procédés Papetiers (LGP2) is a part of the LabEx Tec 21 (Investissements d'Avenir—grant agreement no. ANR-11-LABX- 0030), Thierry Encinas from CMTC - Grenoble for the XRD analysis and the Center of Microscopy at the Federal University of Minas Gerais (<http://www.microscopia.ufmg.br>) for providing the equipment and technical support for experiments involving TEM.

### **Conflict of interest**

The authors declare that they have no conflict of interest.

## References

- [1] Y. Wen, Z. Yuan, X. Liu, J. Qu, S. Yang, A. Wang, C. Wang, B. Wei, J. Xu, Y. Ni, Preparation and Characterization of Lignin-Containing Cellulose Nanofibril from Poplar High-Yield Pulp via TEMPO-Mediated Oxidation and Homogenization, *ACS Sustain. Chem. Eng.* 7 (2019) 6131–6139. doi:10.1021/acssuschemeng.8b06355.
- [2] A. Gupta, W. Simmons, G.T. Schueneman, D. Hylton, E.A. Mintz, Rheological and thermo-mechanical properties of poly(lactic acid)/lignin-coated cellulose nanocrystal composites, *ACS Sustain. Chem. Eng.* 5 (2017) 1711–1720. doi:10.1021/acssuschemeng.6b02458.
- [3] Y. Zhao, U. Shakeel, M. Saif Ur Rehman, H. Li, X. Xu, J. Xu, Lignin-carbohydrate complexes (LCCs) and its role in biorefinery, *J. Clean. Prod.* 253 (2020) 120076. doi:10.1016/j.jclepro.2020.120076.
- [4] A. Lorenci Woiciechowski, C.J. Dalmas Neto, L. Porto de Souza Vandenberghe, D.P. de Carvalho Neto, A.C. Novak Sydney, L.A.J. Letti, S.G. Karp, L.A. Zevallos Torres, C.R. Soccol, Lignocellulosic biomass: Acid and alkaline pretreatments and their effects on biomass recalcitrance – Conventional processing and recent advances, *Bioresour. Technol.* 304 (2020) 122848. doi:10.1016/j.biortech.2020.122848.
- [5] A.K. Kumar, S. Sharma, Recent updates on different methods of pretreatment of lignocellulosic feedstocks: a review, *Bioresour. Bioprocess.* 4 (2017). doi:10.1186/s40643-017-0137-9.
- [6] C.G. Yoo, X. Meng, Y. Pu, A.J. Ragauskas, The critical role of lignin in lignocellulosic biomass conversion and recent pretreatment strategies: A comprehensive review, *Bioresour. Technol.* 301 (2020) 122784. doi:10.1016/j.biortech.2020.122784.
- [7] H. Guo, B. Zhang, Z. Qi, C. Li, J. Ji, T. Dai, A. Wang, T. Zhang, Valorization of Lignin to Simple Phenolic Compounds over Tungsten Carbide: Impact of Lignin Structure, *ChemSusChem.* 10 (2017) 523–532. doi:10.1002/cssc.201601326.
- [8] M. Li, Y. Pu, A.J. Ragauskas, Current Understanding of the Correlation of Lignin Structure with Biomass Recalcitrance, *Front. Chem.* 4 (2016) 1–8. doi:10.3389/fchem.2016.00045.
- [9] M. Li, L. Yi, L. Bin, Q. Zhang, J. Song, H. Jiang, C. Chen, S. Wang, D. Min, Comparison of nonproductive adsorption of cellulase onto lignin isolated from pretreated lignocellulose, *Cellulose.* 27 (2020) 7911–7927. doi:10.1007/s10570-020-03357-6.
- [10] M.H. Sipponen, J. Rahikainen, T. Leskinen, V. Pihlajaniemi, M.-L. Mattinen, H. Lange, C. Crestini, M. Österberg, Structural changes of lignin in biorefinery pretreatments and consequences to enzyme-lignin interactions, *Nord. Pulp Pap. Res. J.* 32 (2017) 550–571. doi:10.3183/npprj-2017-32-04-p550-571.
- [11] A.C. Rodrigues, A.F. Leitão, S. Moreira, C. Felby, M. Gama, Recycling of cellulases in lignocellulosic hydrolysates using alkaline elution, *Bioresour. Technol.* 110 (2012) 526–533. doi:10.1016/j.biortech.2012.01.140.
- [12] H. Nlandu, K. Belkacemi, N. Chorfa, S. Elkoun, M. Robert, S. Hamoudi, Laccase-Mediated Grafting of Phenolic Compounds onto Lignocellulosic Flax Nanofibers, *J. Nat. Fibers.* 00 (2020) 1–10. doi:10.1080/15440478.2020.1738307.

- [13] V. Steinmetz, M. Villain-gambier, A. Klem, I. Ziegler, S. Dumarçay, D. Trebouet, In-situ extraction of depolymerization products by membrane filtration against lignin condensation, *Bioresour. Technol.* 311 (2020) 123530. doi:10.1016/j.biortech.2020.123530.
- [14] M.C. Dias, M.C. Mendonça, R.A.P. Damásio, Influence of hemicellulose content of Eucalyptus and Pinus fibers on the grinding process for obtaining cellulose micro / nanofibrils, *Holzforschung.* 73 (2019) 1035–1046.
- [15] L.E. Silva, A. de A. dos Santos, L. Torres, Z. McCaffrey, A. Klamczynski, G. Glenn, A.R. de Sena Neto, D. Wood, T. Williams, W. Orts, R.A.P. Damásio, G.H.D. Tonoli, Redispersion and structural change evaluation of dried microfibrillated cellulose, *Carbohydr. Polym.* 252 (2021). doi:10.1016/j.carbpol.2020.117165.
- [16] J. Desmays, E. Boutonnet, M. Rueff, A. Dufresne, J. Bras, A new quality index for benchmarking of different cellulose nanofibrils, *Carbohydr. Polym.* 174 (2017) 318–329. doi:10.1016/j.carbpol.2017.06.032.
- [17] Y. Nishiyama, P. Langan, H. Chanzy, Crystal Structure and Hydrogen-Bonding System in Cellulose I $\beta$  from Synchrotron X-ray and Neutron Fiber Diffraction, *J. Am. Chem. Soc.* 124 (2002) 9074–9082. doi:10.1021/ja0257319.
- [18] L.O. Souza, O.A. Lessa, M.C. Dias, G.H.D. Tonoli, D.V.B. Rezende, M.A. Martins, I.C.O. Neves, J.V. de Resende, E.E.N. Carvalho, E.V. de Barros Vilas Boas, J.R. de Oliveira, M. Franco, Study of morphological properties and rheological parameters of cellulose nanofibrils of cocoa shell (*Theobroma cacao* L.), *Carbohydr. Polym.* 214 (2019). doi:10.1016/j.carbpol.2019.03.037.
- [19] J.F. Steffe, *Rheological methods in food process engineering*, Freeman Press, Michigan, 1996.
- [20] K. Dimic-Misic, P.A.C. Gane, J. Paltakari, Micro and nanofibrillated cellulose as a rheology modifier additive in CMC-containing pigment-coating formulations, *Ind. Eng. Chem. Res.* 52 (2013) 16066–16083. doi:10.1021/ie4028878.
- [21] J. Rantanen, K. Dimic-Misic, J. Pirttiniemi, P. Kuosmanen, T.C. Maloney, Forming and dewatering of a microfibrillated cellulose composite paper, *BioResources.* 10 (2015) 3492–3506. doi:10.15376/biores.10.2.3492-3506.
- [22] D.K. Owens, R.C. Wendt, Estimation of the surface free energy of polymers, *J. Appl. Polym. Sci.* 13 (1969) 1741–1747. doi:10.1002/app.1969.070130815.
- [23] G. Chen, J. Dong, J. Wan, Y. Ma, Y. Wang, Fiber characterization of old corrugated container bleached pulp with laccase and glycine pretreatment, *Biomass Convers. Biorefinery.* (2021). doi:10.1007/s13399-020-01200-3.
- [24] C.A. Mooney, S.D. Mansfield, R.P. Beatson, J.N. Saddler, The effect of fiber characteristics on hydrolysis and cellulase accessibility to softwood substrates, *Enzyme Microb. Technol.* 25 (1999) 644–650. doi:10.1016/S0141-0229(99)00098-8.
- [25] C.A. Azevedo, S.M.C. Rebola, E.M. Domingues, F.M.L. Figueiredo, D. V. Evtuguin, Relationship between Surface Properties and Fiber Network Parameters of Eucalyptus Kraft Pulps and Their Absorption Capacity, *Surfaces.* 3 (2020) 265–281. doi:10.3390/surfaces3030020.
- [26] E. Espinosa, F. Rol, J. Bras, A. Rodríguez, Use of multi-factorial analysis to determine



- the quality of cellulose nanofibers: effect of nanofibrillation treatment and residual lignin content, *Cellulose*. 3 (2020). doi:10.1007/s10570-020-03136-3.
- [27] E.J. Foster, R.J. Moon, U.P. Agarwal, M.J. Bortner, J. Bras, S. Camarero-Espinosa, K.J. Chan, M.J.D. Clift, E.D. Cranston, S.J. Eichhorn, D.M. Fox, W.Y. Hamad, L. Heux, B. Jean, M. Korey, W. Nieh, K.J. Ong, M.S. Reid, S. Renneckar, R. Roberts, J.A. Shatkin, J. Simonsen, K. Stinson-Bagby, N. Wanasekara, J. Youngblood, Current characterization methods for cellulose nanomaterials, *Chem. Soc. Rev.* 47 (2018) 2609–2679. doi:10.1039/c6cs00895j.
- [28] H. Tibolla, F.M. Pelissari, F.C. Menegalli, Cellulose nanofibers produced from banana peel by chemical and enzymatic treatment, *LWT - Food Sci. Technol.* 59 (2014) 1311–1318. doi:10.1016/j.lwt.2014.04.011.
- [29] S. Bhattacharjee, Review article DLS and zeta potential – What they are and what they are not ?, *J. Control. Release*. 235 (2016) 337–351. doi:10.1016/j.jconrel.2016.06.017.
- [30] R. Bardet, C. Reverdy, N. Belgacem, I. Leirset, K. Syverud, M. Bardet, J. Bras, Substitution of nanoclay in high gas barrier films of cellulose nanofibrils with cellulose nanocrystals and thermal treatment, *Cellulose*. 22 (2015) 1227–1241. doi:10.1007/s10570-015-0547-9.
- [31] H. Lee, J. Sundaram, L. Zhu, Y. Zhao, S. Mani, Improved thermal stability of cellulose nano fibrils using low-concentration alkaline pretreatment, *Carbohydr. Polym.* 181 (2018) 506–513. doi:10.1016/j.carbpol.2017.08.119.
- [32] M. Imani, K. Dimic-Misic, M. Tavakoli, O.J. Rojas, P.A.C. Gane, Coupled Effects of Fibril Width, Residual and Mechanically Liberated Lignin on the Flow, Viscoelasticity, and Dewatering of Cellulosic Nanomaterials, *Biomacromolecules*. 21 (2020) 4123–4134. doi:10.1021/acs.biomac.0c00918.
- [33] M. Herrera, K. Thitiwutthisakul, X. Yang, P. on Rujitanaroj, R. Rojas, L. Berglund, Preparation and evaluation of high-lignin content cellulose nanofibrils from eucalyptus pulp, *Cellulose*. 25 (2018) 3121–3133. doi:10.1007/s10570-018-1764-9.
- [34] Y.M. Zhou, S.Y. Fu, L.M. Zheng, H.Y. Zhan, Effect of nanocellulose isolation techniques on the formation of reinforced poly(vinyl alcohol) nanocomposite films, *Express Polym. Lett.* 6 (2012) 794–804. doi:10.3144/expresspolymlett.2012.85.
- [35] G.H.D. Tonoli, K.M. Holtman, G. Glenn, A.S. Fonseca, D. Wood, T. Williams, V.A. Sa, L. Torres, A. Klamczynski, W.J. Orts, Properties of cellulose micro/nanofibers obtained from eucalyptus pulp fiber treated with anaerobic digestate and high shear mixing, *Cellulose*. 23 (2016) 1239–1256. doi:10.1007/s10570-016-0890-5.
- [36] R.C. do Lago, A.L.M. de Oliveira, M. Cordasso Dias, E.E.N. de Carvalho, G.H. Denzin Tonoli, E.V. de Barros Vilas Boas, Obtaining cellulosic nanofibrils from oat straw for biocomposite reinforcement: Mechanical and barrier properties, *Ind. Crops Prod.* 148 (2020). doi:10.1016/j.indcrop.2020.112264.
- [37] A.D. French, Idealized powder diffraction patterns for cellulose polymorphs, *Cellulose*. 21 (2014) 885–896. doi:10.1007/s10570-013-0030-4.
- [38] K.R. Hakeem, M. Jawaid, O.Y. Allothman, Rheological Properties and Processing of Polymer Blends with Micro- and Nanofibrillated Cellulose, 2015. doi:10.1007/978-3-319-13847-3.

- [39] O. Nechyporchuk, F. Pignon, M.N. Belgacem, Morphological properties of nanofibrillated cellulose produced using wet grinding as an ultimate fibrillation process, *J. Mater. Sci.* 50 (2015) 531–541. doi:10.1007/s10853-014-8609-1.
- [40] A.I. Koponen, The effect of consistency on the shear rheology of aqueous suspensions of cellulose micro- and nanofibrils: a review, *Cellulose*. 27 (2020) 1879–1897. doi:10.1007/s10570-019-02908-w.
- [41] A. Czaikoski, R.L. da Cunha, F.C. Menegalli, Rheological behavior of cellulose nanofibers from cassava peel obtained by combination of chemical and physical processes, *Carbohydr. Polym.* 248 (2020) 116744. doi:10.1016/j.carbpol.2020.116744.
- [42] C. Qiao, G. Chen, J. Zhang, J. Yao, Structure and rheological properties of cellulose nanocrystals suspension, *Food Hydrocoll.* 55 (2016) 19–25. doi:10.1016/j.foodhyd.2015.11.005.
- [43] J.H. Jordan, M.W. Easson, S. Thompson, Q. Wu, B.D. Condon, Lignin-containing cellulose nanofibers with gradient lignin content obtained from cotton gin motes and cotton gin trash, *Cellulose*. 28 (2021) 757–773. doi:10.1007/s10570-020-03549-0.
- [44] A. Naderi, T. Lindström, A comparative study of the rheological properties of three different nanofibrillated cellulose systems, 31 (2016).
- [45] H.Q. Lê, K. Dimic-Misic, L.S. Johansson, T. Maloney, H. Sixta, Effect of lignin on the morphology and rheological properties of nanofibrillated cellulose produced from  $\gamma$ -valerolactone/water fractionation process, *Cellulose*. 25 (2018) 179–194. doi:10.1007/s10570-017-1602-5.
- [46] S. Yook, H. Park, H. Park, S.Y. Lee, J. Kwon, H.J. Youn, Barrier coatings with various types of cellulose nanofibrils and their barrier properties, *Cellulose*. 27 (2020) 4509–4523. doi:10.1007/s10570-020-03061-5.
- [47] A.H. Tayeb, M. Tajvidi, D. Bousfield, Paper-based oil barrier packaging using lignin-containing cellulose nanofibrils, *Molecules*. 25 (2020). doi:10.3390/molecules25061344.
- [48] I. Solala, R. Bordes, A. Larsson, Water vapor mass transport across nanofibrillated cellulose films: effect of surface hydrophobization, *Cellulose*. 25 (2018) 347–356. doi:10.1007/s10570-017-1608-z.
- [49] W. Wang, F. Gu, Z. Deng, Y. Zhu, J. Zhu, T. Guo, J. Song, H. Xiao, Multilayer surface construction for enhancing barrier properties of cellulose-based packaging, *Carbohydr. Polym.* 255 (2021) 117431. doi:10.1016/j.carbpol.2020.117431.
- [50] K.L. Spence, R.A. Venditti, O.J. Rojas, Y. Habibi, J.J. Pawlak, A comparative study of energy consumption and physical properties of microfibrillated cellulose produced by different processing methods, *Cellulose*. 18 (2011) 1097–1111. doi:10.1007/s10570-011-9533-z.
- [51] N. Lavoine, I. Desloges, B. Khelifi, J. Bras, Impact of different coating processes of microfibrillated cellulose on the mechanical and barrier properties of paper, *J. Mater. Sci.* 49 (2014) 2879–2893. doi:10.1007/s10853-013-7995-0.
- [52] S.P.L. Balasubramaniam, A.S. Patel, B. Nayak, Surface modification of cellulose nanofiber film with fatty acids for developing renewable hydrophobic food packaging, *Food Packag. Shelf Life*. 26 (2020) 100587. doi:10.1016/j.fpsl.2020.100587.

- [53] G.H.D. Tonoli, M.N. Belgacem, J. Bras, M.A. Pereira-Da-Silva, F.A. Rocco Lahr, H. Savastano, Impact of bleaching pine fibre on the fibre/cement interface, *J. Mater. Sci.* 47 (2012) 4167–4177. doi:10.1007/s10853-012-6271-z.
- [54] R. Hossain, M. Tajvidi, D. Bousfield, D.J. Gardner, Multi-layer oil-resistant food serving containers made using cellulose nanofiber coated wood flour composites, *Carbohydr. Polym.* 267 (2021) 118221. doi:10.1016/j.carbpol.2021.118221.
- [55] J. Sheng, J. Li, L. Zhao, Fabrication of grease resistant paper with non-fluorinated chemicals for food packaging, *Cellulose.* 26 (2019) 6291–6302. doi:10.1007/s10570-019-02504-y.
- [56] P. Lahtinen, S. Liukkonen, J. Pere, A. Sneek, H. Kangas, A Comparative study of fibrillated fibers from different mechanical and chemical pulps, *BioResources.* 9 (2014) 2115–2127. doi:10.15376/biores.9.2.2115-2127.
- [57] M. He, G. Yang, J. Chen, X. Ji, Q. Wang, Production and Characterization of Cellulose Nanofibrils from Different Chemical and Mechanical Pulps, *J. Wood Chem. Technol.* 38 (2018) 149–158. doi:10.1080/02773813.2017.1411368.
- [58] I. Solala, M.C. Iglesias, M.S. Peresin, On the potential of lignin-containing cellulose nanofibrils ( LCNFs ): a review on properties and applications, *Cellulose.* 8 (2019). doi:10.1007/s10570-019-02899-8.
- [59] G. Banvillet, E. Gatt, N. Belgacem, J. Bras, Cellulose fibers deconstruction by twin-screw extrusion with in situ enzymatic hydrolysis via bioextrusion, *Bioresour. Technol.* 327 (2021) 124819. doi:10.1016/j.biortech.2021.124819.
- [60] A.J. Benítez, A. Walther, Cellulose nanofibril nanopapers and bioinspired nanocomposites: A review to understand the mechanical property space, *J. Mater. Chem. A.* 5 (2017) 16003–16024. doi:10.1039/c7ta02006f.

## CHAPTER IV: CONCLUSIONS OF THE THESIS

The polymers that constitute the cell wall of plant fibers are closely related to each other and this study has shown that during the process of biorefinery of this biomass, it is extremely important to consider the intrinsic properties of each one and the interactions between these constituents. Both these properties and interactions are responsible for the phenomenon of fiber recalcitrance, which becomes a challenge for the efficient separation and/or degradation of these constituents.

Thus, the obtainment of by-products such as cellulose and its derivatives, hemicellulose, and lignin can be optimized when the recalcitrance factor can be considerably reduced, representing benefits in the quality of the material and energy savings during the biomass conversion process.

In this study, commercial bleached eucalyptus pulps were studied and evaluated with different hemicellulose contents in their composition, and the unbleached pulps were hydrolyzed with laccase and endoglucanase enzymes and were used as raw material to obtain cellulose nanofibrils (CNF) and lignin-cellulose nanofibrils. (LCNF) respectively, using a mechanical nanofibrillator.

Therefore, up to this point, this study showed that the alkaline treatments not only caused different levels of hemicellulose but also caused partial conversion to cellulose II. The positive impact of the change in hemicellulose content and cellulose structure caused in CNF during alkaline treatment with low NaOH concentration (5% w/v) was demonstrated.

The viscosity of the different CNF obtained from fibers with specific hemicellulose content decreased linearly. This occurred because the removal of these polysaccharides reduces the formation of complex networks between CNFs since they have free hydrogen bonding sites that allow cross-linking between cellulose chains. The rheology of CNF suspensions is an essential factor for various applications of this material.

Lignin was also shown to have a positive influence on CNF properties, and the negative aspect of its presence as an obstructive agent for cell wall delamination can be overcome with the use of specific ligninolytic enzymes, such as laccases, which was observed in the reduction of energy consumption during nanofibrillation. Treatment with the laccase enzyme before the endoglucanase enzyme treatment in the unbleached pulps proved to be efficient to avoid the inhibition of the endoglucanase action on cellulose by the presence of lignin.

This study contributed to society with the generation of fundamental knowledge of how the other main components of the cell wall (hemicellulose and lignin) interact with cellulose

and influence the responses of pretreatment of the fibers to mechanically deconstruct them to obtain cellulose nanofibrils. It also contributes to the improvement of industrial technology, involving the development of processes to generate innovative products, especially for the renewable packaging sector with the development of new materials based on cellulose, materials of renewable origin, seeking a more sustainable society concerning petroleum-based materials.

This study not only translates into scientific, technological, and economic impacts, in the case of the development of pre-treatments to reduce energy consumption in the production of CNF and the possibility of applying the material in the development of new packaging and materials, but also in social and environmental impacts by the possibility of generating new employment, and the possibility of using materials from renewable sources, contributing to the immobilization of carbon in the materials produced, and promoting sustainability.

## CHAPTER V: SUGGESTIONS FOR FUTURE WORKS

The following are suggestions for future work:

1. Evaluate the influence of hemicellulose using enzymes (Mainly xylanase enzymes) to avoid the effect of the change in cellulose structure promoted by the action of sodium hydroxide.
2. Evaluate the influence of hemicellulose using a hydrothermal treatment to avoid the effect of the change in cellulose structure promoted by the action of sodium hydroxide.
3. To perform the nanomechanical characterization of the fiber cell wall before and after the treatments to evaluate the effect on recalcitrance.
4. Measure the binding energy of lignin in the fiber structure before and after hydrolysis with the enzyme Lacasse.
5. Evaluate the degree of lignin depolymerization after Lacasse-mediated enzymatic hydrolysis.
6. To evaluate the possibility of simultaneous or continuous enzymatic hydrolysis using the enzymes Lacasse and endoglucanase.

## CHAPTER VI: APPENDICES

### APPENDIX 1: TEMPO - mediated oxidation of cellulosic fibers

#### RESPONSIBLE RESEARCHER:

Matheus CORDAZZO DIAS

matheus.cordazzo-dias@ grenoble-inp.fr

Office: B029 (D2)

Supervisor : N. Belgacem

#### TEMPO - mediated oxidation of cellulosic fibers

##### Lab Security

User must wear safety glasses, gloves, and lab coat

##### Chemicals

Cellulosic fibers ( $C_6H_{10}O_5$ )<sub>n</sub>

TEMPO ( $C_9H_{18}NO$ )









Sodium Bromide (NaBr)

Sodium hypochlorite (NaClO)

Ethanol ( $CH_3CH_2OH$ )

Sodium hydroxide (NaOH) 0.5 M

Hydrochloric acid (HCl) 0.5 M

Product	CAS number	Mol. Weight (g/mol)	Risks
Sodium bromide NaBr	7647-15-6	102.89	-
Sodium hypochlorite NaClO	7681-52-9	74.45	 
2,2,6,6-Tetramethylpiperidine 1-oxyl $C_9H_{18}NO$	2564-83-2	156.25	
Sodium hydroxide NaOH	1310-73-2	40.00	
Hydrochloric acid HCl	7647-01-0	36.46	 
Ethanol $CH_3CH_2OH$	64-17-5	46.07	 

##### Materials:

- |                      |                             |
|----------------------|-----------------------------|
| - pH-meter           | - 100 mL measuring cylinder |
| - Magnetic stirrer   | - Precision balance         |
| - Mechanical stirrer | - Fume hood                 |
| - 250 mL beaker      |                             |

### Amount of NaClO:

---

- **Density:** 1.22 g/cm<sup>3</sup>
- **Molar weight:** 74.45 g/mol
- **Solution concentration:** 12%
- **Molarity:** 12 mmol = 0.012 mol

$$\text{Molarity} = \frac{\text{Mass}}{\text{Molar weight} \times \text{Volume}} \rightarrow 0.012 = \frac{\text{Mass}}{74.45 \times 1} \rightarrow \text{Mass} = 0.8934 \text{ g}$$



$$\text{Mass} = \frac{0.8934 \times 100}{12} \rightarrow \text{Mass} = 7.4450 \text{ g NaClO}$$



$$\text{Density} = \frac{\text{Mass}}{\text{Volume}} \rightarrow \text{Volume} = \frac{7.4450}{1.22} \rightarrow \text{V} = 6.1025 \text{ mL NaClO/1 g cellulose}$$

### Protocol:

---

- Initially, the cellulosic fibers (70 g) were suspended in 2800 mL of distilled water, obtaining a suspension with a concentration of 2.5% (wt%).
- Then, 1.12 g of TEMPO reagent (0.016 g; 0.1 mmol/1 g cellulose) was solubilized in 250 mL of distilled water, where it was constantly stirred for 1 hour. 7 g of NaBr (0.1 g; 0.1 mmol/1 g cellulose) were also solubilized in 100 mL of water under constant stirring for 1 hour. Later, the two reagents were added to the cellulosic fiber suspension and the system was under constant agitation for 20 minutes.
- After this period, 427.1750 mL of 12% NaClO (6.1025 mL; 7.4 g; 12 mmol/1 g cellulose) were gradually added, leaving the system pH at around 10.
- Subsequently, the pH was maintained at around 10 by adding drops of 0.5 M sodium hydroxide solution (NaOH). The reaction carried out for 3 hours with constant stirring and at room temperature.
- After 3 hours of reaction, 100 mL of ethanol were added to stop the reaction and the pH of the system was corrected to 7 by the addition of 0.5 M drops of hydrochloric acid (HCl).
- Finally, the fibers have been washed and the effluents must be stored.

### Effluent treatment

---


Effluent should be put in the “effluent organiques halogénés” container.

### References:



[1] H. Fukuzumi, T. Saito, T. Iwata, Y. Kumamoto, A. Isogai, Transparent and High Gas Barrier Films of Cellulose Nanofibers Prepared by TEMPO-Mediated Oxidation, (2009) 162–165. doi:10.1021/bm801065u.

[2] Y. Wen, Z. Yuan, X. Liu, J. Qu, S. Yang, A. Wang, C. Wang, B. Wei, J. Xu, Y. Ni, Preparation and Characterization of Lignin-Containing Cellulose Nanofibril from Poplar High-Yield Pulp via TEMPO-Mediated Oxidation and Homogenization, ACS Sustain. Chem. Eng. 7 (2019) 6131–6139. doi:10.1021/acssuschemeng.8b06355.

  
Matheus Cordazzo Dias  
Responsible researcher

## APPENDIX 2: Preparation of phosphate buffer solution with pH = 4.5

### RESPONSIBLE RESEARCHER:

Matheus CORDAZZO DIAS

matheus.cordazzo-dias@grenoble-inp.fr

Office: B029 (D2)

Supervisor : N. Belgacem

### Preparation of phosphate buffer solution (pH = 4.5)



#### Lab Security

User must wear safety glasses, gloves, and lab coat

#### Chemicals

Acetic acid glacial (CH<sub>3</sub>COOH)

Sodium acetate trihydrate (C<sub>2</sub>H<sub>3</sub>NaO<sub>2</sub> \* 3H<sub>2</sub>O)

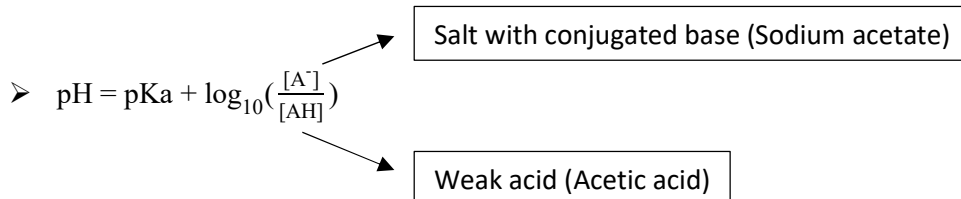
Product	CAS number	Mol. Weight (g/mol)	Risks
Acetic acid glacial CH <sub>3</sub> COOH	64-19-7	60.05	 
Sodium acetate trihydrate C <sub>2</sub> H <sub>3</sub> NaO <sub>2</sub> * 3H <sub>2</sub> O	6131-90-4	136.08	

#### Materials:

- pH-meter
- Magnetic stirrer
- 100 mL beaker
- 1 000 mL volumetric flask
- Fume hood
- Precision balance

#### Henderson-Hasselbalch's equation

pKa acetic acid glacial: 4.76



➤ 
$$4.5 = 4.76 + \log_{10}\left(\frac{[\text{A}^-]}{[\text{AH}]}\right)$$

➤ 
$$10^{(\text{pH} - \text{pK})} = 10^{(-0.2600)} = 0.5495 \rightarrow \text{(salt/acid) ratio (antilog)}$$

**Buffer solution desired molarity = 0.05 M → Total mol**

$$\text{Moles salt} = 0.05 \times \left( \frac{0.5495}{(0.5495+1)} \right) = 0.0177 \text{ mol of sodium acetate}$$

$$\text{Moles acid} = 0.05 \times \left( \frac{1}{(0.5495+1)} \right) = 0.0323 \text{ mol of acetic acid}$$

Then,

$$\text{➤ } \text{pH} = 4.76 + \log_{10} \left( \frac{0.0177}{0.0323} \right)$$

$$\text{➤ } \text{pH} = 4.76 + \log_{10}(0.5480)$$

$$\text{➤ } \text{pH} = 4.76 + (-0.2612)$$

$$\text{➤ } \text{pH} = 4.4988$$

**Molar weight (MW) of acetic acid = 60.05 g/mol**

**Molar weight (MW) of sodium acetate trihydrate = 136.08 g/mol**

**For CH<sub>3</sub>COOH:**

$$M = \frac{m}{\text{MW} \times V} \longrightarrow 0.0323 = \frac{m}{60.05 \times 1} \longrightarrow m = 0.0323 \times 60.05 = 1.9396 \text{ g (1.8472 mL)}$$

**For C<sub>2</sub>H<sub>3</sub>NaO<sub>2</sub> \* 3H<sub>2</sub>O:**

$$M = \frac{m}{\text{MW} \times V} \longrightarrow 0.0177 = \frac{m}{136.08 \times 1} \longrightarrow m = 0.0177 \times 136.08 = 2.4086 \text{ g}$$

**Protocol:**

---


- Transfer 2.4086 g of sodium acetate trihydrate and 1.8472 mL of glacial acetic acid for 1 000 mL volumetric flask.
- Dissolve in water and make up to the mark with the same solvent.
- Let the solution in a magnetic stirrer for 5 minutes.
- Adjust the pH of solution if necessary.

**Reference:**

[1] Lawrence J. Henderson (1908). "Concerning the relationship between the strength of acids and their capacity to preserve neutrality". *Am. J. Physiol.* 21 (2): 173–179. doi:10.1152/ajplegacy.1908.21.2.173.

[2] Hasselbalch, K. A. (1917). "Die Berechnung der Wasserstoffzahl des Blutes aus der freien und gebundenen Kohlensäure desselben, und die Sauerstoffbindung des Blutes als Funktion der Wasserstoffzahl". *Biochemische Zeitschrift.* 78: 112–144.

[3] National Center for Biotechnology Information. PubChem Database. Acetic acid, CID=176, <https://pubchem.ncbi.nlm.nih.gov/compound/Acetic-acid>.

  
Matheus Cordazzo Dias  
Responsible researcher

### APPENDIX 3: Preparation of phosphate buffer solution with pH pH 5

#### RESPONSIBLE RESEARCHER:

**Matheus CORDAZZO DIAS**

matheus.cordazzo-dias@ grenoble-inp.fr

Office: B029 (D2)

Supervisor : N. Belgacem

#### Preparation of phosphate buffer solution (pH = 5)



##### Lab Security

User must wear safety glasses, gloves, and lab coat

##### Chemicals

Acetic acid glacial ( $\text{CH}_3\text{COOH}$ )

Sodium acetate trihydrate ( $\text{C}_2\text{H}_3\text{NaO}_2 \cdot 3\text{H}_2\text{O}$ )

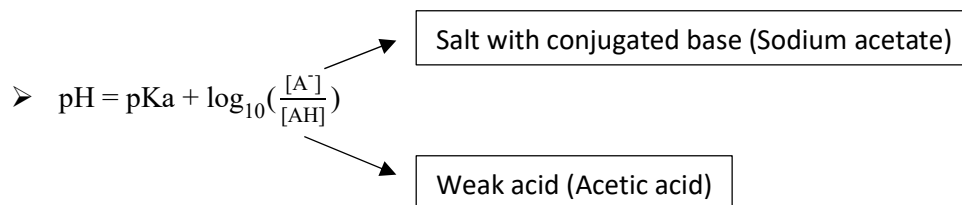
Product	CAS number	Mol. Weight (g/mol)	Risks
Acetic acid glacial $\text{CH}_3\text{COOH}$	64-19-7	60.05	 
Sodium acetate trihydrate $\text{C}_2\text{H}_3\text{NaO}_2 \cdot 3\text{H}_2\text{O}$	6131-90-4	136.08	

##### Materials:

- |                    |                             |
|--------------------|-----------------------------|
| - pH-meter         | - 1 000 mL volumetric flask |
| - Magnetic stirrer | - Fume hood                 |
| - 100 mL beaker    | - Precision balance         |

### Henderson-Hasselbalch's equation

pKa acetic acid glacial: 4.76



$$5.0 = 4.76 + \log_{10}\left(\frac{[\text{A}^-]}{[\text{AH}]}\right)$$

$$10^{(\text{pH} - \text{pKa})} = 10^{(0.2400)} = 1.7378 \rightarrow \text{(salt/acid) ratio (antilog)}$$

**Buffer solution desired molarity = 0.05 M → Total mol**

$$\text{Moles salt} = 0.05 \times \left(\frac{1.7378}{(1.7378+1)}\right) = 0.0317 \text{ mol of sodium acetate}$$

$$\text{Moles acid} = 0.05 \times \left(\frac{1}{(1.7378+1)}\right) = 0.0183 \text{ mol of acetic acid}$$

Then,

$$\text{pH} = 4.76 + \log_{10}\left(\frac{0.0317}{0.0183}\right)$$

$$\text{pH} = 4.76 + \log_{10}(1.7322)$$

$$\text{pH} = 4.76 + 0.2386$$

$$\text{pH} = 4.9986$$

**Molar weight (MW) of acetic acid = 60.05 g/mol**

**Molar weight (MW) of sodium acetate trihydrate = 136.08 g/mol**

**For CH<sub>3</sub>COOH:**

$$M = \frac{m}{\text{MW} \times V} \longrightarrow 0.0323 = \frac{m}{60.05 \times 1} \longrightarrow m = 0.0183 \times 60.05 = 1.0989 \text{ g (1.0445 mL)}$$

**For C<sub>2</sub>H<sub>3</sub>NaO<sub>2</sub> \* 3H<sub>2</sub>O:**

$$M = \frac{m}{MW \times V} \longrightarrow 0.0177 = \frac{m}{136.08 \times 1} \longrightarrow m = 0.0317 \times 136.08 = 4.3137 \text{ g}$$

**Protocol:**

---

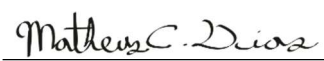
- Transfer 2.4086 g of sodium acetate trihydrate and 1.8472 mL of glacial acetic acid for 1 000 mL volumetric flask.
- Dissolve in water and make up to the mark with the same solvent.
- Let the solution in a magnetic stirrer for 5 minutes.
- Adjust the pH of solution if necessary.

**Reference:**

[1] Lawrence J. Henderson (1908). "Concerning the relationship between the strength of acids and their capacity to preserve neutrality". *Am. J. Physiol.* 21 (2): 173–179. doi:10.1152/ajplegacy.1908.21.2.173.

[2] Hasselbalch, K. A. (1917). "Die Berechnung der Wasserstoffzahl des Blutes aus der freien und gebundenen Kohlensäure desselben, und die Sauerstoffbindung des Blutes als Funktion der Wasserstoffzahl". *Biochemische Zeitschrift.* 78: 112–144.

[3] National Center for Biotechnology Information. PubChem Database. Acetic acid, CID=176, <https://pubchem.ncbi.nlm.nih.gov/compound/Acetic-acid>.

  
Matheus Cordazzo Dias  
Responsible researcher

## APPENDIX 4: Enzymatic hydrolysis mediated by the Laccase enzyme (60 LAMU/g)

### RESPONSIBLE RESEARCHER:

**Matheus CORDAZZO DIAS**

matheus.cordazzo-dias@ grenoble-inp.fr

Office: B029 (D2)

Supervisor : N. Belgacem

### Laccase mediated enzymatic hydrolysis

#### Lab Security

User must wear safety glasses, gloves, and lab coat

#### Chemicals

- Cellulosic fibers ( $C_6H_{10}O_5$ )<sub>n</sub>
- Laccase from *Aspergillus* sp. (Novozym 51003) Activity:  $\geq 1000$  Laccase Units (LAMU/g)
- Acetic acid glacial ( $CH_3COOH$ )
- Sodium acetate trihydratate ( $C_2H_3NaO_2 \cdot 3H_2O$ )

Product	CAS number	Mol. Weight (g/mol)	Risks
Laccase enzyme SAE0050	80498-15-3	-	
Acetic acid glacial $CH_3COOH$	64-19-7	60.05	
Sodium acetate trihydratate $C_2H_3NaO_2 \cdot 3H_2O$	6131-90-4	136.08	

#### Materials:

- |                    |                     |
|--------------------|---------------------|
| - pH-meter         | - 250 mL beaker     |
| - Magnetic stirrer | - Precision balance |
| - Reactor          |                     |



**Enzymatic charge:**

Cellulosic fibers	Novozym 51003 = 1000 LAMU/g
200 g	60 LAMU/g

$$Mass_{enzyme} = \frac{(200 \times 60)}{1000} = 12 \text{ g of enzyme solution at 60 LAMU/g}$$

**Preparation of acetate buffer solution (pH = 4.5):**

- Transfer 2.4086 g of sodium acetate trihydrate and 1.8472 mL of glacial acetic acid for 1 000 mL volumetric flask.
- Dissolve in water and make up to the mark with the same solvent.
- Let the solution in a magnetic stirrer for 5 minutes.
- Adjust the pH of solution if necessary.

**Protocol:**

- 
- The cellulose pulp is diluted to 1.4% and placed in a heated reactor. A temperature 40°C and a stirring of ~300 rpm is fixed. Do this step during the preparation of buffer and enzyme solutions.
  - When the temperature has stabilized, add the buffer solution until a pH 4.5 is reached (a pH control and a temperature control are required throughout the reaction phase).
  - Add the enzyme solution.
- Leave to react for 2 hours. Constantly monitor the pH.

**5. Stopping the reaction.**

- To stop the reaction, heat to 80°C for 10 minutes, then cool to 25°C.

The suspension is recovered, filtered with a 1 micron membrane, and dispersed in 2% deionized water. Add a few drops of chloroform to the suspension as a biocide.

Store the suspension at 3°C.

*Matheus C. Dias*  
 Matheus Cordazzo Dias  
 Responsible researcher

## APPENDIX 5: Enzymatic hydrolysis mediated by the Cellulase enzyme (300 ECU/g)

### RESPONSIBLE RESEARCHER:

**Matheus CORDAZZO DIAS**

matheus.cordazzo-dias@grenoble-inp.fr

Office: B029 (D2)

Supervisor : N. Belgacem





### Cellulase mediated enzymatic hydrolysis

#### Lab Security

User must wear safety glasses, gloves, and lab coat

#### Chemicals

- Cellulosic fibers ( $C_6H_{10}O_5$ )<sub>n</sub>
- FiberCare Cellulase 4890 ECU/g enzyme solution (Sigma-Aldrich C2730-50mL)
- Acetic acid glacial ( $CH_3COOH$ )
- Sodium acetate trihydratate ( $C_2H_3NaO_2 \cdot 3H_2O$ )

Product	CAS number	Mol. Weight (g/mol)	Risks
FiberCare® Cellulase 4890 ECU/g enzyme solution	9012-54-8	-	
Acetic acid glacial $CH_3COOH$	64-19-7	60.05	 
Sodium acetate trihydratate $C_2H_3NaO_2 \cdot 3H_2O$	6131-90-4	136.08	

#### Materials:

- |                    |                     |
|--------------------|---------------------|
| - pH-meter         | - 250 mL beaker     |
| - Magnetic stirrer | - Precision balance |
| - Reactor          |                     |

**Enzymatic charge:**

Cellulosic fibers	FiberCare 4890 ECU/g
100 g	300 ECU/g

$$Mass_{enzyme} = \frac{(100 \times 300)}{4890} = 6.14 \text{ g of enzyme solution at 300 ECU/g}$$

**Preparation of acetate buffer solution (pH = 5):**

- Transfer 4.3137 g of sodium acetate trihydrate and 1.0445 mL of glacial acetic acid for 1 000 mL volumetric flask.
- Dissolve in water and make up to the mark with the same solvent.
- Let the solution in a magnetic stirrer for 5 minutes.
- Adjust the pH of solution if necessary.

**Protocol:**

- 
- The cellulose pulp is diluted to 1.4% and placed in a heated reactor. A temperature 50°C and a stirring of 250 rpm is fixed. Do this step during the preparation of buffer and enzyme solutions.
  - When the temperature has stabilized, add the buffer solution until a pH 5 is reached (a pH control and a temperature control are required throughout the reaction phase).
  - Add the enzyme solution.
- Leave to react for 2 hours. Constantly monitor the pH.

**5. Stopping the reaction.**

- To stop the reaction, heat to 80°C for 10 minutes, then cool to 25°C.

The suspension is recovered, filtered with a 1-micron membrane, and dispersed in 2% deionized water. Add a few drops of chloroform to the suspension as a biocide.

Store the suspension at 3°C.